# Modeling Corrosion in Suspension Bridge Main Cables

**Efe Karanci**

Submitted in partial fulfillment of the
requirements for the degree of
Doctor of Philosophy
in the Graduate School of Arts and Sciences

**COLUMBIA UNIVERSITY**

2017

# ABSTRACT


**Modeling Corrosion in Suspension Bridge Main Cables**

**Efe Karanci**

Accurately determining the current state of a suspension bridge's main cables is a critical component to reliably assessing the safety of the bridge. The primary cause for the deterioration of cable strength with time is universally recognized to be the corrosion of high-strength steel wires, which together comprise the main cable. Hidden from view by the cable wrapping, this corrosion often goes undetected for years and is typically only discovered during costly and intrusive inspections. Furthermore, current inspection methods provide an incomplete picture of the variation in wire condition across the cable cross-section. As a result, cable strength estimation techniques that rely solely on inspection data introduce a considerable degree of uncertainty. Finally, a method has not been developed for estimating the continuing decline in cable strength due to ongoing corrosion. A recent direction in research attempts to address the shortcomings of current inspection methodologies and the intent of this thesis is to further build upon these findings.

In these recent studies, environmental conditions inside main cables are monitored to obtain information regarding the corrosive nature of the cable's internal environment. The first goal of this thesis is to further this research direction by introducing a corrosion rate model for bridge wires that relates the monitored environmental parameters within a cable to the corrosion rate of bridge wires. Initially, temperature, relative humidity, pH, and $Cl^-$ concentration have been identified as the most

relevant variables for predicting the corrosion rate of a bridge wire. By applying machine learning methods to a corrosion dataset in conjunction with these monitored environmental inputs, a long-term corrosion rate model for bridge wires has been developed that is capable of capturing variability associated with these environmental parameters.

This long-term corrosion rate model is then applied to establish a methodology that will allow bridge owners and engineers to estimate the remaining strength of a main cable at any point in time. This is accomplished through the use of continually monitored environmental parameters which are input into the corrosion rate model. Incorporating the long-term corrosion rate model developed in this thesis with current strength estimation techniques, the methodology presented in this thesis for the estimation of the remaining strength of suspension bridge cables may be readily adapted to other bridges and can be used to complement the current best practices for bridge inspection.

# TABLE OF CONTENTS

# LIST OF FIGURES

# LIST OF TABLES

# ACKNOWLEDGMENTS

This has been a remarkable journey that truly tested me. Along the way, I received guidance and support of many people for which I'll forever be grateful.

Firstly, I would like to thank my advisor, Prof. Raimondo Betti, for giving me the opportunity to carry out this research, and all the knowledge imparted along the way. I thank him for his maddening rigor that drove me nuts at times, but at the same time enormously improved the quality of the work presented in this thesis. Above all, I thank him for his belief in me and continuous support over all these years.

I spent my fair share of time in the Carleton Lab while performing a great number of experiments. I sincerely appreciate the help I received from the past and present employees of the lab. Thank you all!

As the second worst writer Prof. Betti has seen, I required a ton of help with my writing. I am forever indebted to Ryan, Cem, Grace, Oya, Elisabeth, Ali, Emre, and Maya for the countless hours reading my drafts and their vital edits and critique.

More personally, I am very fortunate to have shared many unforgettable moments with wonderful friends throughout my Ph.D. Thanks to my friends in the Civil Department for their intellectual and

motivational support, in particular, Adrian, Eleni, Elisabeth, Logan, Jesse, Wei, Ali, Berk, Cengiz, and Yuwei. Baris, Can Alpdo, Ahmet: your friendship kept me sane, grounded, and focused at all the right times. Cem: I will always remember that moment in Dusseldorf when I was in complete despair and how you implanted the hope and determination that took me to the finish line.

Finally, and most importantly, my thanks and love to my family. My late grandfather Mehmet Fuat Yucesoy - for making me want to live up to your example and principles. Mom - for always being an inspiration and a constant source of support. Dad - for pushing me to be better—and in turn teaching me how to push myself—and instilling the relation between the head and the brain inside of it. Ayse - for always checking up on me and threatening to finish your Ph.D. before mine.

# CHAPTER 1. INTRODUCTION

ON Friday noon, July the twentieth, 1714, the finest bridge in all Peru broke and precipitated five travelers into the gulf below. This bridge was on the high-road, between Lima and Cuzco and hundreds of persons passed over it every day. It had been woven of osier by the Incas more than a century before and visitors to the city were always led out to see it. It was a mere ladder of thin slats swung out over the gorge, with handrails of dried vine. Horses and coaches and chairs had to go down hundreds of feet below and pass over the narrow torrent on rafts, but no one, not even the Viceroy, not even the Archbishop of Lima, had descended with the baggage rather than cross by the famous bridge of San Luis Rey. St. Louis of France himself protected it, by his name and by the little mud church on the further side. The bridge seemed to be among the things that last forever; it was unthinkable that it should break. The moment a Peruvian heard of the accident he signed himself and made a mental calculation as to how recently he had crossed by it and how soon he had intended crossing by it again. People wandered about in a trance-like state, muttering; they had the hallucination of seeing themselves falling into a gulf.

Thornton Wilder, *The Bridge of San Luis Rey* [1]

## Overview

Suspension bridges are known for their aesthetic, efficiency, and especially their ability to span longer distances than any other type of bridge. The long spans characteristic of suspension bridges enable crossings over vast expanses of water and valleys previously deemed insurmountable. Consequently, suspension bridges have become one of the most vital aspects of modern infrastructure. The key structural components and form of the modern suspension bridge remain virtually unchanged and date all the way back to James Finley's designs in the early 19$^{th}$ century [2]. In particular, suspension bridges rely on main cables comprised of thousands of high-strength

bridge wires to make feasible the immense spans for which these bridge are known. John Roebling's main cable erection scheme developed in the second half of the 19th century is still widely used in the construction of new bridges, more than 150 years after Roebling's first major suspension bridge was constructed [3]. The main cables are the most critical components of a suspension bridge: not only do they support the loads from the roadway and transmit them to foundation structures, they are also non-redundant elements. In other words, loss of a main cable invariably leads to catastrophic collapse of the bridge structure.


Figure 1: The Menacing of the East River Bridge. By Matt Buchholz, 2013 [4]. Reproduced with permission of the artist.

During the 20th century, as design challenges posed by flood, snow, and wind loads for new structures were conquered one after the other, the primary concern of designers and bridge owners shifted from the mastery of bridge design to ensuring the safety of existing suspension bridges. Barring a sea monster attack (), the main perceived threat to the prolonged safety of existing bridges was posed by material deterioration. Since then, national and local government spending on the maintenance and repair on a global scale has exceeded the spending on the construction of new bridges [5]. While suspension bridges are equally as vulnerable as the other types of bridges to the damaging effects of time, they are far more costly to repair and maintain [6]. Moreover, suspension bridges are typically on major transportation routes where an interruption of service can have a paralyzing effect on the public.

Corrosion of bridge wires, which together comprise the main cable, is universally recognized as the primary cause of deterioration of such bridges. Corrosion is an extremely complex phenomenon that depends on a multitude of corrosion-inducing environmental effects. Due to the safety concerns as well as the tremendous costs associated with maintenance related work on suspension bridge main cables, it is crucial to understand how corrosion affects the strength of these cables along with the environmental conditions that drive the deterioration mechanisms.

Commencing during construction, periodic inspections serve a critical part in confirming the safety and longevity of a bridge. Findings from inspections provide bridge owners with the information necessary to make informed management decisions such as periodic maintenance, rehabilitation of deteriorated components, and even occasionally the replacement of major parts or the entire structure as deemed required. The current inspection procedure for suspension bridge main cables

relies on visual assessments of the wire conditions and laboratory testing of wire samples removed from the main cables [7]. As illustrated later in this chapter, the prevailing methods employed to evaluate the remaining strength of a cable rely on data collected from these inspections that is both limited and subjective in nature. Furthermore, current inspection guidelines fail to offer methods to estimate the deterioration in cable strength due to ongoing corrosion with time as the remaining cable strength can only be estimated at the time of the inspection. A recent direction in research laid out the groundwork to address the shortcomings of current inspection methodologies. In these studies, sensing systems were used to monitor environmental parameters such as temperature and relative humidity inside main cables to obtain information regarding the corrosive nature of the cables' internal environment. Sloane et al. [8] demonstrated that internal fluctuations inside a cable can be reliably monitored using sensors installed at various depths within the cable's cross-section.

The initial goal of this thesis is to further these exciting developments by introducing a corrosion rate model for bridge wires that relates the monitored environmental parameters within the main cable cross-section to the corrosion rate of an individual bridge wire. In previous studies, it has been shown that a number of environmental variables directly impact the rate of corrosion of bridge wires [9–12]. However, owing to the complicated nature of the corrosion process, models attempting to link the corrosion rate of a metal to environmental variables have generally been restricted to specific applications with a limited range of environmental parameters. This is further complicated by the wide range of environmental conditions to which bridge wires are exposed as illustrated by numerous bridge inspections conducted over the last few decades [13–15]. Nonetheless, machine learning methods using datasets that cover the appropriate range of inputs have been shown to be effective in modeling similar complex phenomena [16,17].

The long-term corrosion rate of metals can be described by the exponential expression

$$C(t) = At^n$$

where $A$ is the annual corrosion rate for a metal free of corrosion products, $t$ is the time in years and $n$ is an exponent dependent on the type of metal as well as the prevalent environmental conditions. The framework used in this thesis is a data-based approach using machine learning methods to develop a predictive model that estimates wire corrosion rates from measured environmental inputs. The following questions will be answered in an effort define this relationship:

a) Which environmental variables are most relevant to the prediction of wire corrosion rates?
b) Can the annual (short-term) corrosion rate of a bridge wire be predicted accurately from measured environmental variables?
c) Can the annual corrosion rate predictions be extended to the prediction of long-term wire corrosion rates according to exponential expression $C(t) = At^n$? What is the value of the exponential constant $n$?

Subsequently, the second goal of this thesis is to establish a methodology that allows bridge engineers to estimate the remaining strength of a main cable at any point in time using continually monitored environmental parameters. The proposed method integrates the long-term corrosion rate model developed in this thesis with state-of-the-art cable strength estimation methodologies currently employed by researchers and bridge consultants alike.

The remainder of this chapter provides necessary background information and expands on the issues associated with the current inspection and cable condition evaluation methodologies.

# Background

## Early History and Development

Primitive versions of suspension bridges—virtually unknown to the Western world until the 15th century—were frequent and essential links in mountainous regions of the world, such as the Himalayas and ancient China, as early as the third century B.C [2]. When conquistadors arrived in Peru, they had never witnessed anything akin to the spans of braided cables strewn throughout the region across expansive valleys and river gorges. Despite their strength, cables of these early bridges were fiber ropes made of natural vines and were easily damaged or deteriorated [2,18]. Today, these primitive bridges no longer see much use with the exception of a select few in Japan (e.g. Kazura Bridge in Tokushima Prefecture, rebuilt every two years [2]) and Peru (Queswachaca Bridge in Cuzco region, rebuilt every year).

The 16th century saw a number of rope suspension bridges with short service lives built in Western Europe for military applications. Wrought iron quickly replaced plant based fibers as the material of choice for cable construction due to its higher strength and longevity. Some of the earliest examples of bridges that used wrought iron chains as the main cables include an army bridge built across the Oder River in Prussia in 1734, and later, the Winch Bridge built in 1741 in Middleton, UK. In these early schemes, the bridge walkway was not separated from the cables: the pedestrians' path of travel followed the catenary curve of the main cables. As the need to carry horse-drawn carriages, cars, and trains across great expanses grew, the structural form of the suspension bridge evolved to

offer adequate stiffness to prevent excessive deflections attributed to heavier traffic as well as to provide a flat roadway separated from the catenary shape of the main cables. James Finley built the first iron chain suspension bridge that fit these criteria in Jacob's Creek, Pennsylvania in 1801 [2]. Finley listed the following features in the patent application for this type of bridge design:

- Installed anchorages and towers
- Separation of the main cables from the deck
- Suspended hangers extending from the main cables
- Attachment of the deck to the suspenders

Many consider the Jacob's Creek Bridge to be the beginning of the modern suspension bridge era [2,3]. Initially a great success, over the subsequent two decades approximately 40 additional bridges were built following Finley's patented design. However, the North American boom in suspension bridges was soon overshadowed by numerous bridge collapses within years of completion. In addition to the lack of consideration and understanding of wind and snow loading in bridge design, a principal culprit of these collapses was the failure of iron linked chain cables due to defects associated with the raw materials and fabrication of chains from iron rings. While the use of iron chains greatly prolonged the life of suspension bridges relative to those constructed using plant based ropes, this innovation fell short of providing the level of dependability required in one of the most critical types of transportation infrastructure. The Lehigh Gap Bridge built in 1826—the last of Finley's bridges—was the last iron chain cable bridge built in North America.

Despite the unfortunate fate of many of Finley's suspension bridges, his bridge concept gained wide recognition in Europe. Samuel Brown, a captain in the British Navy, invented the eyebar chain which proved the next significant improvement to the suspension bridge. An eyebar is a flat or

round bar with holes at either end and was forged from wrought iron at the time. Eyebar chain quickly gained acceptance in Britain due to their superior strength and fewer defects compared to linked chain cables. The Menai Suspension Bridge in Wales (176 m span), designed by the Scottish engineer and architect Thomas Telford and completed in 1826, is one of the earlier examples of the British eyebar chain suspension bridges. The sixteen wrought iron chains of the bridge each consisted of five rows of 187 eyebar links, each 2.4 m long, running side by side and linked by fishplates and bolts to make up a total of 935 total eyebar links per chain. While the original wrought iron chains were replaced with steel ones over the full length of the bridge in 1938 over concerns about metal fatigue and corrosion in the eyes of the chain links, the bridge stands to this day, albeit carries limited traffic. The Clifton Bridge, designed by Isambard Kingdom Brunel in 1864 had the longest span in the world—214 m—at the time of construction. Still in use today, the Clifton Bridge marked the end of the British eyebar chain bridge era.

The next major development in suspension bridge cables was the adoption of wire cable to replace the eyebar chain. The Seguin brothers observed the benefits of wire cable over eyebar chain as early as 1820s. Their main realization was that, unlike the eyebar chain where a defect in a single link of chain would endanger the safety of the cable, breakage of a few wires in the wire bundle comprising a cable would not result in an appreciable loss in overall cable strength. Their first suspension bridge built with wire cables in 1824, the Pont de Tournon over the Rhone River in France, was such a success that more than 200 suspension bridges were built in France between 1830 and 1850. The cables of these early French suspension bridges were manufactured off-site by stretching numerous parallel running wires to a predetermined sag between temporary structures that stand in for the actual bridge towers and bundling the wires into a prefabricated strand. Completed

parallel-wire strands were then transported to the bridge site for assembly. This procedure placed a constraint on the size of the manufactured strands that was governed by the capacity of the transportation and erection equipment.

A French engineer by the name of Louis-Joseph Vicat questioned the efficiency of manufacturing strands off-site. This led to his invention of the *aerial spinning* method in which cables are erected on-site. Even though, the aerial spinning method had clear advantages over prefabricating the strands at the time, the adoption was slow in France. It was not until a brilliant engineer in the United States transformed Vicat's concept into a modern method that to this day is considerered the basis of suspension bridge construction. John Roebling, in as early as 1841, described the modern bridge cable that is still widely used in this form over 175 years later as [19]:

> "The nature of my invention consists in the combination of any number of wires, laid parallel to each other, so that they form a round cylinder, and occupy the same position respectively for their entire length; all the wires to be uniformly strained in thus collecting them, and the whole to be wrapped with wire, either at intervals or throughout the whole length. The wrapping may be made of annealed wire, so as to form a close cover."

## Modern suspension bridge

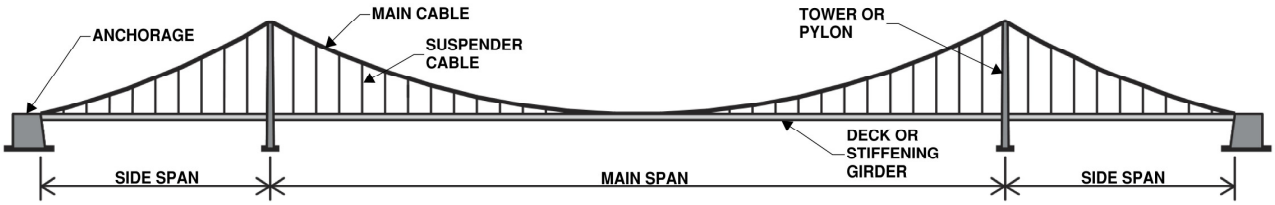


Figure 2: Structural components of a suspension bridge

In a suspension bridge the roadway is suspended from suspension cables. The five main structural components as shown in Figure 2 are:

1. Main Cables: Primary load-carrying members that support the entirety of the loads from the roadway—including the weight of the bridge deck, traffic, snow, wind, and ice loads—and transfer these loads to towers and anchorages at the ends.
2. Anchorages: structures—typically massive concrete blocks or rock—that carry the tensile forces from main cables at both ends. Gravity-type anchorages where the cable force is resisted by the self-weight of the anchorage block is the most common. In the less frequently used tunnel-type anchorages the cable force is resisted by friction between an anchor block and the surrounding bedrock. Anchoring main cables as a unit to the anchorage at a single position is challenging due to the large tensile forces in the cables. For this reason, the main cables are spread into strands, each consisting of 300-500 bridge wires, and anchored separately. Figure 3 shows this arrangement where individual strands are looped around a strand shoe which in turn is anchored to an anchorage block via anchor bolts.

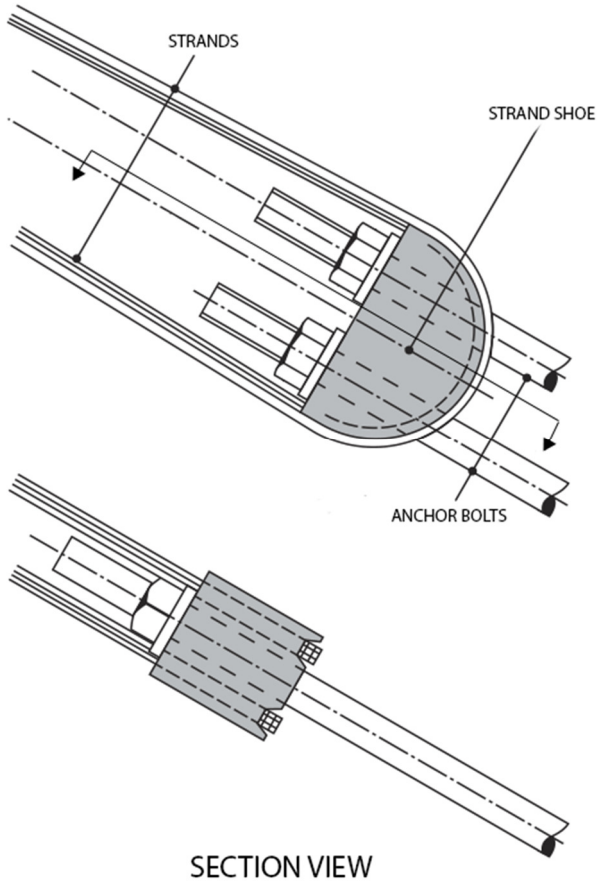


Figure 3: Strand shoe used for anchoring main cable strands into anchorage block

3. Towers or Pylons: Vertical structures that transmit vertical loads from main cables to the foundation elements. In almost all major suspension bridges, the main cables run over a *saddle* at the top of each tower. Some of the earlier bridges were built with roller type saddles that allowed some movement at the tower top to reduce bending forces imposed to the towers, whereas newer bridges utilize a fixed saddle (Figure 4).

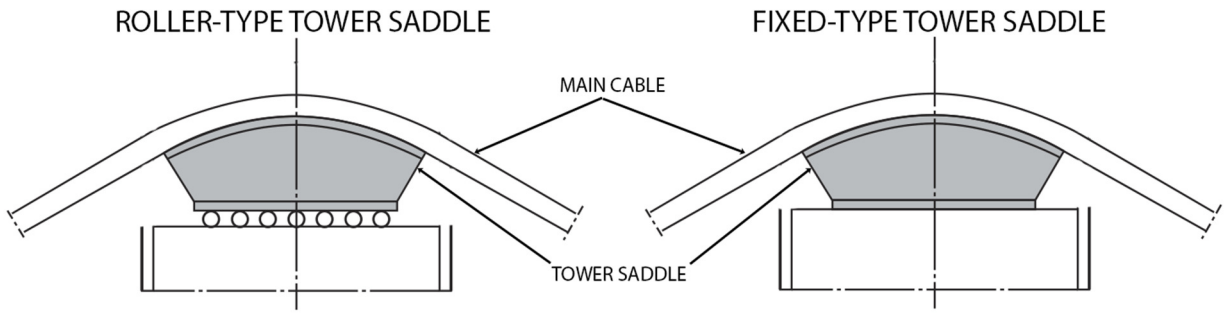


Figure 4: Connection between Main Cable and Tower

4. Suspender Cables: Smaller vertical cables that suspend the roadway from the main cables.
5. Deck or stiffening girder: longitudinal structures that support imposed live loads such as traffic and provide dynamic stability to the bridge.

Suspension bridges, by the inherent characteristic of their efficient structural form, lack a high degree of redundancy. The lower margin of error stemming from lack of redundancy was the main reason why failures were commonplace in the earlier days of suspension bridges. Over the course of the 19$^{th}$ and 20$^{th}$ centuries, bridge designers developed a comprehensive understanding of loading due to snow, flood, and wind on bridges and how to design for them. The advances in bridge design techniques and analysis were often achieved through investigating failures and learning from the underlying causes. Perhaps the most famous example of this advancement is the Tacoma Narrows Bridge. This bridge was constructed at a time where each consecutive bridge design furthered the boundaries of spans and slenderness. The Golden Gate Bridge had been completed only a few years before, and boasted an extreme slenderness of 1:168 in the depth-to-span ratio of its stiffening truss. The Tacoma Narrows Bridge, completed in 1940 with a deck constructed with plate girders had a depth-to-span ratio of only 1:350 [3]. Despite this extreme slenderness, the bridge had adequate factor of safety against live loads from traffic and static wind pressures. From the get go, the bridge

displayed considerable vertical oscillations in the wind. After only a few months in service, and following the breaking of a number of inclined tie cables—cables that tied down the bridge deck to the ground to reduce movement due to wind motions—due to wind motions, the oscillations started to take the form of torsional movements that became progressively more powerful. Eventually the suspender cables began to break, ultimately causing the collapse of the roadway. After this catastrophe, the field of aerodynamic stability became the main focus of bridge design research. The Tacoma Narrow Bridge failure influenced the design of the suspension bridges since the 1940s, including the strengthening of the Golden Gate Bridge. In the following two decades, the stiffening truss-type girders with large flexural and torsional rigidity dominated the design of suspension bridges in the United States. Starting with the Severn Bridge (opened 1966, UK), box girders with streamlined shapes and large torsional stiffness—to reduce the dynamic effects of wind—replaced the stiffened-girder type deck.

## Recognition of the Corrosion Threat

Ever since bridge designers mastered the effects of snow, floods, and wind, cable corrosion has become the primary concern for designers and bridge owners. The lack of redundancy in suspension bridges applies especially to the main cables: loss of a main cable invariably leads to the total collapse of the bridge. Numerous cases of cable failure have been seen since early 1900's leading to major repairs or complete cable replacement [20].

Two suspension bridges from France, the Tancarville Bridge over the Seine River (opened in 1959) and Pont d'Aquitaine over the Garonne River (opened in 1967), and the Moselle Bridge in Wehlen, Germany (opened in 1949) are examples of corrosion leading to costly replacement of main cables.

The Tancarville Bridge with its 608 m main span is one of the first large suspension bridges built in Europe, following an era until the 1950s during which most major suspension bridges were built in the United States. In the 1990s severe corrosion of the original non-galvanized helical strand cables was discovered and cables of the bridge had to be replaced between 1996-1999 [21]. Cable replacement of the Pont d'Aquitaine due to similar issues followed shortly after in 2002 [22]. Severe corrosion of the main cables of the Moselle Bridge necessitated a complete reconstruction of the superstructure, main cables and their anchorages, but retained the towers [6].

Another suspension bridge in Europe, the Forth Road Bridge in Scotland was completed in 1964, and at the time of completion had the fourth longest main span in the world. Significant corrosion within the main cables and many broken wires were observed during the first internal inspection in 2003 [23]. Following this discovery, repairs and preventive measures—such as fitting the entire length of the main cables with acoustic monitoring to detect further wire breaks and installation of a dehumidication system to keep wires dry—were taken. These safety measures came at a great expense: the dehumidification system installed in 2007 cost £8M and lasted two years. In 2009, a legislation was introduced to build a new bridge alongside the Forth Road Bridge to extend its lifespan by diverting the bulk of traffic to the new bridge—the Queensferry Crossing—scheduled to open towards the end of 2017 after many delays.

The United States has the greatest number of aging suspension bridges in the world and main cable deterioration due to corrosion has been well-known and documented [7]. Several cases can be readily listed to illustrate the extent of cost and burden caused by the corrosion of main cables. The General U.S. Grant Bridge was completed in 1927 and has long history of cable corrosion problems

[24]. Following the discovery of severe corrosion of the main cables during an inspection in 1939 and then another in 1978, the main cables were replaced twice during the lifetime of the bridge. In 1996, after having spent $9M following the second re-cabling to rehabilitate portions of the bridge, further rehabilitation was not found cost-effective and the bridge was permanently decommissioned in 2001. The main cables of the Waldo-Hancock Bridge (opened in 1931) in Maine were immediately strengthened by temporary supplemental cables when inspections performed in 1990s uncovered extensive deterioration of the main cables [21]. The bridge was retired in 2006 and replaced with a cable-stayed bridge. Broken wires found in the 1980s prompted major rehabilitation efforts on the main cables of the Bear Mountain, Mid-Hudson, and Williamsburg Bridges [7,13,24].

The extreme importance of suspension bridges as a part of transportation networks and the high economic burden of inspection, maintenance, and rehabilitation work on main cables necessitates developing a highly developed understanding of how corrosion affects these cables. Suspension bridges are similarly vulnerable to effects of time and need for upgrades as other types of bridges, but they are considerably more expensive to repair and renovate [5]. A multitude of factors—such as the design of the main cable, materials used, and the environmental conditions—all play important roles on the cable corrosion. Therefore, it is essential to develop a deeper understanding of the main cables and their building blocks—the bridge wire.

## The Main Cable

In modern suspension bridges, main cables are typically composed of hundreds of parallel bridge wires that are bundled and compacted into a round cable body. The *aerial spinning* method, originally developed by John A. Roebling in the 1800s [19] and vastly improved over the years, is still used today in the construction of main cables. In the most primitive version of the spinning method, a single bridge wire is pulled from one anchorage, up and over both towers (or pylons), and on to the other anchorage. The wire is then looped around the strand shoe and hauled back towards the other end. In current practice, multiple sets of wires—8 wires or greater—are simultaneously spun from both anchorages, travelling at around 1,500 ft/min (around 5 times the speed of Roebling's spinning wheel at the time). During the spinning operation, individual wires are combined into bundles called *strands*, which are then arranged into a hexagonal shape. Upon the completion of the final strand, the main cable is compacted by a traveling hydraulic press and tightly wrapped by an additional galvanized steel wire into the final circular form.

In recent years, the prefabricated parallel wire strand (PPWS) method that greatly reduces the construction time needed in the aerial spinning method has been introduced. In this method, prefabricated hexagonal strands composed typically of 61, 91, or 127 wires are drawn from one anchorage to the other and connected to the anchorage via sockets set at both ends of the strand. The PPWS method was used in the construction of the Akashi Kaikyo Bridge in Japan (opened in 1998)—the current record holder for the longest suspension bridge main span with a span of 1,991 m.

## Erection of the cable

During cable erection—using either one of the AS or PPWS methods—the hexagonal pattern of the strands is positioned in either vertical or horizontal orientation, as shown in Figure 5. Either pattern has been applied to main cables of various sizes. The George Washington Bridge (completed 1931) and the Verrazano Narrows Bridge (completed 1964) are two examples from New York City where the horizontal arrangement was used. Examples to the application of vertical arrangement are the Golden Gate Bridge (San Francisco, CA, opened 1937), the Forth Road Bridge (Scotland, opened 1964), and the Humber Bridge (Hull, England, opened 1981). The vertical arrangement is preferred in newer bridges since it allows the use of vertical spacers between each row of strands in order to position the strand at the correct location within the main cable with ease.

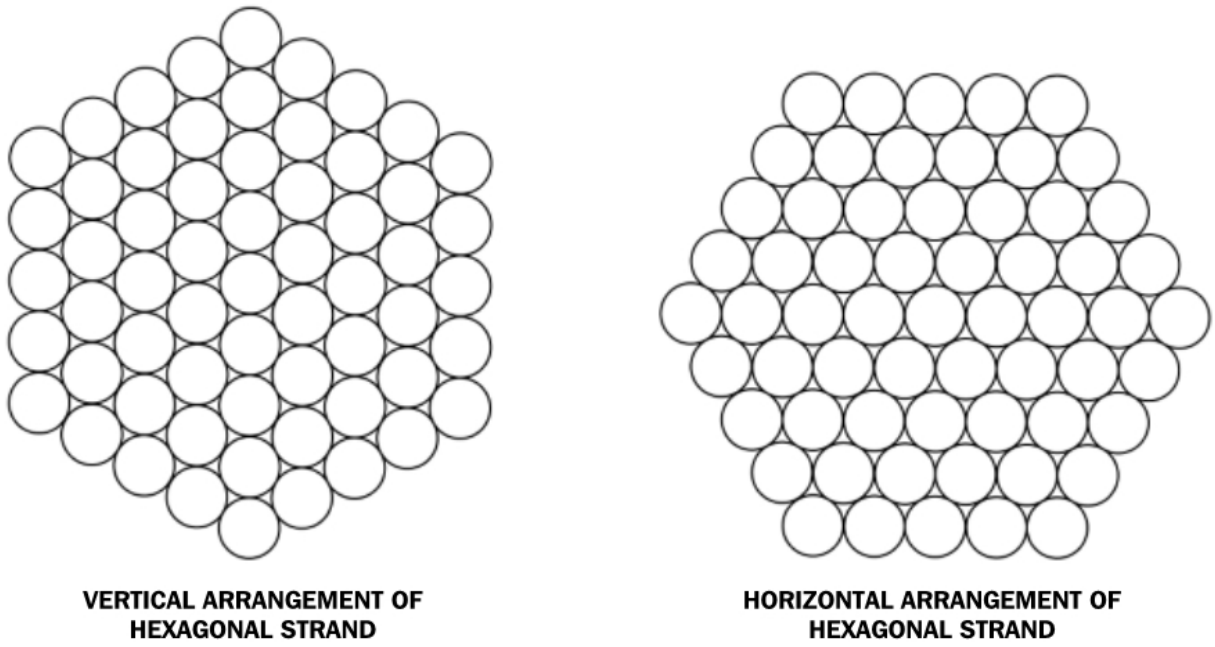


Figure 5: Hexagonal arrangement of bridge wires within a strand

Following the compaction of bridge wires or PPWS, *cable bands* that connect the main cable and the suspender ropes are installed along the main cable at a specific spacing. Cable bands typically consist of two vertically split semi-circular halves and clamp the main cable with high-strength bolts (Figure 6). Generally, vertical grooves at the exterior faces of the cable band are provided to guide the suspension ropes (Figure 7). Depending on the inclination of the cable at each cable clamp, the friction required to prevent the slip of the cable band varies—the highest friction force is required near the tops of the towers where the steepest slope of the main cable occurs. For this reason, cable bands near the mid-span where the cable is nearly horizontal are clamped with smaller number of bolts compared to near bands near the tower tops. In European bridges and most of the newer suspension bridges built after the turn of the century, the traditional looping of the suspender ropes over the cable clamp has been substituted with connections between vertical gussets provided at the cable band to clevises provided at the end of each suspender rope. Figure 8 shows the application of this system on the Akashi Kaikyo Bridge.

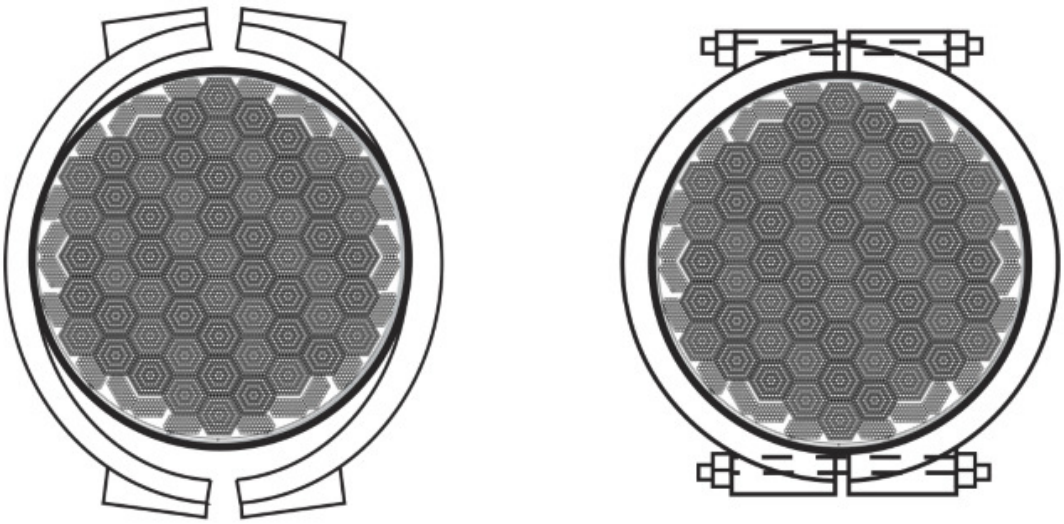

Figure 6: Section view - two-part, vertically split cable band

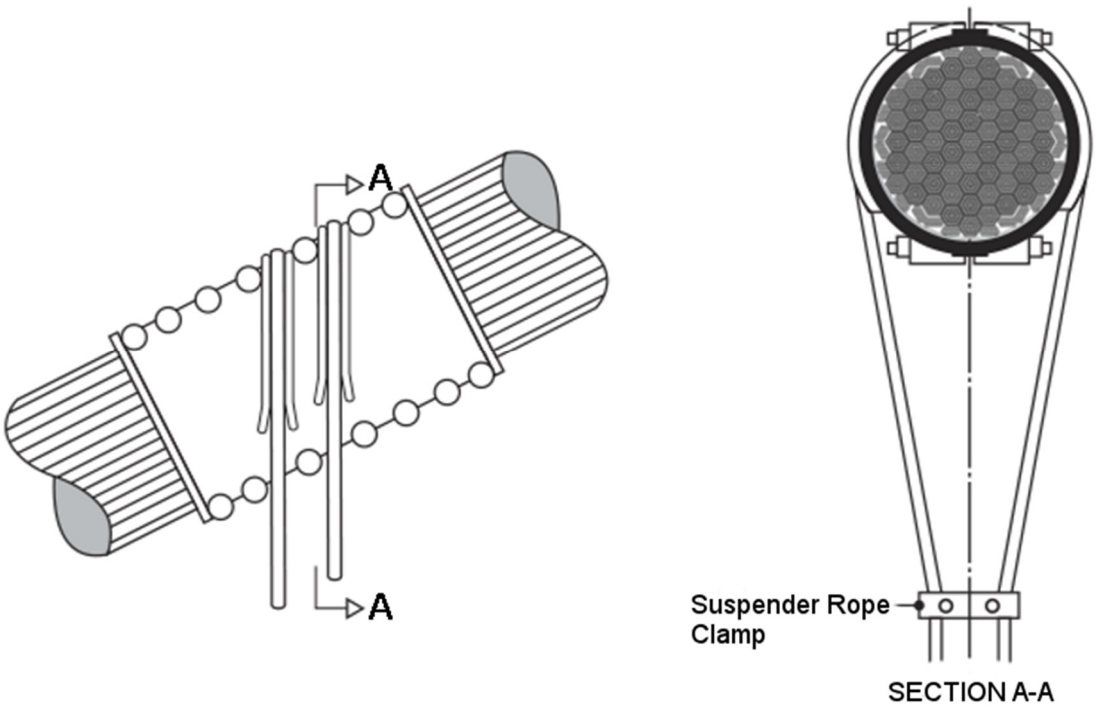


Figure 7: Left: Elevation - grooves on exterior face of cable band shown. Right: Section at the cable band. Suspender ropes looped around the clamp shown. Hanger clamps below the main cable may be provided to reduce the space between suspender ropes, as shown.

In most suspension bridges built after the 19th century, suspender and cable band spacing is between 6 to 18 m (20 to 60 ft), the trend following longer spacing for newer bridges. Suspenders of the Williamsburg Bridge (completed 1903) in New York City are spaced 6.1 m (20 ft) apart, whereas the Akashi Kaikyo Bridge has its suspenders spaced at 14.2 m (46.6 ft).

Following the installation of the cable bands, the main cable is wrapped between the cable bands with a galvanized wire. This wire used in this wrapping has traditionally been a galvanized wire of around 3.5 mm. In more recent bridges, Z-shaped wires that provide a better seal have replaced the round wrapping wires.

Figure 8: Akashi Kaikyo Bridge cable clamp

## The Bridge Wire

Wires used in cable supported bridges are called *bridge wire* and made from carbon steel. Typically, bridge wires used in suspension bridge main cables are 4.5-5.5 mm in diameter whereas wires of diameter up to 7 mm are used in the strands of cable-stayed bridges. In the United States, most suspension bridges constructed in the 1900s were built with wires with a nominal diameter of 4.88 mm before the application of galvanization [3,24].

The production of wire starts from raw materials in the form of steel billets. Steel mills produce steel rods of approximately 7-10 mm through hot rolling processes. The wires exhibit a fine-grained microstructure after heat treatment and quenching operations, a process commonly called *patenting*. The steel rods are then delivered from the steel mill to the wire manufacturer's plant and surface treated to remove any rust and scales from the surface. The steel rods are then fed to drawing (cold-working) machines and drawn through dies of decreasing diameter in about 3-4 passes to achieve the desired diameter, mechanical strength, and toughness [21,24,25]. The final microstructure following the cold-working operation is a fine-grained pearlite. After the drawing, wires are annealed, pickled to remove surface impurities. At this stage, most bridge wires are hot-dip galvanized or electroplated with zinc for corrosion protection.

Finally, wires are coiled on to reels that contain up to 100 km of continuous spliced wire, and transported to the construction site to be spun on the bridge. Some of the newer bridges are constructed with prefabricated strands where individual wires are bundled into hexagonal shaped strands following the galvanization process and coiled onto reels.

Chemical composition of the bridge wire is similar to common carbon steels. Alloying elements such as Si, Mn, Cu, Ni, and Cr are present in low quantities; therefore, bridge wires can be classified as low-alloy steels [24,26]. Carbon content is higher than structural steels to achieve higher yield and ultimate tensile strength. One disadvantage of achieving higher strength through cold-working is the loss of ductility such that the breaking strain is only around one-fifth of structural steel [21,24]. Table 1 shows the typical mechanical properties and chemical composition of bridge wires.

Table 1: Typical properties of bridge wire [3,6,21,24,25]

| Property | | Conventional Bridge Wire (4-7 mm wires) | Unit |
|---|---|---|---|
| Minimum Yield stress | | 1100-1300 | MPa |
| Ultimate Tensile Strength | | 1500-2000 | MPa |
| Minimum Strain at Breaking | | 4 | % |
| Modulus of Elasticity | | 205 | GPa |
| Typical Chemical Composition | | | |
| | C | 0.75-0.85 | % |
| | Mn | 0.55-0.75 | % |
| | Si | 0.15-0.3 | % |
| | P | 0.03 (0.04 maximum) | % |
| | Cu | 0.05 | % |
| | Ni | 0.05 | % |
| | Cr | 0.05 | % |
| | S | 0.02 (0.04 maximum) | % |

Over the years, advances in production techniques and refinements in the chemical composition continually improved the tensile strength of bridge wires. 1,600 MPa was the prevailing minimum tensile strength until the end of 1900s [3]. Mayrbaurl reported tensile strengths varying between 1,644 to 1,695 MPa for wires from three suspension bridges [27]. In the 2000s, wires with a guaranteed minimum tensile strength of 1,800 MPa have become readily available from a number of suppliers and wires with a minimum tensile over 1,960 MPa have been produced [28]. The Akashi Kaikyo Bridge in Japan, completed 1998 and the current record holder for the greatest main span in the world with a span of 1,991 m, was constructed using wires with a guaranteed minimum tensile strength of 1,800 MPa.

Galvanization requirements for bridge wires are specified for each specific bridge. ASTM A586 [29], the standard for zinc-coated structural strands, is taken as a general guideline for bridge wires.

ASTM A586 lists three weight classes of galvanized coatings that are designated as Class A (300 g/m$^2$), Class B (600 g/m$^2$), and Class C (900 g/m$^2$). With some exceptions, most long-span suspension cable bridges consist of wires protected by Class A coating. Wires are almost universally produced as a steel core of 4.9 mm in diameter and then galvanized with Class A coating produce a finished diameter of 5.0 mm.

Williamsburg Bridge in New York City is a notable exception to the galvanization usage. The designers of the famous bridge opted against the use of galvanized wires and instead used a protective coating of slushing compound mixed with graphite to act as a lubricant.

## Corrosion of Bridge Wire

### Corrosion Mechanisms

Deterioration of bridge wires is caused by corrosion. Bridge wires corrode when they come in contact with moisture. For the galvanized bridge wire, zinc coating at the outer surface will undergo corrosion first, protecting the steel wire until the zinc coating is consumed. Zinc oxidizes to zinc oxide (ZnO), a white powdery compound that is insoluble in water. In the presence of moisture, ZnO reacts with dissolved atmospheric carbon dioxide and sulfur dioxide to form various passivating layers such as zinc carbonate ($ZnCO_3$), zinc hydroxide ($Zn(OH)_2$), and zinc sulfate ($ZnSO_4$) [7,30]. As corrosion continues, each zinc compound generally increases in quantity and may transform into other compounds depending on the environmental factors [31]. In clean atmospheric environments $ZnCO_3$ is typically found to be the dominant compound and forms a

compact film that dissolves very slowly and prevents permeation of oxygen and water, essentially slowing down corrosion processes. On the other hand, $ZnSO_4$ is highly soluble and erodes from the metal surface easily—causing faster depletion of the zinc coating.

Following the depletion of the zinc coating, corrosion of the steel bridge wire commences at the surface. The corrosion rate of a bridge wire depends on its chemical properties and the environmental conditions that it is subjected to. There are two main types of corrosion associated with bridge wires: (i) uniform or atmospheric corrosion; (ii) pitting corrosion [7,15,20,24].

Uniform corrosion is the most common form of corrosion and is responsible for the largest material lost from a wire by volume. Surface area of a wire exposed to a corrosive environment is converted into an oxide layer through electrochemical reactions, resulting in a loss of metal area. The corrosion by-product formed on the wire surface consists of a reddish brown colored hydrous ferrous oxide ($Fe_2O_3$), commonly known as rust. Many factors affect when corrosion processes occur: rainfall, humidity, air movement, and temperature control the period in which a wire is exposed to moisture. pH, chlorides, and atmospheric pollutants such as $SO_2$, $SO_3$, $H_2S$, $NH_3$, $NO_2$, and $NO_3$ all play a role as corrodants [24,32,33]. Thermal gradients during the day and throughout the year lead to various levels of condensation on the wires, creating alternating wet/dry cycles. Condensation rates are especially high at the outer portions of the cable due to direct exposure to sunlight and the elements. As a result, wires near the cable exterior typically experience higher uniform corrosion rates compared to interior wires [24]. Rate of uniform corrosion is generally reported in terms of corrosion depth per year such as mm/yr or μm/yr.

Localized corrosion types include crevice corrosion, galvanic corrosion, intergranular corrosion, dealloying, stress corrosion cracking, and hydrogen-induced cracking [24,32,34,35]. Among these,

the most common is pitting corrosion. In pitting corrosion, corrosion occurs at a greater rate at a localized region where metal loss is concentrated at this limited area, creating pits on the surface. Pitting will occur where localized damage creates unprotected regions within protective coatings. Notches in wire galvanization is an example of such a defect. Formation of pits is difficult to predict and can lead to sudden and brittle failure of a bridge wire. Depth of pitting can be expressed in terms of a *pitting factor*—the ratio of the greatest metal penetration depth due to pitting to the average penetration due to uniform corrosion [32]. A pitting factor close to unity would indicate corrosion attack on the metal is uniform.

*Stress Corrosion Cracking* (SCC) occurs when a metal is exposed to a corrosive environment while simultaneously stressed due to tensile forces. SCC failures tend to be brittle and commonly accompanied by a reduction in ultimate elongation of the wire. *Hydrogen-induced cracking* is a similar mode of failure where cracking is caused by hydrogen atoms penetrating a metal at the grain boundaries through a corrosion reaction or cathodic polarization. Steels containing interstitial hydrogen do not always display visible damage but lose their ductility in most cases; a phenomenon known as hydrogen embrittlement. Hydrogen-induced cracking usually occurs only when the steel is subjected to high applied or residual tensile stress—a condition characteristically met for bridge wires.

## Corrosion Rate of Bridge Wires

Throughout their lives, bridge wires are exposed to varying environmental conditions such as temperature and moisture fluctuations. With regard to the corrosion rate of metals, the most important environmental variables are temperature, pH (acidity), ion/contaminant concentration, humidity and extended periods of wetness [32,36]. Analysis of inspection reports on suspension bridges in the New York City area concluded that water penetration into the interior of the cable is a common occurance and pH values as low as 4 was observed [13,14]. Eiselstein and Caligiuri's [15] study revealed that the wires comprising the main cables of the Williamsburg Bridge in New York City remained damp for more than 135 days of the year and exposed to water that contained significant concentrations of contaminants. Throughout the year, moist air and rainwater penetrate into the cable due to imperfections in the protective cover, poor compaction of the wires, cracks in the caulking at cable bands, and puncture of the elastomeric barrier near the tower saddle [24]. Furuya et al. [11] reported water accumulation inside the main cables of suspension bridges in Japan, within only ten years of service.

Suzumura and Nakamura [12] studied the internal environment of the main cable under ambient conditions and showed that the relative humidity (RH) varies significantly across the cross section of the cable throughout the day. Sloane et al. [8] studied the variability of temperature (T) and relative humidity (RH) using a full-size mock-up cable specimen enclosed in an environmental chamber and instrumented with RH and T sensors: their measurements showed elevated RH levels near the surface, whereas the center of the cable stayed at much lower levels. Additionally, while the temperature at the outer regions of the cable cross section fluctuated in sync with the applied

external temperature, the temperature at the center lagged behind and showed monotonic changes. In a similar study, Furuya et al. [11] instrumented a 650 mm diameter cable model with thermometers and reported that while the temperature at the center and the lower parts of the cable section showed small fluctuations, the temperature at the cable's sides and upper portion closely followed the trend of the external temperature variation.

In summary, the environmental conditions each bridge wire experiences depend not only on the geographic location of the bridge itself but also on the location of the wire within the cable cross-section and along the length of the cable. This variability of environmental conditions could be the leading reason why wires removed from the same cable display vastly differing levels of deterioration.

In their pioneering study on the corrosion of bridge wires, Eiselstein and Caligiuri [15] simulated field conditions by cyclic testing wires from the Williamsburg Bridge using synthetic acid rain. The results of the accelerated corrosion tests indicated that corrosion progresses linearly with the number of testing cycles. Eiselstein and Caligiuri estimated that each of their wet/dry cycles is equivalent to a range of [1-2.7] days of outdoor exposure in New York City. They estimated the current corrosion rate for Williamsburg Bridge wires to be between 15.2 and 63.5 μm/year of metal penetration.

Past studies on bridge wires confirm the dependence of corrosion rate on environmental variables. Betti et al. carried out extensive cyclic corrosion tests on bridge wires subjected to corrosive environments [9,10,37]. Their results indicate that decreasing pH level and increasing chloride ion

concentration of the solution used in cyclic testing both lead to higher corrosion rates. Suzumura et al. published numerous papers on bridge wire corrosion, in summary revealing that: (i) corrosion is unlikely to occur when relative humidity is below 60%, unless high concentrations of chlorides are present; (ii) corrosion rate is constant under unchanging environmental conditions; (iii) corrosion rate increases exponentially with temperature based on tests carried out at 0, 10, 20 and 40˚C [11,12,38,39].

Significant effort has gone into establishing analytical models for the prediction of corrosion rate of metals as a function of environmental variables. However, due to the complexity and the nonlinear nature of the underlying physicochemical phenomena, the models developed have been shown to be restricted to specific geographical regions and limited in capturing the nonlinear nature of the corrosion process. In corrosion science, the time-dependent corrosion of metals is often described by the simple exponential expression:

$$C(t) = At^n$$

where *C(t)* – cumulative corrosion loss (in terms of thickness or section loss) after *t* years, *A* – annual corrosion rate for a metal, *n* – exponent which depends on the type of metal and surrounding environment, typically in the range [0-1]. Values of *n* for steel in urban-industrial atmospheres are in the range [0.25-0.59] [40,41].

## Methods of Preventing Corrosion

Main cables of suspension bridges are protected from corrosion by multiple levels of protection:

- The first line of defense is the paint systems and coatings applied to the main cable to provide a barrier against water infiltration into the cable. Generally, the coating is an elastomeric acrylic type that resists rust and moisture while retaining its flexibility.
- Underneath the coating, the cable is wrapped with wires or other materials. This wrapping has traditionally been a soft, annealed galvanized round wire, circumferentially wrapped around the cable under tension. The round wires have been replaced with interlocking S-shaped wires that create a more water-tight wrapping in the late 1900s [21]. In recent bridges, the wire wrapping is supplemented or replaced with neoprene, plastic, and other wrapping materials.
- At the next level, the compacted cable inside the wrapping is usually covered with a protective lead or zinc paste as a sealant and corrosion protection. The voids between wires are filled with synthetic and natural corrosion inhibitors such as linseed oil and non-petroleum based oils to prevent or slow down corrosion within the main cable. Typically, oil is introduced at the highest point of the cables, the tower saddles, with the expectation that it will flow down the cable and surround as much of the surface area of wires as possible. Oiling tends to introduce its own complications: oil leakage and bulging of the cable wrapping at the lower portions of the cable have been observed at numerous occasions [7,21]. The effectiveness of oiling has been a constant question and in recent years bridge owners have veered away from performing oiling operations.

- Galvanization of bridge wires serves as the final layer of protection.

An important step in recent years to improve corrosion protection of suspension bridge main cables is the emergence of cable dehumidification as a mitigation strategy for new and existing suspension bridges [21,23,42,43]. Dehumidification involves over-wrapping the cable into an air-tight enclosure and driving dried-air through the cable to remove built-up moisture and maintain a dry environment. It is not yet possible to state definitively that dehumidification will prevent future corrosion and strength loss and whether this strategy can be implemented as a standalone solution or as part of a hybrid strategy to achieve the necessary level of protection.

Findings from inspections discussed in the previous section point to the fact that the traditional main cable protection system consisting of wrapping wire and paste, followed by an over-coating of paint does not manage to keep moisture out of the cable nor provide adequate corrosion protection.

## Main Cable Inspections

In recent years, inspections of main cables of suspension bridges have uncovered extensive corrosion of high-strength steel bridge wires. The failure of the eyebar chain cable of the Silver Bridge—a suspension bridge opened in 1928 that connected Ohio to West Virginia over the Ohio River—in 1967 led to the development of the current bridge inspection standards in both the United States and the rest of the world [21]. At present, NCHRP Report 534 published in 2004 [7] on the inspection and strength evaluation of suspension bridge cables and the accompanying primer published in 2012 [44] are widely accepted as the industry standard [3,21]. The Bridge Inspection

Manual (BIM) [45] published by the New York State Department of Transportation (NYSDOT) and the Bridge Inspector's Reference Manual (BIRM) [46] are two other publications that provide guidelines for inspection of suspension bridges in the United States.

The NCHRP guidelines recommend three levels of inspection: (i) periodic visual inspections; (ii) biennial "hands-on" inspections; (iii) internal inspections.

i. Periodic visual inspections focus on the external appearance of the cable and monitor any visible damage to the paint or cable wrapping, and caulking. During these inspections, entire length of the underside of the cable is inspected by binoculars. Cable is examined for any evidence of water penetration such as water dripping from the wrapping wire and from the weep holes in cable band grooves.

ii. Biennial inspections require hands-on inspection of the paint, caulking, wire wrapping, and underneath the cable and cable bands. If the biennial inspection uncovers conditions pointing to the presence of internal corrosion, the cable is inspected internally in that location in the near future.

iii. Internal inspections are performed to determine the cable's condition and strength. The NCHRP guidelines suggest conducting internal inspections in 30-year intervals and reducing the recommended interval to as little as five years if substantial wire corrosion is uncovered. In most inspections, a minimum of three panels—section of cable between consecutive cable bands—along the main cable are selected for inspection: one each at the low point of the main span and one of the side spans, and one at about midway between the tower top and low point of either the main span or the side span. During the

internal inspection selected panels of the cable are unwrapped and the cable is wedged at a number of radial positions. Wires visible during the wedging operation are visually inspected and assigned corrosion stages based on the level of corrosion observed. Following the visual inspection, recommended number of sample wires assigned to each corrosion stage are cut and removed for laboratory testing of wire properties. A new wire is spliced to the cut ends of each wire sample to restore continuity.

The four corrosion stages or grades assigned to wires during the internal inspections were developed by Hopwood and Havens [47] and adopted by the NCHRP inspection guidelines [7]. These corrosion stages shown in Figure 9 are defined as:

Stage 1—spots of zinc oxidation on the wires;

Stage 2—zinc oxidation on the entire wire surface;

Stage 3—spots of brown rust covering up to 30% of the surface of a 3-inch to 6-inch length of wire;

Stage 4—brown rust covering more than 30% of the surface of a 3-inch to 6-inch length of wire.


Figure 9: Corrosion stages developed by Hopwood and Havens

## Cable Strength Estimation

Assessing the safety of suspension bridges relies on determining the remaining strength of bridge cables in their deteriorated state. The degree of deterioration of bridge wires from the same main cable has been found to vary considerably [13,24,48]. Wires in practically new condition were observed alongside heavily corroded ones within the same cable cross-section. As wire corrosion is a highly complex process that depends on many environmental factors, it is very challenging to determine the deteriorated strength of specific wires. Owing to the limited number of sample wires that can be removed from the main cable for testing, the most prevalent strength estimation methods of main cables rely on probabilistic methodologies. In these methodologies, various types of extreme value distributions and random variable based Monte Carlo simulation techniques are applied to data obtained from the testing of sample wires removed during internal inspections. The standard procedure to obtain the cable strength following the removal of wire samples consists of: (i) cutting the wires in unit-length segments (typically one foot length); (ii) testing each unit-length segment for ultimate tensile strength; (iii) estimating probability distribution of the strength of unit-length segments; (iv) calculating the strength of a wire of *prescribed length* based on the probability distribution of the strength of the unit-length segments; (v) calculating the strength of the entire cable cross-section comprised of a known number of wires.

The term *prescribed length* used in Step (iv) is called the clamping or development length and usually denotes a length of wire that corresponds to a few cable band spacings. Over this length, a broken wire can recover its load-carrying capacity due to friction forces between wires caused by cable clamping and wrapping; however, defining the clamping length is not a trivial task due to

variations in cable compaction, different inclination of the cable at each cable bands, and variations in wrapping wire tension [21]. If a wire of this prescribed length is comprised of *n* unit-length segments, its strength is determined as the minimum strength value amongst the *n* unit-length segments—the unit-length segment with the lowest strength being the weakest link. The report on the safety of the Williamsburg Bridge prepared by Steinman et al. [48] quantified a clamping length of 60 ft, corresponding to the length of two panel lengths or distance covered by three consecutive cable bands. This length has since been used in numerous studies within the industry and academia [49–52]. Recently, Waisman et al. published extensively on quantifying the development length of parallel wire cables [53,54]. Their findings suggest that the development length can be considerably less than the commonly used three cable band spacing.

Step (v) requires a means of calculating the entire cable strength from the calculated strengths of individual wires. NCHRP guidelines [7] recommend three strength models developed by Perry [55] for this purpose: (i) Ductile-Wire Model; (ii) Brittle-Wire Model; (iii) Brittle-Ductile Model.

(i) Ductile-Wire Model: In this model, the assumption is that the wires making up the cable cross-section share in the cable force until all of the wires break simultaneously and the entire cable breaks as a single unit. In order for this to happen, the wires need not have equal strength but they must be: (1) ductile; and (2) elongate elastically and then plastically to the same degree. The cable strength is the summation of individual wire strengths.

(ii) Brittle-Wire (Limited Ductility) Model: In this model, an individual wire may fail when the strain or the stress in the wire reaches a certain level and that wire ceases to share the

cable force. Each wire in the cable can only elongate up to that specific wire's ultimate strain. For a specific strain value, each intact wire is carrying a tensile force that corresponds to strain in that wire's stress-strain diagram. When a wire fails, the force carried by that wire is distributed to all the remaining unbroken wires in the cable, proportionally to each wire based on the respective force carried by each before the wire failed. The cable strength is determined by increasing the cable strain incrementally and calculating the number of wires reaching their elongation limit at each step. The cable force is calculated as the total force carried by the intact wires at each strain level. At a certain strain wires start failing faster than the cable force increases: this maximum force attained is the cable strength.

(iii) Brittle-Ductile Model: This model considers the wires that fail at very low strains and discounts them from the total number of wires making up the cable. The remaining intact wires are assumed to be ductile and the cable calculation is the same as for the Ductile Model, except the reduction in the number of contributing wires.

## Challenges in Cable Inspections and Strength Estimation

Currently, agencies in the United States responsible for suspension bridge maintenance are required to follow inspection plans mandated by the National Bridge Inspection Standards that provide limited information regarding the status of bridge wires. These plans require inspections typically on a biennial basis, involving only a visual inspection of the protective covering or coating [44]. If such inspections reveal signs of potential deterioration in the interior of the cable, "in-depth" inspections are then performed to inspect within the cable cross-section. These inspections,

however, are performed only at a few selected locations at the bridge owner's discretion and provided the maintenance budget allows for such an expenditure.

Internal cable inspections are very costly undertakings. The recent internal inspection of the Forth Road Bridge (Scotland, completed 1964) in 2012 cost the bridge authority over $4M—even after cost reducing adjustments such as reducing the number of panels inspected were made to the initially proposed scope of work. One of the main challenges of working on suspension bridge cables is that the cables are typically directly above the vehicular and pedestrian traffic. Unless the bridge is closed to traffic during inspections, the public faces increased health and safety risks. In order to reduce these risks, at a minimum, the roadway immediately below the main cable being accessed is closed. To be able to perform the inspection work, access platforms need to be provided hundreds of feet up in the air. Access to internal wires requires removing the cable's external covering that frequently contains red lead paste. As the red lead paste ages, it becomes brittle and friable and needs to be contained and safely disposed to eliminate environmental and health hazards.

Following visual inspections, laboratory tests are performed on the limited number of wires removed during the inspection to determine wire properties. Even in the most thorough inspection projects, the ratio of bridge wires extracted for testing to the total number of wires that make up the cable remain very small. Furthermore, the removed sample wires are of limited length and much shorter than the overall length of the main cable. The variation in the degree of wire deterioration within the cable cross-section—coupled with the impracticability of testing a significant percentage of the wires in the cable's cross-section—creates a great challenge in estimating the remaining

strength of main cables. Cable strength evaluation relies on tensile test data from a limited number of wires removed and the visual gradation of wires into various stages of corrosion [7]. Visual assessment hinges on the inspector's ability to assign the appropriate corrosion stage based on a set of qualitative criteria. Distinguishing between stage 3 and 4 wires is a difficult task for even the most experienced inspectors and can have a considerable impact on the estimated cable strength. As a result, the current methods involve considerable uncertainty as the information extracted during inspections does not reflect the condition of the entire cable and rely on subjective visual classification of wires.

As previously noted, NCHRP guidelines for inspection of suspension bridges recommends a 30-year interval for internal inspections [7]. Since data is not available between inspections, the current inspection methodologies offer a snapshot of the condition of the cable only at the time of the inspection and merely at the few selected locations that happen to exhibit external indications of deterioration. Furthermore, a means of estimating the declining cable strength due to ongoing corrosion is not provided. In short, the current inspection and evaluation methods fail to provide adequate and sufficiently reliable data for the assessment of cable strength (and safety) and its evolution with time.

In order to address the shortcomings of the present inspection methods, recent studies have investigated the use of indirect sensing technologies where a network of sensors installed within the cable cross-section continually monitor environmental variables related to the corrosion of bridge wires, such as temperature and relative humidity [8,56]. Sloane et al. [8] demonstrated the feasibility of a monitoring system installed on a suspension bridge by instrumenting a 1:1 scale

replica of a suspension bridge main cable. The mock-up cable was 6.1 m long—representative of the distance between two adjacent vertical suspenders—and comprised of 9,271 wires. Temperature and relative humidity sensors were installed at various locations across the cross-section to continuously monitor these parameters during testing. An environmental chamber was constructed to expose the mock-up cable to a variety of cyclic environmental conditions, consisting of rain, heat, and cooling. The constructed sensor network was able to measure the fluctuations of the temperature and relative humidity at various depths within the cable. A natural progression from this study is the development of a method to include environmental sensor data in the estimation of the remaining strength of the main cables—the main goal of this thesis.

## Thesis Structure

The thesis is structured as follows:

**Chapter 2** explores the effect of environmental variables on the corrosion rate of bridge wires and a means to assess wire deterioration through an Indirect Sensing Method. In this exploration, cyclic corrosion tests are performed at varying levels of selected environmental variables to validate the expected corrosion behavior of bridge wires. In addition, the measured data establishes additional points for the data-driven corrosion model developed in the following chapters. Linear Polarization Resistance (LPR) sensors are tested in the same cyclic environment to evaluate their performance in realistic conditions.

**Chapter 3** develops a data-based corrosion rate model for bridge wires that forms the crux of this thesis. As a first step, a corrosion database is compiled and used to select the most relevant environmental variables in predicting the corrosion rate of bridge wires. Once this selection has been made, a model for the prediction of the annual (short-term) corrosion of bridge wires is developed using a larger database.

**Chapter 4** extends the previous chapter's work to the long-term corrosion of bridge wires. This long-term corrosion model is then applied to the estimation of the remaining strength of suspension bridge main cables subjected to changing environmental conditions.

**Chapter 5** is devoted to the conclusions and recommendations for future research.

# CHAPTER 2. CORROSION RATE OF BRIDGE WIRES – EXPERIMENTAL TESTING

## Introduction

Environmental variables such as temperature, relative humidity, pH, and chloride content within the cable are the controlling agents for the corrosion rate of bridge wires. These factors need to be related to the corrosion rate of the wires subjected to them. Extensive testing on carbon steel has been done by many researchers over the past few decades [57–73]. Data collected from these studies were used to develop numerical or categorical corrosion rate expressions, generally through regression analyses. However, very few studies have focused their attention on high-strength carbon steel wires used in suspension bridges. In-depth inspection of the main cables of the Williamsburg Bridge during the 80's revealed significant corrosion of the wires [18]. In the last two decades, numerous corrosion studies on bridge wires were carried out by a research team at Columbia University [19-23], and a group of researchers in Japan [24-27]. This chapter investigates the impact of various environmental variables on the corrosion rate of bridge wires through experimental procedures. The corrosion data compiled from the studies presented here will be used in Chapter 3 in the development of a corrosion model that links environmental parameters to wire corrosion rate.

Cyclic corrosion tests were developed in 1960's and 1970's to test industrial maintenance coatings [2, 3]. Cyclic corrosion tests expose specimens to a series of different environments in a repetitive cycle.

This cyclic approach enables simulating environments that naturally oscillate due to atmospheric conditions. Cyclic corrosion testing has been shown to be a more realistic way of evaluating corrosion performance compared to traditional, steady state exposures [4]. Relative corrosion rates, corrosion structure and morphology observed in cyclic corrosion tests are excellent predictors of corrosion performance in real service environments. This has been particularly shown for zinc and steel corrosion [5, 6].

Cyclic cabinet testing simulates the changing outdoor environment such as corrosive ions, temperature and humidity [7]. Most previous studies performed on the corrosion testing of suspension cable bridges had employed a version of cyclic testing. Eiselstein and Caligiuri [8] used an immersion-dry cycle to estimate the rate of corrosion-induced damage. Their corrosive solution was prepared to match the chemical composition of "acid rain" that was collected from the Williamsburg Bridge in New York City. Betti and Vermaas et al. [7, 9-12] used solutions of higher acidity and salinity, applied as fog sprays in order to further increase the corrosion rate. Suzumura et al. [13-16] employed wet-dry cycles by wetting gauzes wrapped around bridge wires through periodic water sprays. Instead of preparing saline solutions, a method of depositing salt particles on the surface of test specimens prior to cyclic testing was selected.

In this study, an array of solutions ranging from mild to high corrosiveness were used as fog sprays. Cyclic tests were also run at different temperatures to investigate the impact of temperature on the corrosion rate.

## Cyclic Corrosion Experiments

Cyclic corrosion tests conducted in this study employed an array of solutions, ranging from mildly to highly corrosive, as fog sprays in a corrosion chamber to create environments at different levels of the selected environmental variables. The corrosion cycle used in this study is similar to the Cyclic Acidified Salt Fog Test A2 outlined in ASTM specification G85-02 [74]. The 3 hour, three-step cycle consisted of (i) 10 min of salt fog; (ii) 120 min of high humidity; (iii) 50 min of low humidity. A total of 18 tests consisting of 48 cycles were performed using, in each test, 10 samples of 254 mm long wire segments 4.88 mm in diameter. Chloride content and pH of fog solutions were varied, along with the temperature at which each test was run to investigate the impact of such variables on the corrosion rate of carbon steel. Fog solutions were adjusted with acetic acid ($CH_3COOH$) to attain pH values of 3.0, 4.0, and 6.0. Since pH values lower than 3 have not been reported for bridge cables, the pH values used in this study are representative of conditions that occur in the actual cable environment. $Cl^-$ ion content was regulated by NaCl to achieve 100 and 500 ppm $Cl^-$ solutions and tests were run at 30, 35 and 45˚C. RH conditions are the same for all tests, at an average value of 80% over the duration of each test.

At the end of each test, the total corrosion in terms of mass loss was calculated from the difference between the final weight, after the removal of corrosion products, and the initial weight of the sample. This loss was then converted to corrosion depth considering the nominal diameter of the wires (4.88 mm).

## Results of Cyclic Corrosion Tests

The dataset from the cyclic corrosion laboratory tests consists of a total of 180 measurements, 10 per each of the 18 tests performed. Mean weight loss (in grams) and the associated mean corrosion depth for the 10 specimens in each experiment are shown in Table 2.

Table 2: Cyclic test conditions and results

| Test No. | Temperature (˚C) | pH | Chlorides (ppm) | Mean Weight Loss (g) | Mean Corrosion Depth (μm) |
|---|---|---|---|---|---|
| 1 | 30 | 6 | 100 | 0.2696 | 14.87 |
| 2 | 35 | 6 | 100 | 0.3020 | 16.67 |
| 3 | 45 | 6 | 100 | 0.3249 | 17.93 |
| 4 | 30 | 4 | 100 | 0.3204 | 17.68 |
| 5 | 35 | 4 | 100 | 0.3543 | 19.56 |
| 6 | 45 | 4 | 100 | 0.3838 | 21.19 |
| 7 | 30 | 3 | 100 | 0.3539 | 19.56 |
| 8 | 35 | 3 | 100 | 0.3760 | 20.76 |
| 9 | 45 | 3 | 100 | 0.4409 | 24.35 |
| 10 | 30 | 6 | 500 | 0.2829 | 15.61 |
| 11 | 35 | 6 | 500 | 0.3147 | 17.37 |
| 12 | 45 | 6 | 500 | 0.4025 | 22.23 |
| 13 | 30 | 4 | 500 | 0.3398 | 18.76 |
| 14 | 35 | 4 | 500 | 0.3840 | 21.20 |
| 15 | 45 | 4 | 500 | 0.4382 | 24.20 |
| 16 | 30 | 3 | 500 | 0.3746 | 20.68 |
| 17 | 35 | 3 | 500 | 0.4292 | 23.70 |
| 18 | 45 | 3 | 500 | 0.5068 | 28.00 |

Figure 10 shows the results of the cyclic corrosion tests (corrosion depth/cycles) from Test 16 (Table 2), Barton et al.'s accelerated corrosion tests [9], and Eiselstein and Caligiuri's cyclic immersion tests [15]. Test 16 is selected for this comparison since it was run under similar conditions to Betti et al.'s tests. The comparison reveals that the corrosion rate observed in the present study is similar to that of Betti *et al.*'s. This similarity is expected since both studies use the same modification of the cyclic salt fog test A2 outlined in ASTM Specification G85-02 [74]. However, Eiselstein and Caligiuri's tests were carried out under milder conditions, and this led to considerably lower corrosion rates. Their study estimated annual corrosion rate of bridge wires to be in the range of 15.2 and 63.5 µm/year for exposure in New York City. Using the median of this range (40 µm/year) and comparing with the corrosion depth after 48-cycles, each cycle in Test 16 is estimated to be equivalent to 3.9 days of exposure or roughly half a year of exposure for the entire test duration.

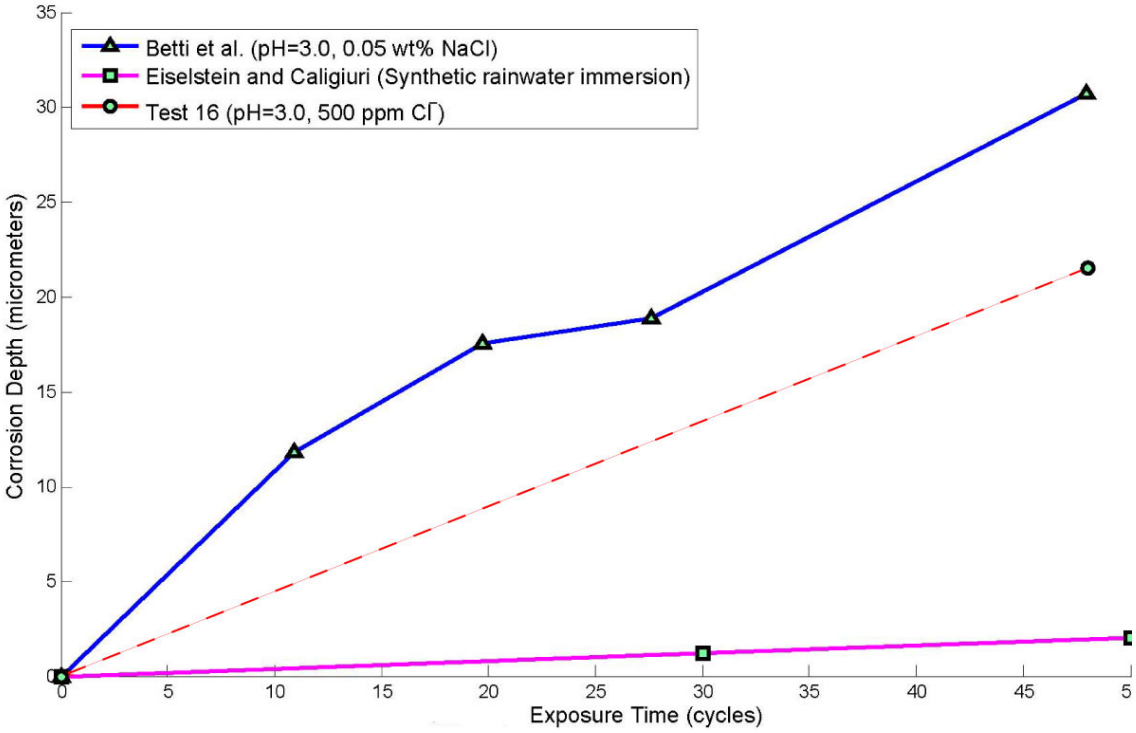

Figure 10: Comparison of corrosion rates for various studies: Barton et al. [9], Eiselstein and Calgiuri [15], current study

The individual effects of the environmental variables pH, $Cl^-$ concentration, and temperature on the corrosion rate observed in the cyclic tests are in agreement with metallic corrosion theory and findings from previous studies [9,12,75] and will be discussed next.

## Effects of Chloride Ion Concentration

Increasing $Cl^-$ ion concentration leads to higher corrosion rates since the $Cl^-$ ion breaks down the otherwise protective passive film layer present on the metal surface. In the accelerated cyclic tests conducted in this study, two different concentrations of chloride solutions, with 100 and 500-*ppm*, were used. These chloride concentrations bracket the 0.05% weight (*~300-ppm*) *NaCl* solution used by Barton et al. [9]. Figure 11 shows the estimated corrosion depths for chloride solutions of different pH values, at 30, 35, and 45 $^{\circ}C$ temperature. From the plots, it is clear that corrosion rate increases with higher chloride ion concentration. Taking the average of all test results, corrosion rate for 500-*ppm* solutions is 11% higher than that for 100-*ppm* solutions. These results corroborate the findings of Suzumura et al. [12] that corrosion rate increases as the $Cl^-$ concentration increases for tests performed at various temperatures.

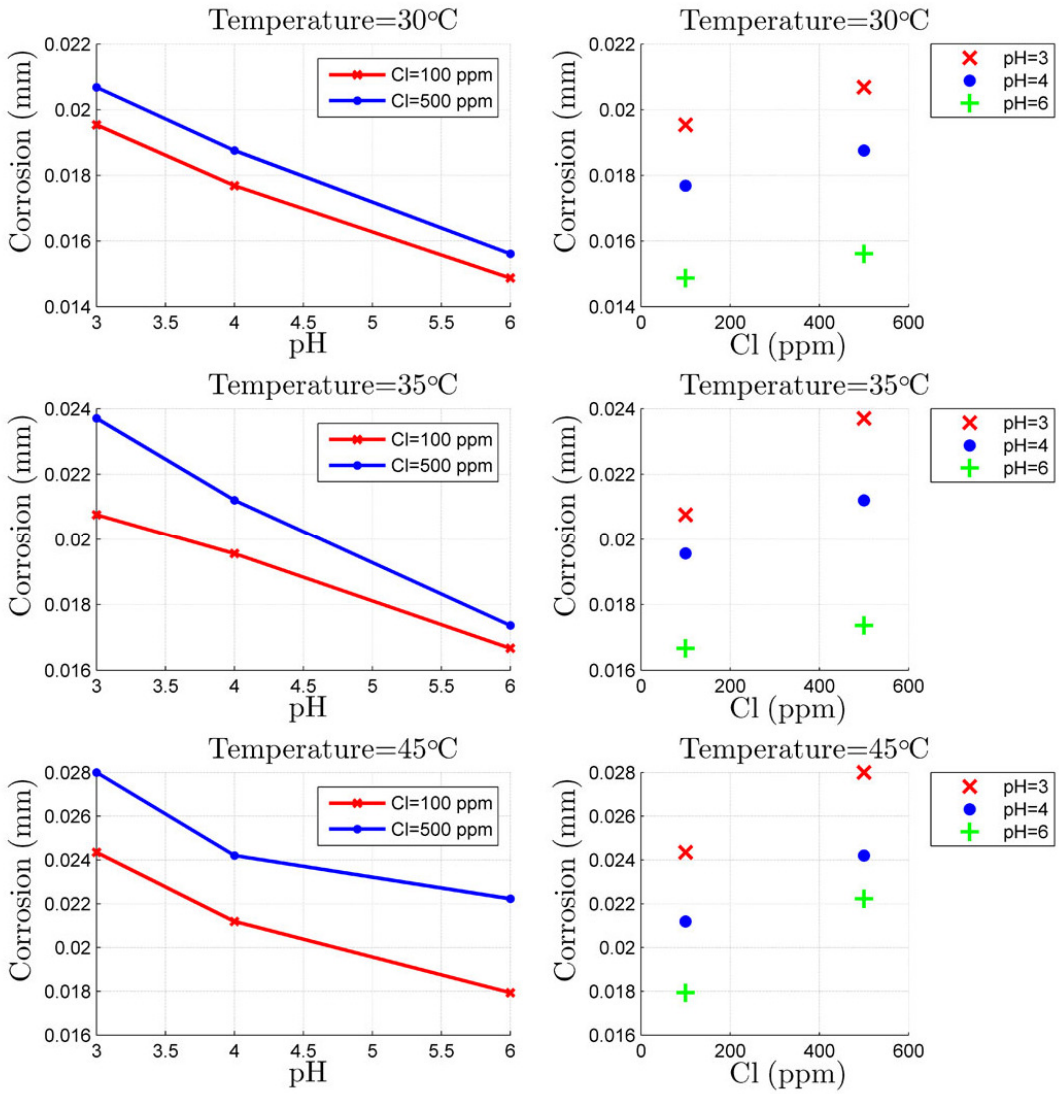


Figure 11: Corrosion depth (mm) vs. pH and $Cl^-$ at T=30, 35, 45°C

## Effects of Temperature

Looking at the effect of temperature on the variability of the corrosion rate, temperature affects the corrosion rate in different ways: (i) by altering the solubility, and thus the concentration of a constituent; (ii) by changing the ionization constant of water, and consequently the pH value; (iii) by drying corrosive surfaces to reduce corrosion rate [76]. When corrosion rate is determined solely

by metal oxidation, corrosion rate follows an exponential law with an increase in temperature [75]. Figure 12 shows the variation of average corrosion depths with temperature (30, 35 and 45 ˚*C*) for solutions of pH=3.0, 4.0, and 6.0, and $Cl^-$ concentrations of 100 and 500 ppm. The plots display increasing corrosion depths for higher temperatures. The average corrosion rate measured in the tests increases by 33% when the temperature raises from 30 to 45 ˚*C*.

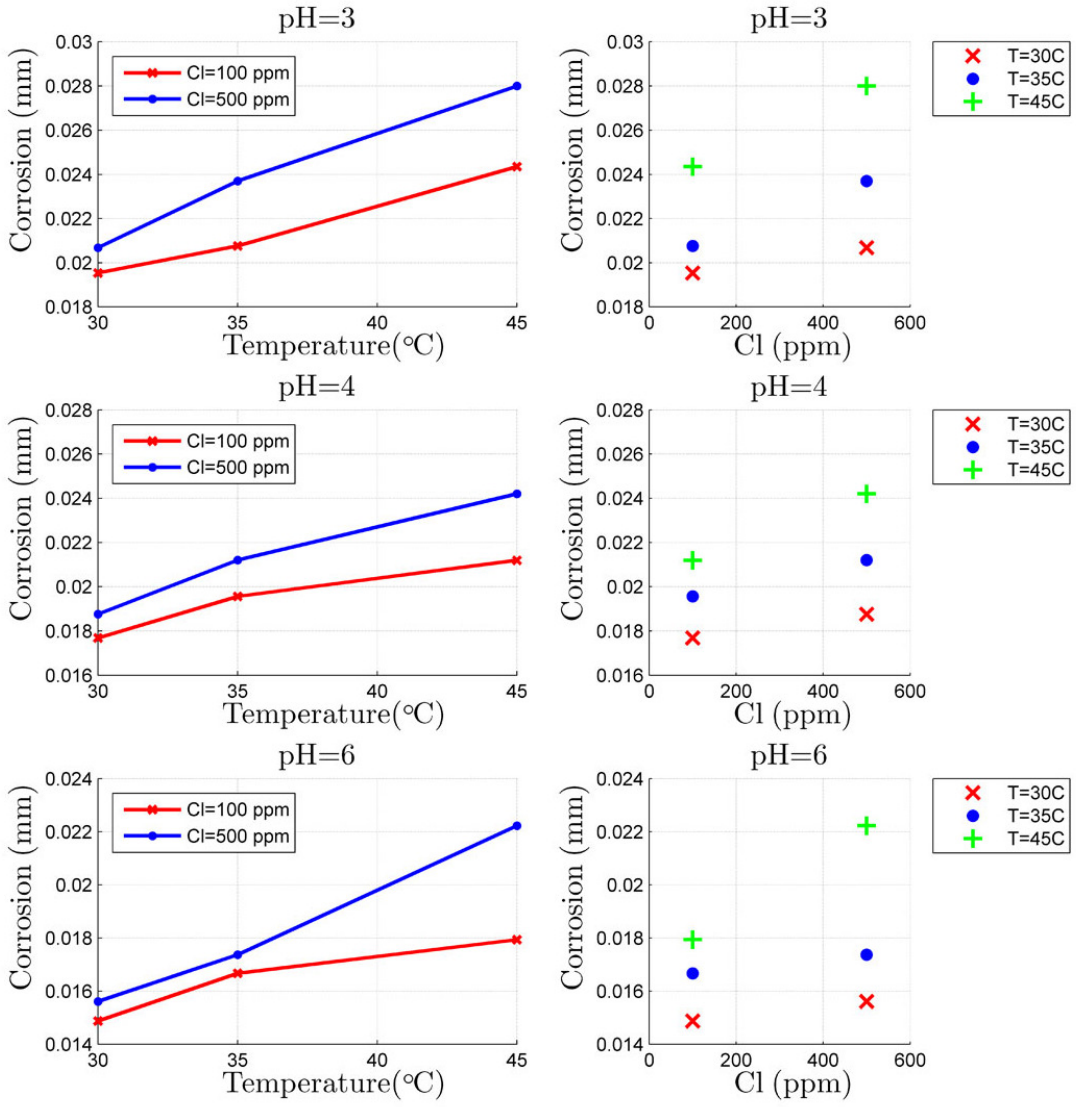


Figure 12: Corrosion depth (mm) vs. temperature and $Cl^-$

Suzumura et al. [12] studied the effect of temperature on the corrosion rate by comparing mass loss values of bridge wires kept at 0, 10, 20, and 40 $^{\circ}C$ under constantly wet conditions. Their findings indicated that corrosion rate increases exponentially with the test temperature. While it is not possible to confirm an exponential trend with the data collected in this study at only three temperature levels, the results are in agreement with Suzumura et al.'s in that corrosion rate of bridge wires increase with temperature.

## Effects of pH Level

Carbon steel shows a complex dependence of the corrosion rate on the pH value. At low pH, the corrosion mechanism is dependent not only on the hydrogen ion concentration but also on the concentration of the counter-ions present. In near-neutral conditions (5<pH<9), pH no longer plays a direct role in the corrosion process [75], while under acidic conditions rust layers on the metal surface tend to dissolve [77].

Figure 13 shows the variations of average corrosion depths with pH for $Cl^-$ concentrations of 100 and 500-*ppm*, at 30, 35, and 45 $^{\circ}C$. The plots show that the corrosion rate increases with decreasing pH, or alternatively, with increasing hydrogen ion concentration. The increase in the corrosion rate did not show an exponential trend when tests were conducted in mildly acidic test solutions (pH=4.0 and pH=6.0), since the pH dependency of the corrosion rate becomes a factor only under strongly acidic conditions. Acetic acid $(CH_3COOH)$ has been shown to accelerate the corrosion rate of carbon steel in strongly acidic conditions, starting around pH=3.5 and reaching a maximum effect around pH=2.5 for carbon steel [78].

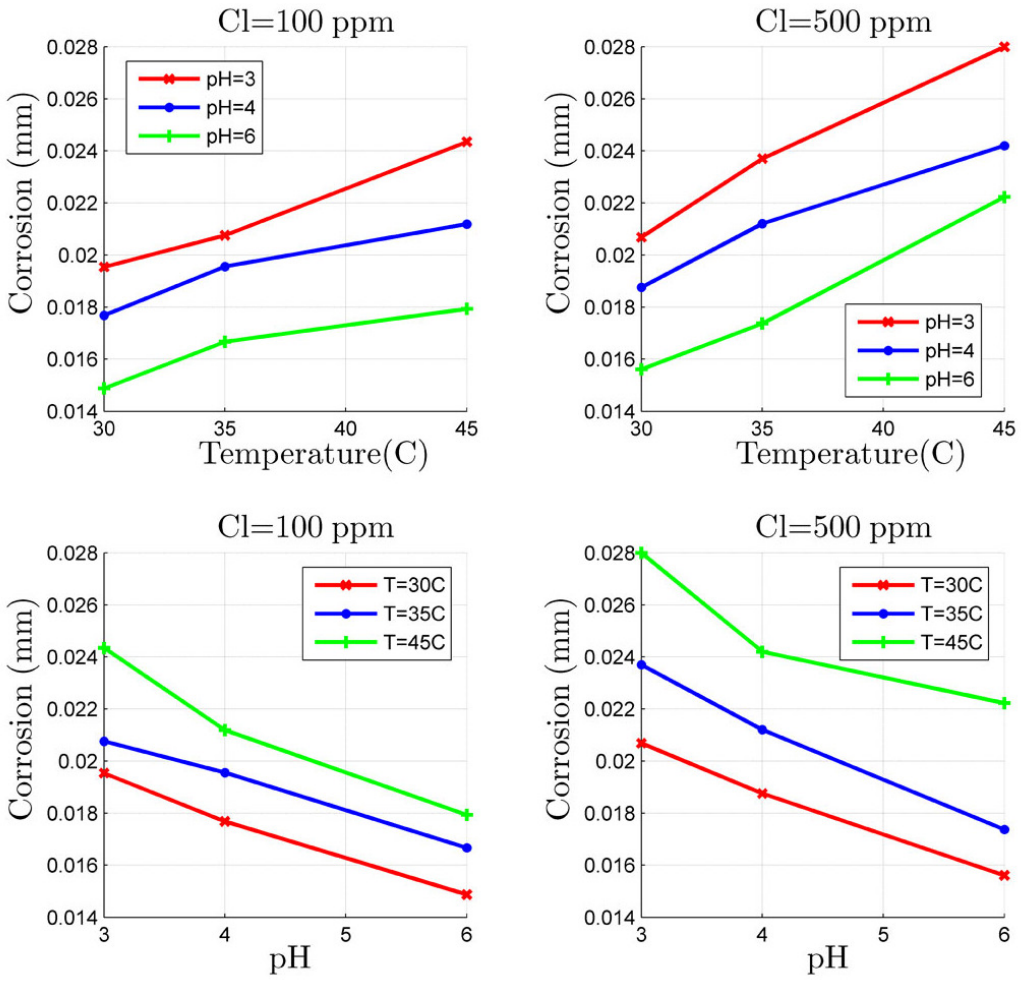


Figure 13: Corrosion depth (mm) vs. temperature and pH for T=30, 35, 45˚C

## Linear Polarization Resistance (LPR) Sensors

Linear polarization is an electrochemical technique where a potential scan is applied to a freely corroding sensor element and the resulting current response is measured. This small perturbation is applied step-wise, starting below the free corrosion potential (the open-circuit potential) and

terminating above the free corrosion potential. Linear Polarization Resistance (LPR) sensors supplied by Analatom, Inc.—a company that specializes in structural health monitoring products—were tested in cyclic corrosion environments. Analatom LPR sensors are two-electrode sensors consisting of a working electrode and a counter/reference electrode (Figure 14). The potential between the two electrodes is measured directly, eliminating the need for a third reference electrode typical of three-electrode procedures. The 150 μm wide fingers of the working electrode are aligned with the 450 μm wide fingers of the counter/reference electrode in an interlocking configuration, leaving an interdigitation gap between the two electrodes. The interdigitation distance between the electrode fingers determine the sensitivity of the sensors; a narrower gap allows an easier charge exchange and leads to more sensitive readings. In this study, three kinds of sensors with different interdigitation distances were tested. They will be referred to as 150 μm, 300 μm, and 1200 μm sensors, the name indicating the interdigitation gap between the electrodes. A smaller interdigitation gap results in a larger number of electrodes. The electrodes are 20 mm long and 9.5 mm wide (Figure 14) and are made from standard shim stock of AISI 1080 steel, which has a chemical composition similar to that of the bridge wires (Table 3). In this manner, the effect of sensor sensitivity stemming from material property fluctuation could be minimized. The electrodes are mounted on a Kapton film, a non-conducting polymer not susceptible to corrosion.

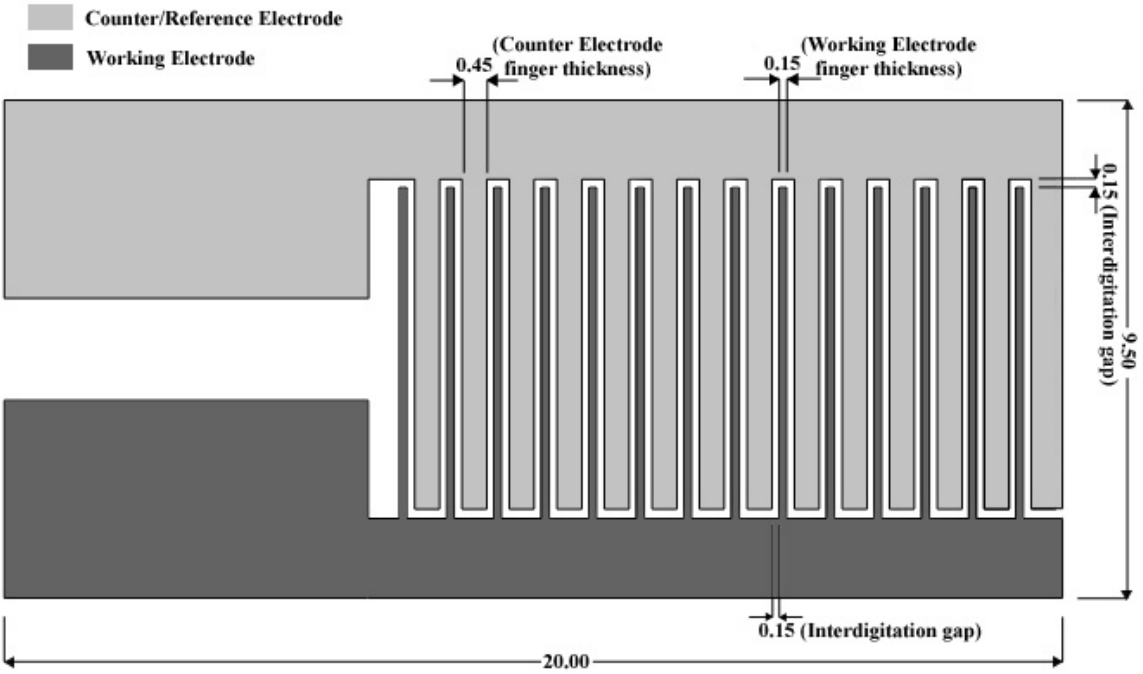


Figure 14: Layout of the Analatom LPR Sensor (dimensions for 150 μm sensor shown in mm units)

These type of sensors can be considered as an array of counter and working electrodes (in Figure 14, a network of 14 sensors). A data acquisition unit performs a voltage sweep about the open-circuit potential of the LPR sensor, through a circuit that uses two operational amplifiers. The input voltage to the circuit is provided by the D/A converter of the micro-controller, which can provide a voltage in the 0.0 - 1.5 volts range. The output voltage is proportional to the current through the LPR sensor: from the operational amplifier circuit, this voltage is measured by the micro-controller's A/D converter, which can sense voltages in the same voltage range. The slope of the input voltage vs. output voltage curve is proportional to the polarization resistance and it is calculated from a least-squares data fit on the data collected from the voltage sweep. Polarization resistance data from the sensors are then recorded and converted into corrosion rate values.

Table 3: Chemical compositions of AISI 1080 Steel vs. Standard Bridge Wire

| Chemical Composition | AISI 1080 Steel | Standard Bridge Wire |
|---|---|---|
| Carbon (C) | 0.75-0.88% | 0.75-0.85% |
| Manganese (Mn) | 0.60-0.90% | 0.55-0.75% |
| Phosphorus (P) | 0.04% max | 0.04% max |
| Sulfur (S) | 0.05% max | 0.04% max |

## Preliminary Testing

The 1100 liter capacity Q-Fog Cyclic Corrosion Tester shown in Figure 15 was used to run the cyclic tests. The corrosion tester is capable of running different cycles (fog, dry-off, and humidity) repetitively to reproduce outdoor cyclic conditions.


Figure 15: Q-Fog Cyclic Corrosion Tester

The sensors were first tested for their durability and ability to function under cyclic variation of relative humidity. A two-step cycle consisting of a high and a low humidity step was repeated continuously. At the start of the high humidity step, relative humidity within the chamber rises to 100% and remains constant for the rest of the phase. In the low humidity phase the moist air inside the chamber is purged and the relative humidity drops to approximately 30%.

Figure 16 shows two of the 49-wire bundles used in this test. LPR sensors were placed in various locations on the surface of and inside the bundles. The sensors showed high sensitivity to humid environments and were very successful in capturing the start of corrosion reactions. Figure 17 shows an LPR sensor showing the onset of corrosion.

Figure 16: 49-wire bundles prepared to be placed in the corrosion chamber

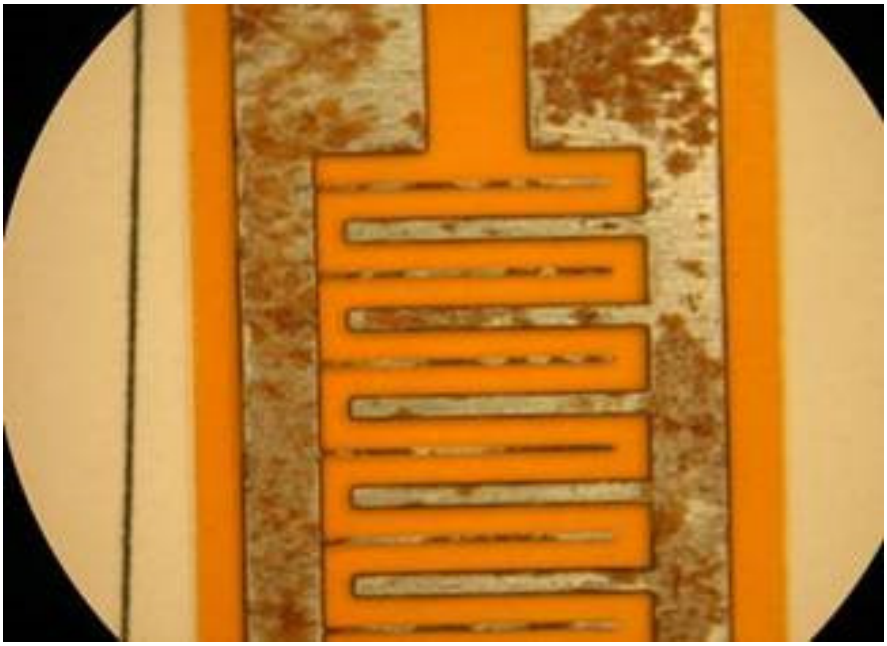

Figure 17: Onset of corrosion on an LPR sensor

Figure 18 shows corrosion rate readings from two sensors, one located on the surface (yellow line) and the other located at the center of a bundle (blue line) during a single high humidity step. The green ramp function indicates the start and the end of this step. With the start of the humidity phase, relative humidity inside the chamber increases gradually and reaches 100% shortly. From the figure, it can be observed that the sensor mounted on the surface of the bundle detects corrosive activity earlier and at a higher rate than the sensor inside the bundle. This was expected since the wire bundle acts as a barrier against the moisture.

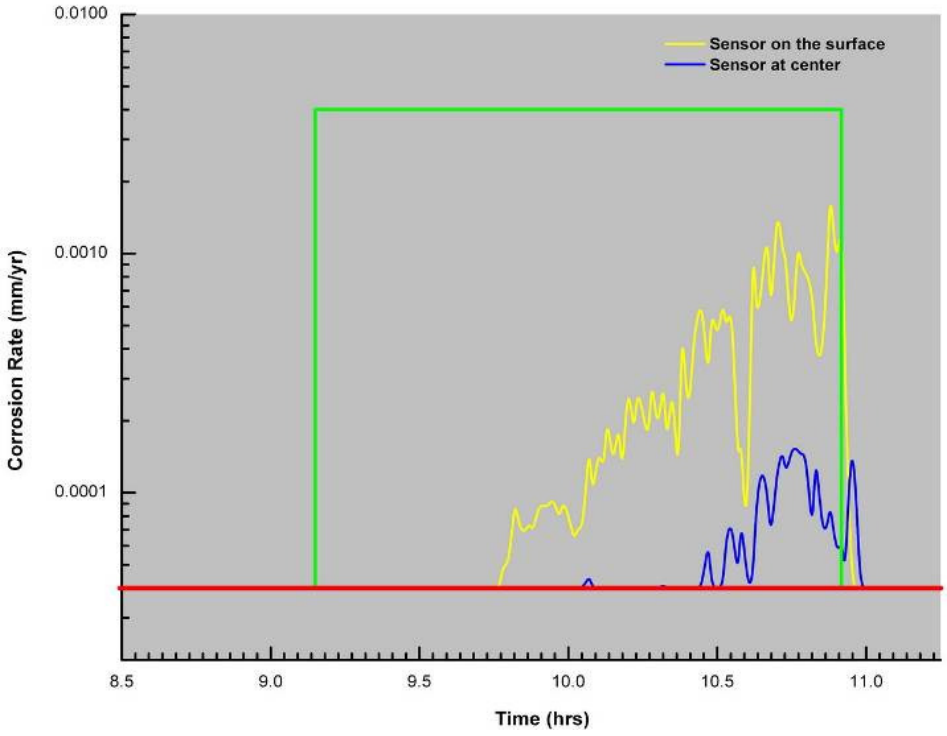


Figure 18: Close-up of a humidity step: yellow – sensor on the surface, blue – sensor at the center of the bundle, green – duration of the humidity cycle.

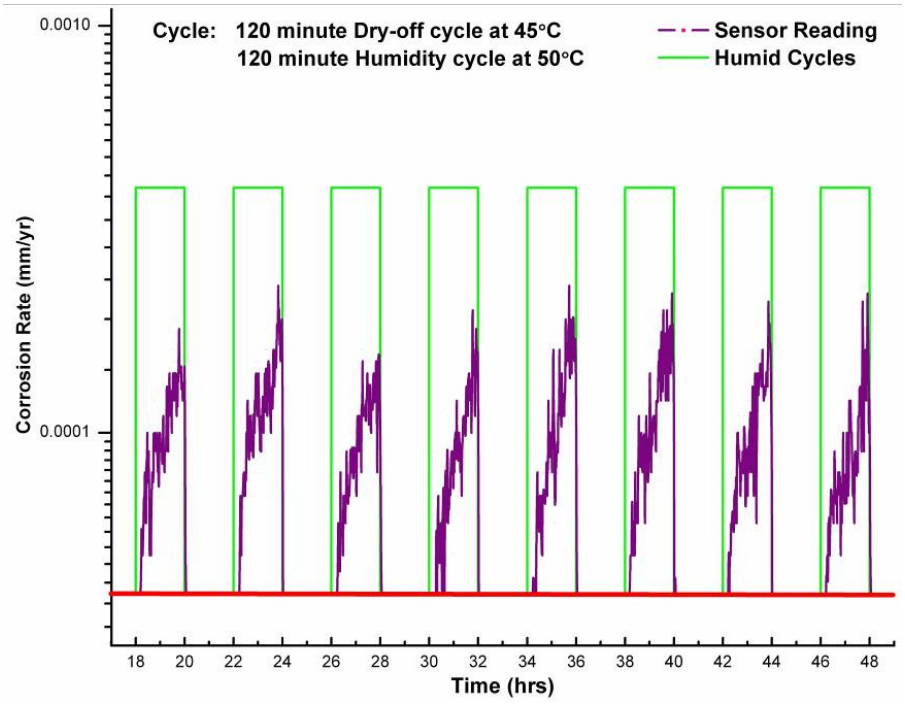


Figure 19: Corrosion rate vs time in cyclic humidity testing of a sensor

The next step of the testing aimed at examining the consistency of the sensors when they were subjected to the same humidity cycle for an extended duration of time. Figure 19 shows corrosion rate readings from an LPR sensor subjected to repetitive cycles. Each cycle lasted for 4 hours and consisted of a 120-minute humid cycle at 50$^{o}$ C and a 120-minute dry cycle at 45$^{o}$ C. Since the goal of this testing program was to calibrate the sensor readings to the wire corrosion rate, it was important to keep the sensors away from saturation: this is the reason why the corrosion rate readings are kept quite low. It is important to note that the measured corrosion rate is the actual corrosion rate of the sensor itself and not that of the bridge wire. To determine the correlation between the sensor and wire corrosion rate, it is essential to prevent the saturation of the sensor. Corrosion rate readings obtained from sets of sensors with the same interdigitation distance and under the same environmental conditions were found to be consistent over time and in agreement with each other.

Several tests consisting of humidity, dry-off and fog cycles were run to test the survival of sensors in harsh environments. During the fog cycles, aggressive solutions of low pH and high chloride content were sprayed on the sensors in a fine mist form. Figure 20 shows an LPR sensor after a week of testing with a solution of pH=2.5 and 3.5% NaCl in weight. Most of the sensors ceased to function after a week of cyclic testing under these severe conditions. The LPR sensors performed better in milder tests of humid-dry cycles in the 25-60˚C range and fog sprays of pH=3.5 and higher. Almost all of the sensors were functional after a month of cyclic testing under these conditions, with only a few sensor failures.

Figure 20: Corroded LPR sensor after one week test

## Experimental Program

After evaluating the performance and establishing the soundness of LPR sensors, cyclic tests were run to collect calibration data for the LPR sensors. A series of tests was conducted in which LPR sensors and bridge wires stripped of their zinc coating were placed at the same time in the cyclic corrosion chamber and subjected to the same environment. Corrosion rate readings from the sensors were recorded and integrated over time while, for the wires, the mass loss from before and after the testing was measured. By correlating the sensors' reading with the wires' mass loss, it was possible to obtain a proportionality constant that allows to convert the sensors' reading to that of the wires.

An array of LPR sensors (up to 6 for an experiment) were mounted on a plexi-glass board, to be placed in the vicinity of the bridge wire samples (10 wire samples for each experiment). The sensors were connected to a data acquisition unit (DAQ) supplied by Analatom Inc., which communicated with a computer via a serial port. The DAQ was capable of recording polarization resistance

readings from up to eight channels at specified intervals. During each test, polarization resistance ($R_p$) data from the LPR sensors was recorded at one minute intervals for the duration of the test. These readings are used for calibrating the sensors against the measured mass loss for bridge wires undergoing the same tests.

In 6 of these experiments (1, 2, 4, 5, 6, 7 in Table 2), wires were placed together with sensors so to get recordings needed for sensor calibration.

## Calibration of Sensors

In Table 4, the list of the experiments where the sensors were tested for calibration and the type of sensors used are presented. The experiment numbers correspond to cyclic tests shown in Table 2.

Table 4: Type and number of LPR sensors used in experiments

| **Sensor Type** | **Test No:** | **1** | **2** | **4** | **5** | **6** | **7** |
|---|---|---|---|---|---|---|---|
| **150-µ** | | 1 | 1 | - | 2 | 2 | 2 |
| **300-µ** | | - | - | - | 2 | 2 | 2 |
| **1200- µ** | | - | - | 1 | 2 | 1 | 2 |

In order to obtain the bridge wire corrosion rate from LPR sensors, a relationship between the corrosion rate of a wire and the polarization resistance reading from a sensor is needed. The corrosion rate is calculated from the measured polarization resistance and from the mass loss measurement of the corroding wire using the concept of equivalent weight and Faraday's Law. Equivalent weight $EW$ is the weight of an element that reacts with 1 Faraday of charge, thus contributing to the corrosion and overall loss of material in the basic oxidation process for metals: $M \rightarrow M^{z+} + ze^{-}$. $EW$ is

calculated from the known atomic weight *(AW)* of the metal and number of electrons lost per atom of the metal *(z)* as:

$$EW = \frac{AW}{z} \tag{1}$$

In order to relate the mass loss of metal to the current flow, we begin by stating Faraday's law:

$$Q = z \times F \times M \tag{2}$$

where,

$Q$ = charge in Coulombs resulting from the reaction of corroding metal

$F$ = Faraday's constant, 96,485.34 Coulombs/mole

$z$ = number of electrons lost per atom of the metal

$M$ = number of moles of metal reacting

For the number of moles lost for the metal $M$, the mass loss $W$ can be calculated as:

$$W = M \times AW \tag{3}$$

Combining equations (1), (2), (3) and substituting for $z$ and $M$, the mass loss $W$ can be related to charge $Q$ by the relation:

$$W = \frac{EW \times Q}{F} \tag{4}$$

Corrosion rate can be calculated from mass loss $W$ using the density and sampling area of the corroding metal from the basic identities:

$$W = \rho \times V = \rho \times Area \times T \tag{5}$$

$$Q = I_{corr} \times t \tag{6}$$

where,

$\rho$ = density of metal

$V$ = volume of corroding metal, corresponding to the sampling area

$Area$ = sampling area

$T$ = thickness of corrosion layer, corresponding to the sampling area

$I_{corr}$ = corrosion current

$t$ = time in seconds

From Eq. (6),

$$\rho \times Area \times T = \frac{EW \times I_{corr} \times t}{F} \tag{7}$$

$$\frac{T}{t} = \frac{I_{corr} \times EW}{\rho \times Area \times F} \tag{8}$$

The rate of change of thickness $\left(\frac{T}{t}\right)$ is the corrosion rate ($CR$) of the metal:

$$CR = \frac{I_{corr} \times K \times EW}{\rho \times Area} \tag{9}$$

where, $K$ is a constant that accounts for Faraday's constant $F$ in Eq. (8) and changes units of corrosion from seconds to years. $I_{corr}$ can be substituted to yield:

$$CR = \frac{1}{R_p}\left(\frac{B \times K \times EW}{\rho \times Area}\right) = \frac{B'}{R_p} \tag{10}$$

where $B'$ is the overall proportionality constant in units of mm-ohms/year. In order to determine $B'$, LPR sensors and ungalvanized bridge wires were tested together in various cyclic corrosion tests described in the previous section.

## Determination of the Overall Proportionality Constant $B'$

From the mass loss experiments with actual bridge wires, we determined the exact corrosion loss for each test. Both the recorded polarization resistance values and the corrosion mass loss values were used to estimate the overall proportionality constant $B'$ in Eq. (10).

The sampling frequency for $R_p$ during the corrosion test was one recording per minute. Hence, the estimated thickness loss induced by corrosion during a given minute can be obtained by converting the corrosion rate *CR* in mm/year to mm/minute and then multiplying with a duration of 1 minute:

$$C_{1-\min} = CR\ (mm/year) \times \frac{1\ \min}{60\ \min/hr \times 24\ hr/day \times 365\ day/year} = \frac{CR}{525,600}\ (mm) \qquad (11)$$

Substituting for $CR$ the expression presented in Eq. (10) leads to an expression for the thickness loss during a given minute as:

$$C_{1-\min} = \frac{B'}{R_p} \times \frac{1}{525,600} \quad (mm) \qquad (12)$$

where $R_p$ is obtained directly from the measurements. The total thickness loss for the duration of the 3(hr)x60(min)x48(cycle)=8,640-min experiments, $C_{Exp}$ will then be expressed as:

$$C_{Exp} = \sum_{t=0}^{t=8640\min} \frac{B'}{R_p(t)} \times \frac{1}{525,600} = \frac{B'}{525,600} \sum_{t=0}^{t=8640\min} \frac{1}{R_p(t)} \qquad (mm) \qquad (13)$$

where the summation is intended for all the values recorded during the experiment. In this case, the proportionality constant $B'$ can be obtained from:

$$B' = \frac{C_{Exp} \times 525,600}{\sum_{t=0}^{t=8640\min} \frac{1}{R_p(t)}} \qquad \left(mm - ohms/year\right) \qquad (14)$$

As an example, the calculation of $B'$ for the 150 µ LPR sensor used in Test 1 will be carried out. In this test, only one 150 µ LPR sensor was placed in the chamber together with the wires. Figure 21 shows the inverse of $R_p$ readings for this sensor during the first eight cycles of Test 1. Each data point on the plot corresponds to the inverse of $R_p$ at a given instant in time and is proportional to the instantaneous (1-minute) corrosion rate value at that recording time, following the relation given by Eq. (12). The integration of this time series (multiplication of these values by the sampling interval of 1 minute and summation of all these products) yields the denominator of Eq. (14).

Figure 22 shows the integrated area for the first eight cycles of Test 1. The total area for the entire duration of the test (its integration) is $7.1020 \times 10^{-3}$ min/ohms.

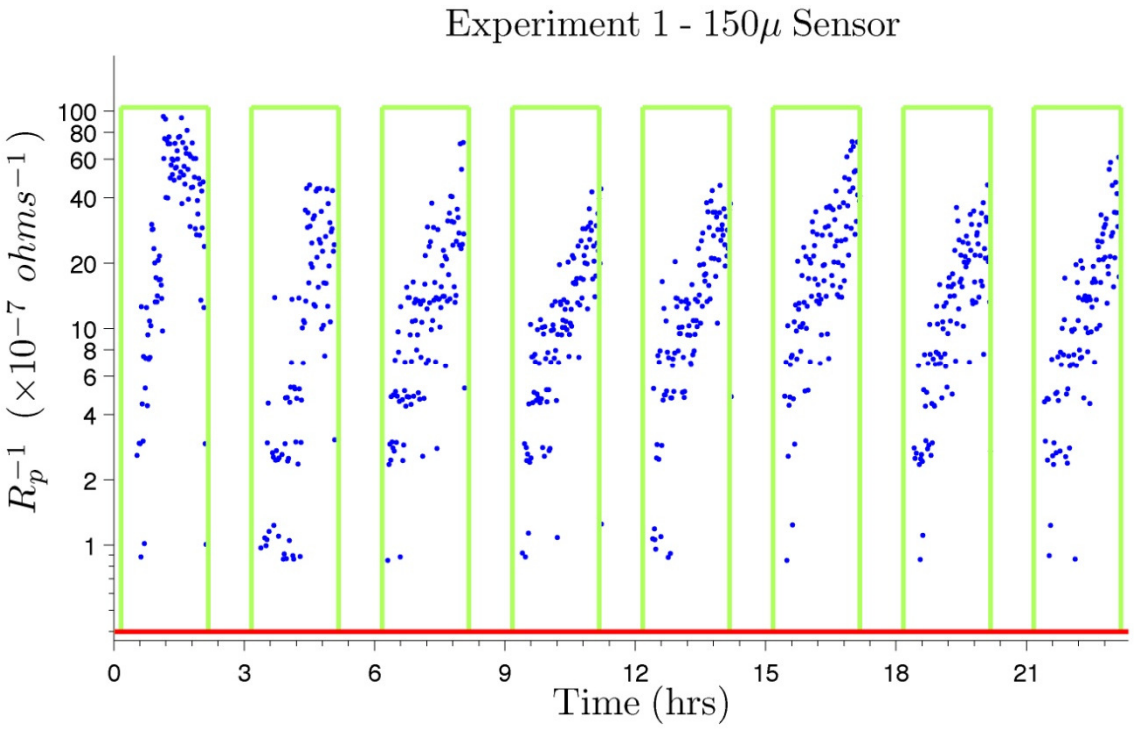


Figure 21: The Inverse of Polarization Resistance vs Time

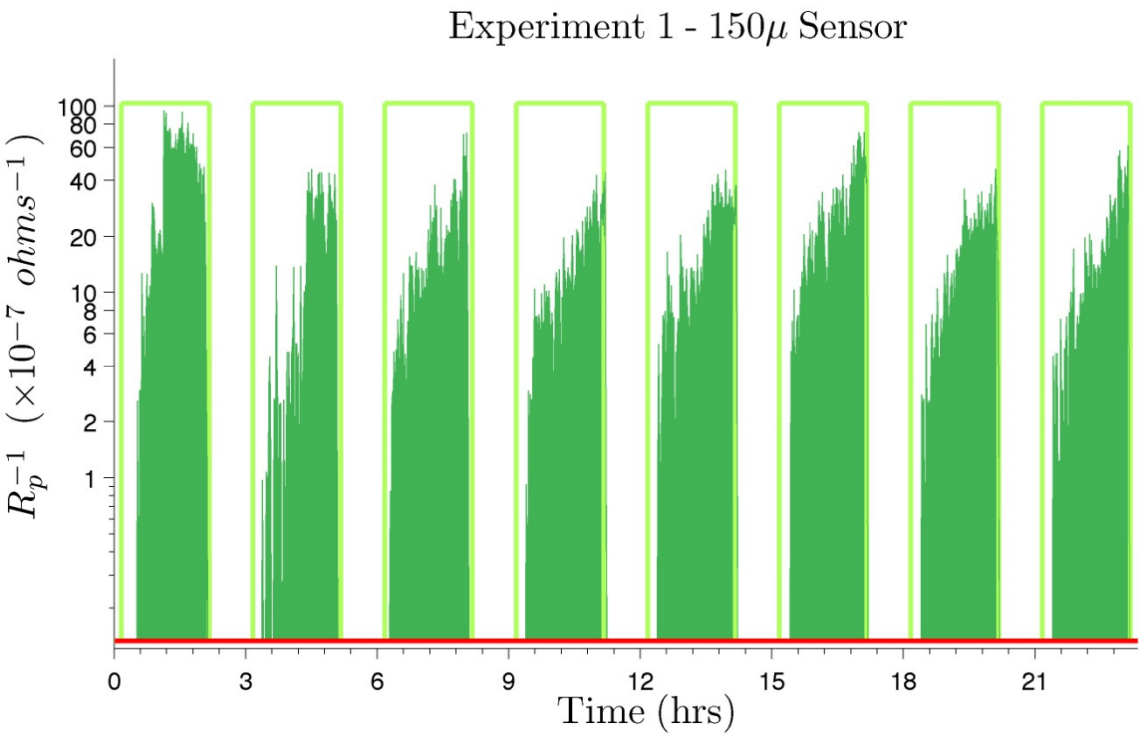


Figure 22: Integration of $R_p(t)^{-1}$

The average thickness loss measured for the ten specimens tested in Test 1 is 14.87 µm. This is obtained by weighing the wires before and after the experiment, as previously described. The overall proportionality constant $B'$ for the sensor can then be calculated as:

$$\sum_{t=0}^{t=8640\,\text{min}} \frac{1}{R_p(t)} = 7.1020\times10^{-3}\left(\text{min}/ohms\right)$$

$$C_{Exp-1} = 14.87\ (\mu m)$$

$$B' = \frac{C_{Exp-1}\times 525{,}600}{\sum_{t=0}^{t=8640\,\text{min}} \frac{1}{R_p(t)}} = \frac{14.87\ (\mu m)\times {}^{1(mm)}/_{1000\,(\mu m)}\times 525{,}600\left(\text{min}/year\right)}{7.1020\times10^{-3}\left(\text{min}/ohms\right)}$$

$$= 1100491 \quad \left(\frac{\text{mm-ohms}}{\text{year}}\right)$$

Hence, when using measurements from 150 µ LPR sensors, dividing the calculated value of *B'* by $R_p$ will provide an instantaneous measurement of the corrosion rate of the wire. Figure 23 displays the instantaneous corrosion rate values calculated using the overall proportionality constant $B'$ calculated above.

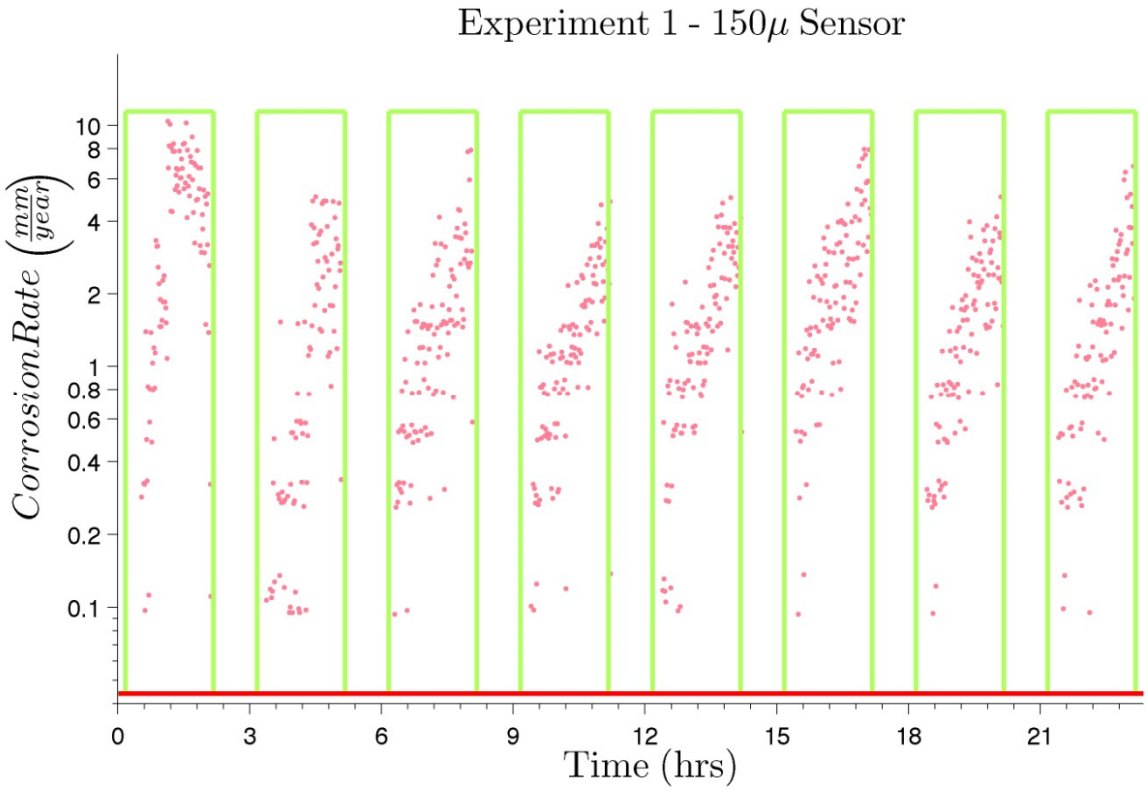


Figure 23: Instantaneous corrosion rates vs time

Figure 24-26 show the calculated overall proportionality constants from the experiments for 150 µ, 300 µ, and 1200 µ sensors, respectively. The mean values of the constants are also displayed. The constants for 150 µ and 300 µ are virtually identical. However, the constant calculated for the 1200 µ sensors is two orders of magnitude smaller. This cannot be explained by the decreased sensitivity due to the larger interdigitation gaps of 1200 µ sensors. Instead, compared to the 150 µ and 300 µ sensors, higher polarization resistance values would be expected for the 1200 µ sensors. Consequently, 1200µ

sensors should have had higher constants than the rest. Apart from this peculiarity with the order of magnitude of the constants calculated for 1200 μ sensors, the variance in the constants calculated for the three sensor types are all reasonably low, displaying the consistency of the results. This suggests that the proportionality constants obtained for LPR sensors are accurate and can be used as a reliable means of measuring the corrosion rate of bridge wires.

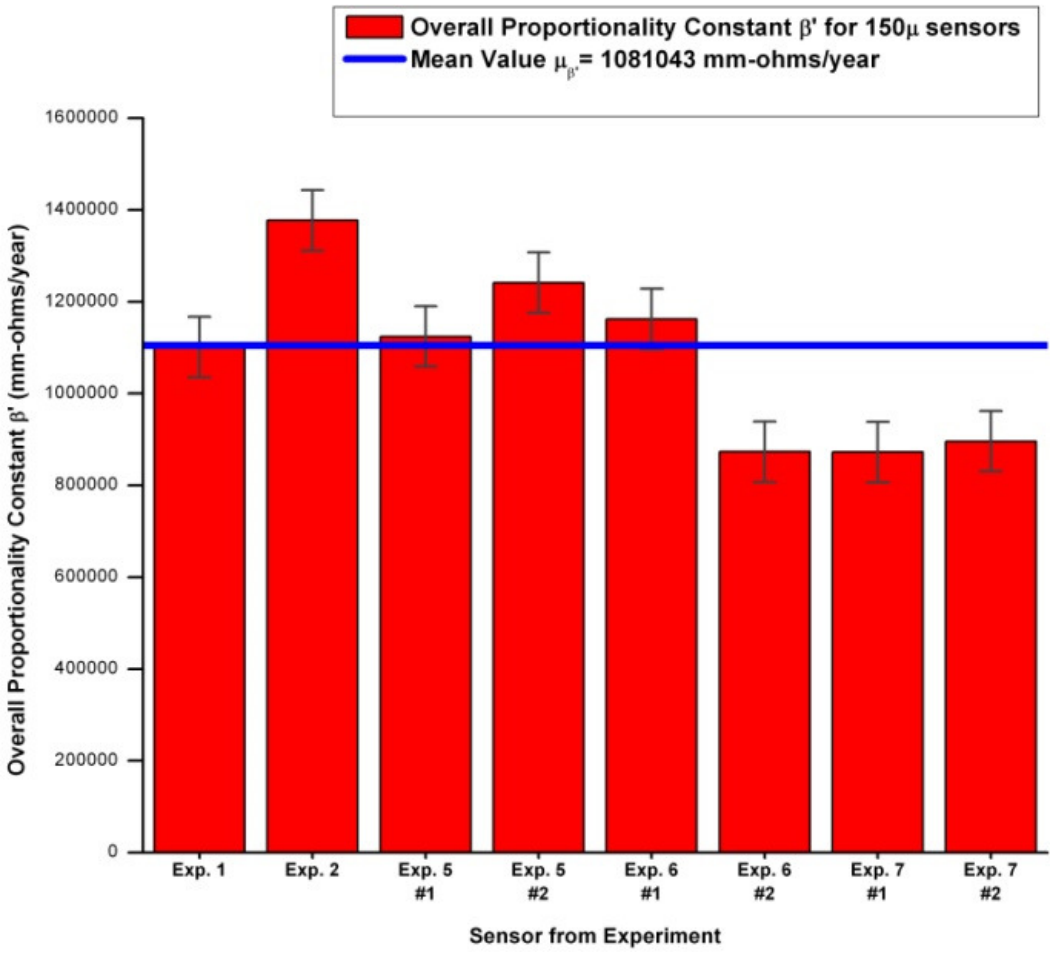


Figure 24: Proportionality Constant for the 150 μm sensors

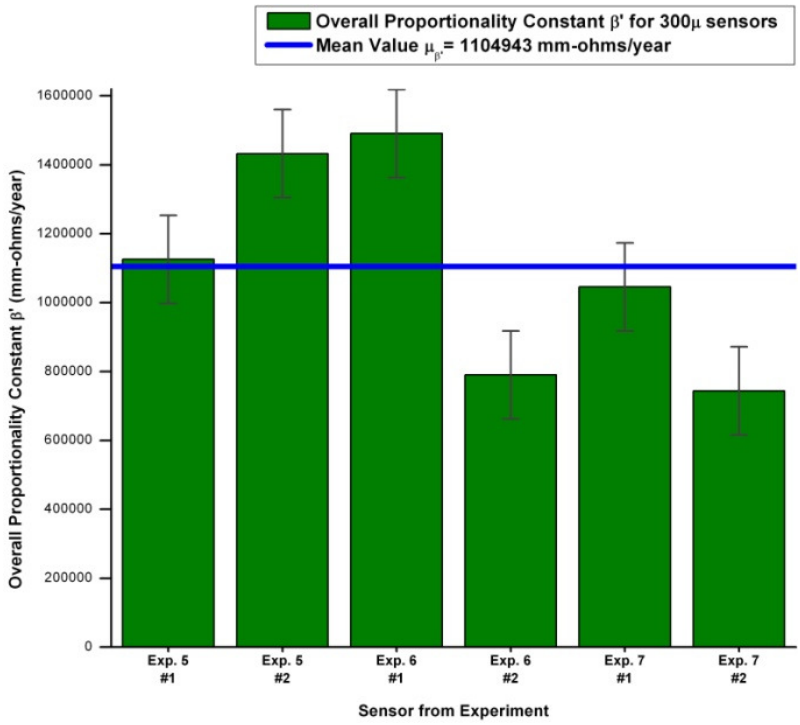


Figure 25: Proportionality Constant for the 300 μm sensors

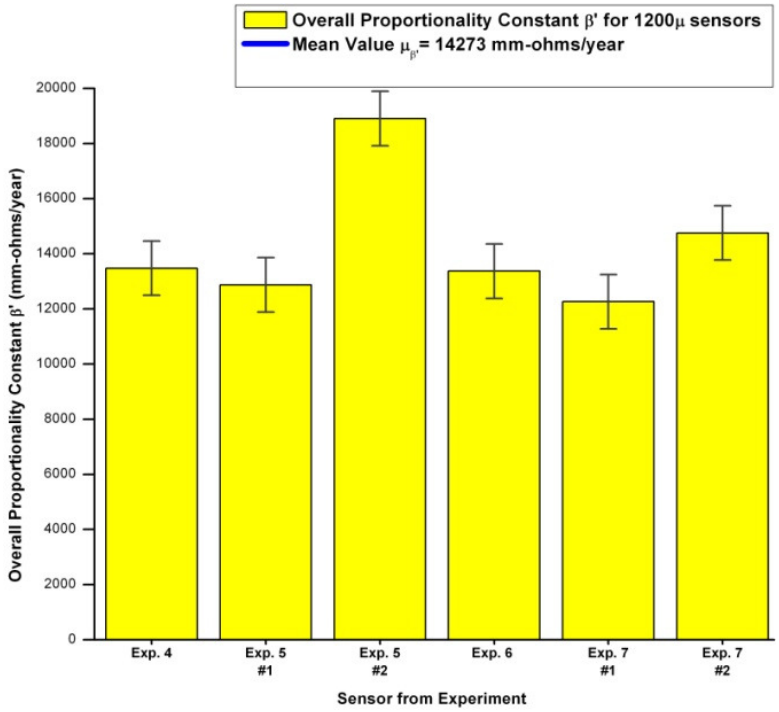


Figure 26: Proportionality Constant for the 1200 μm sensors

## Conclusions of the Experimental Testing of LPR Sensors

LPR sensors provided by Analatom Inc. were tested and calibrated against mass loss measurements of bridge wires. The LPR sensors are very successful in detecting the onset of corrosive activity. They also perform well under characteristic suspension bridge cable environment, confirmed by the very low failure rate during the tests. Calibration data for the sensors indicate that they can be used as consistent and accurate instruments for the measurement of corrosion rate of bridge wires. 150 μ sensors are the primary candidate for bridge application on the account of their higher sensitivity compared to the 300 μ and 1200 μ types, without exhibiting an apparent penalty for reliability or quality in corrosion rate sensing.

# CHAPTER 3. ANNUAL CORROSION RATE

## Introduction

Accurately determining the current state of a suspension bridge's main cables is critical in assessing the safety of the bridge. These cables are composed of thousands of individual bridge wires, each of which deteriorates over time at a different rate. Previous research, with the aim of improving the current inspection methods, have investigated the use of: (1) Non-destructive testing (NDT) technologies for direct detection of corrosion damage to bridge wires and (2) a network of sensors to continually monitor the cable's internal conditions and provide information to assess the cable's deterioration over time [8,56]. This and the next chapter propose a time-dependent corrosion rate model for bridge wires that relies on the monitored environmental variables (temperature, relative humidity, pH, etc.) from the cable interior. Such a model can then be used to estimate the reduction in a bridge wire's cross-section and, consequently, the remaining cable strength.

To this end, the previously reported experimental data on the corrosion rate of carbon steel is compiled into a database and analyzed using machine learning methods to determine the set of environmental variables that generate the best corrosion rate prediction accuracy. Statistical measures are used to validate the variable selection process and to determine the prediction accuracy. To expand the database available in the literature, cyclic corrosion tests—described in the previous chapter—were performed by subjecting bridge wire samples to varying levels of the selected environmental variables. Graphical analyses are used to compare the experimental findings

to those available in the literature. Cyclic corrosion test data is scaled into ranges defined by atmospheric conditions of suspension bridge cable environment and used to augment the previous experimental data. Finally, a model that predicts the annual corrosion rate of bridge wires as a function of the selected environmental variables is developed using the augmented dataset. This model will be used in an integrated methodology to estimate the remaining cable strength, as shown in the next chapter.

## Corrosion of High-Strength Bridge Wires

The corrosion rate of a bridge wire depends on its chemical properties and the environmental conditions that it is subjected to. Bridge wires are typically made of carbon steel and hot-dip galvanized with zinc for corrosion protection. The zinc coating will undergo corrosion first, protecting the steel wire until the zinc coating is consumed. Following the depletion of the zinc coating, corrosion of the steel bridge wire will commence at the surface.

Bridge cables are constantly exposed to varying environmental conditions such as temperature and moisture fluctuations. The environmental conditions a bridge wire is exposed to depend not only on the geographic location of the bridge itself but also on the location of the wire within the cable cross-section and along the length of the cable.

As discussed in Chapter 1, the time-dependent corrosion of metals is described by the exponential expression

$$C(t) = At^n \tag{15}$$

where *C(t)*–cumulative corrosion loss (in terms of thickness or section loss) after *t* years, *A*–annual corrosion rate for a metal, *n*–exponent which depends on the type of metal and surrounding environment, typically in the range [0-1]. Values of *n* for steel in urban-industrial atmospheres are reported to be in the range [0.25-0.59] [40,41].

In essence, environmental conditions play a direct and integral role in the corrosion of bridge wires and therefore need to be linked to the time-dependent corrosion expression in Eq. (15). This link can be established through either an analytical method that models the physicochemical corrosion process or a data-based method that investigates the relationship between environmental inputs and measured corrosion loss through the direct analysis of experimental data. Deriving an analytical equation that is all-encompassing and applicable to the broad range of environmental conditions within the cable interior is extremely difficult. Depending on the conditions such as the ion concentrations of the solution in contact with the metal, temperature, etc., the same metal may undergo a number of different chemical reactions, all of which may occur at significantly different rates. Owing to this complexity, analytical corrosion models found in the literature are appropriate under limited and specific conditions. In contrast, data-based models have been used to model complex problems such as the estimation of corrosion rate from environmental inputs and shown to produce accurate predictive models, provided there exists a sufficiently large dataset that covers the range of inputs specific to the problem at hand [16,17]. Consequently, data-based methods are used in this work to establish the annual corrosion rate *A* in Eq. (15) as a function of environmental inputs such as T, pH, RH, etc. so that the expression of the cumulative corrosion loss in Eq. (15) can now become:

$$C(t, T, pH, RH, etc.) = A(T, pH, RH, etc)t^n \tag{16}$$

## Methodology: Development of Corrosion Rate Model

In developing a methodology for estimating remaining cable strength, it is essential to have a model that predicts the corrosion rate of each wire within the cable. This corrosion rate depends on the interaction of bridge wires with their environment that is characterized by physical quantities such as T, pH, RH, etc.

Previous studies on bridge wires over the last decade by Betti et al. [9,10,37] and Nakamura et al. [11,12] provide deep insight into the effects of environmental parameters on the corrosion of bridge wires. However, the amount of data available from these experiments is insufficient to develop a data-based predictive function for the corrosion problem, which depends on multiple environmental variables. For this reason, a more extensive database of environmental variables as input and the associated annual corrosion rate as output is needed to: (1) select which environmental variables need to be monitored to achieve the best corrosion rate prediction accuracy; (2) develop the annual corrosion rate estimation model based on these selected environmental variables.

Once a database that is sufficiently exhaustive and that covers the range of inputs specific to the bridge wire corrosion problem is established, it can be used to develop a data-based predictive model. Machine learning methods are computational algorithms that are often used to build predictive models from observed data [17]. There are two types of machine learning algorithms: supervised and unsupervised learning algorithms. In contrast to unsupervised learning approaches that are used for finding hidden patterns in datasets without known output values, supervised learning approaches use datasets that include both input data and the known corresponding output

values and seek to build a model that can predict the output value when presented with new input data. Since our goal is to create a predictive model from a database that consists of environmental variables (T, pH, RH, etc.) as the input and the corresponding measured annual corrosion rate $A$ in Eq. (16) as the output, supervised learning methods are used in this work.

## General Formulation: Machine Learning Algorithms

Consider the problem at hand of estimating the annual corrosion rate from the measured environmental parameters using the dataset $(T, pH, RH, ..., A)_i, i = 1, 2, \ldots, N$ or in condensed form $(\mathbf{x}, y)_i, i = 1, 2, \ldots, N$ where $\mathbf{x}$ represents a column vector of inputs containing physical quantities that can be measured such as T, pH, RH, etc., $y$ is a scalar representing the measured annual corrosion rate $A$, and $N$ is a scalar representing the number of input-output pairs in the entire dataset. In supervised learning, the dataset is typically split into two parts: a training dataset and a test dataset. The training dataset contains a substantial portion of the dataset (it contains $N_{tr}$ input-output pairs from the available $N$) and is used by a supervised learning algorithm to train a predictive model that minimizes the errors between the observed outputs from the dataset and the corresponding predicted output values. The remaining data comprises the test dataset (contains $N_{test} = N - N_{tr}$ input-output pairs from the available $N$) and is used to determine the performance of the model. Since the test dataset is independent of the data used to train the model, it can be used to estimate any quantitative measure of performance that is appropriate for the data. In corrosion rate prediction, the predicted value is continuous (i.e. can take any positive value), and traditional

error measures such as the root mean squared error (RMSE) and mean absolute error (MAE) can be used to determine the prediction accuracy.

One factor that has a considerable impact on the success of a learning algorithm is the removal of variables or *features* that are irrelevant or redundant with respect to the supervised learning problem at hand from the dataset. In the context of corrosion rate prediction, a feature is any one of the measured environmental variables such as T, pH, RH, etc. Consider a dataset that consists of $v$ input variables (or features): $(V_1, V_2, \ldots V_v)$ where $V_.$'s represent different input variables. The aim of *feature subset selection* is to find a subset of the original features of a dataset (e.g. $(V_3, V_4, V_7)$) so that a learning algorithm, using data containing only the selected features, generates a function with the highest prediction accuracy.

Many supervised learning algorithms deal with the prediction of values, or regression, which can be used for corrosion rate prediction. In this study, three algorithms were selected: (1) linear regression, (2) Artificial Neural Networks (ANN) and (3) Support Vector Regression (SVR). Among the three, linear regression and ANN methods are well documented in the literature [17,79] and so only a brief account of the SVR method and how it relates to the corrosion rate estimation is given here.

In applying supervised learning algorithms, our goal is to find a function that accurately predicts the annual corrosion rate $A$ when presented with measured environmental inputs (*T, pH, RH*, etc.). Consider the given training data $(\mathbf{x}, y)_i, i = 1, 2, \ldots, N_{tr}$. In the case of corrosion rate modeling, measurements of environmental parameters such as T, pH, RH, etc. comprise the input vectors $\mathbf{x}_i$

while the corresponding measurements of annual corrosion rate $A$ are represented by the output values $y_i$. In SVR analysis, the goal is to find a function $\hat{y}(\mathbf{x})$ that has a constrained amount of deviation $\varepsilon$ from the observed targets $y_i, i = 1,2,...N_{tr}$ for the entire set of training data, and at the same time has the least complexity to prevent overfitting. For the simple case of linear functions, SVR algorithms seek the optimal coefficients for the function of the form

$$\hat{y}(\mathbf{x}) = \mathbf{w}^T \cdot \mathbf{x} + b \tag{17}$$

where $\mathbf{w}$ is the weight vector (a column vector representing the regression coefficient for each environmental variable), $(.)^T$ denotes the transpose operation, and $b$ is a constant. In Eq. (17), the least complex—or the *flattest*—function that is always within $\varepsilon$ from the observed targets $y_i$ is achieved by minimizing the norm of the weight vector $\mathbf{w}$.

The dot product in Eq. (17) can be replaced with a *kernel function* to increase the computational power of linear SVR. This replacement is called *kernel substitution* where the input data is mapped into an equivalent dual representation in which the predictions are based on linear combinations of a kernel function evaluated at the training data points. Using the kernel function notation, Eq. (17) can be expressed as:

$$\hat{y}(\mathbf{x}) = \sum_{j=1}^{N_{SV}} \nu_j \, k(\mathbf{x}_j, \mathbf{x}) + b \tag{18}$$

where $\mathbf{x}$ is an input vector for which the value of the predictive function $\hat{y}(\mathbf{x})$ is sought, $\mathbf{x}_j, j = 1,2,...,N_{SV}$ are *support vectors* that are a subset of original inputs $\mathbf{x}_i, i = 1,2,\ldots,N_{tr}$ from the training dataset, $N_{SV}$ is the number of support vectors, $\nu_j$ are non-zero optimization constants, and $k(.,.)$ represents the kernel function operating on $\mathbf{x}$ and $\mathbf{x}_j$. As can be seen from Eq.(18), the

predictive regression function $\hat{y}(\mathbf{x})$ can be completely described as a linear combination of the support vectors $\mathbf{x}_j$ (which in turn are a subset of the training inputs $\mathbf{x}_i$), optimization constants $\nu_j$, and constant $b$. SVR models are trained by solving a quadratic optimization problem from which the optimization constants $\nu_j$ and the subset of the training dataset that make up the $N_{SV}$ support vectors $\mathbf{x}_j$ are determined [80]. In this study, the LIBSVM library that uses the Sequential Minimal Optimization (SMO) method for the solution of the optimization problem is used [81].

Table 5 displays the four common SVR kernels used in this study.

Table 5: SVR kernels used in this study

| kernel type | kernel function | | kernel parameters |
|---|---|---|---|
| linear | $k(\mathbf{a},\mathbf{b}) = \mathbf{a}^T \cdot \mathbf{b}$ | (19) | - |
| polynomial | $k(\mathbf{a},\mathbf{b}) = (\gamma(\mathbf{a}^T \cdot \mathbf{b}) + c_0)^d$ | (20) | $\gamma > 0$ : coefficient of polynomial<br>$c_0 \geq 0$ : additive constant<br>$d \in \mathbb{N}$ : degree of polynomial |
| radial basis function (RBF) | $k(\mathbf{a},\mathbf{b}) = e^{-\gamma\|\mathbf{a}-\mathbf{b}\|^2}$ | (21) | $\gamma > 0$ : width of the RBF |
| sigmoid | $k(\mathbf{a},\mathbf{b}) = \tanh\left(\gamma(\mathbf{a}^T \cdot \mathbf{b}) + c_0\right)$ | (22) | $\gamma > 0$ : coefficient of sigmoid<br>$c_0 < 0$ : additive constant |

Note: $\mathbf{a}, \mathbf{b}$ are column vectors.

## Methods of Model Validation

Estimating the performance of a model developed by supervised learning algorithms is necessary for both choosing a suitable learning algorithm and determining future prediction accuracy. During the training of a learning algorithm, an objective error function such as the root-mean-squared error (RMSE), $\sqrt{\frac{\sum_{i=1}^{N_{tr}} (\hat{y}(\mathbf{x}_i) - y_i)^2}{N_{tr}}}$, between the estimated output and the measured output is minimized. However, the true measure of performance for a learning algorithm is its prediction accuracy on *unseen* data outside the training set: either a test set that was held out from the original dataset or future data once it becomes available. Failure of a learning algorithm that shows a good fit to the training set in achieving similar performance on unseen data, or in other words failing to generalize to unseen data, is called *generalization error*. *Cross-validation* has been shown to prevent this error in the model selection process for real-world datasets similar to the one used in this study [16].

In cross-validation (CV), the original dataset $D$ that consists of $N$ input-output pairs is randomly split into *k* mutually exclusive subsets, or *folds*, $D_1, D_2, ..., D_k$ of approximately $N/k$ pairs each. The learning algorithm is trained and tested *k* times; for each fold $j, (j = 1, 2, ..., k)$ a predictive model is created by training on the subset of the original data without the j-th fold ($D \setminus D_j$) and tested on the j-th fold $D_j$ to measure the model performance. At the end of cross-validation, $k$ performance measures are obtained for each trained model, from which the average performance and standard deviation of errors can be calculated to measure the accuracy of the learning algorithm on the

original dataset. 10-fold cross-validation ($k$=10) was used in this study as it has been shown to reduce the variance in model errors across different folds for datasets of similar size to the ones used in this study [16].

Two of the supervised learning methods used in this study (ANN and SVR) require the selection of kernel and tuning parameters that have a direct effect on the prediction performance of the trained models. Table 6 lists the parameters to be optimized for each method used in this study. The SVR algorithm has two internal parameters, $C, \varepsilon$ , and additional kernel parameters depending on the kernel type selected. The parameters to be tuned for the Multi-Layer Perceptron (MLP) type of ANN are the number of neurons ($n_H$), and the type of activation function ($g_H$) for the hidden layer. In order to find the model with the highest prediction accuracy, optimal parameters need to be found from a search space that is appropriate for each parameter. The search for optimal parameters is driven by a grid-search approach for discrete parameters ($n_H$, $g_H$, d) and an evolutionary computation approach [82] for continuous ones ( $C, \varepsilon, \gamma, c_0$ ).

Table 6: Parameters for learning algorithms used

| Learning Method | | Parameters | |
|---|---|---|---|
| SVR | Kernel Type | Kernel parameters | SVR parameters |
| | Dot Product | - | $C, \varepsilon$ |
| | RBF | $\gamma$ | |
| | Polynomial | $\gamma, d, c_0$ | |
| | Sigmoid | $\gamma, c_0$ | |
| ANN (MLP)[a] | | Parameters $n_H$, $g_H$ | |

a ANN with sigmoid, linear, tanh, sine, logarithmic, and Gaussian activation functions was tested.

Three performance metrics are considered to evaluate the prediction performance of trained models in this study: (1) root mean squared error (RMSE); (2) mean absolute error (MAE); and (3) $R^2$. The first two metrics are scale-dependent measures that have the same unit (*μm/year*) as the estimated output variable – the annual corrosion rate. The MAE is an average of the *N* absolute errors $|e_i| = |\hat{y}_i - y_i|$, where $\hat{y}_i$ is the predicted value and $y_i$ the measured value, for $i = 1, 2, \ldots, N$. It can be used to gather a general idea of the prediction performance of a trained model by comparing it with a typical range of predicted values. The RMSE is the square root of the second moment of the error and, therefore, incorporates both the variance and the bias of the predictive model. It is used in this study during feature selection and model training stages to evaluate the performance of trained models. The $R^2$ coefficient of determination is a unitless statistical measure, between 0 and 1, that indicates how well data fits a predictive model:

$$R^2 = 1 - \frac{SS_E}{SS_T} = 1 - \frac{\sum_{i=1}^{N}(y_i - \hat{y}_i)^2}{\sum_{i=1}^{N}(y_i - \bar{y})^2} \quad (23)$$

Where $\bar{y}$ is the mean of the $N$ measured values $y_i$, $SS_E$ is the sum of squared prediction errors, $SS_T$ is the total sum of squared differences of each $y_i$, and $\bar{y}$. An $R^2$ of 1 indicates that the predictions of the model perfectly fit the measured data.

Now that the general concepts of the data-based methodology and the data to be used have been presented, the two-step procedure to determine the predictive corrosion rate model will be discussed in detail as follows: (1) selection of the subset of the environmental variables that yields the highest prediction accuracy; (2) development of the annual corrosion rate estimation model based on the selected environmental variables.

## Selection of the Most Relevant Environmental Variables

The data-based methodology for finding the subset of environmental variables that leads to the highest prediction accuracy can be summarized as: (1) creating combinations of available environmental variables (e.g. (T, pH, RH)); (2) training predictive models for each combination using a learning algorithm; (3) testing the models on test data to find the best performing subset. An additional challenge is faced since the majority of the considered learning algorithms have their own parameters (e.g. kernel parameters for SVR, the number of neurons and layers for ANN) that need to be tuned to produce the best results. It has been shown that selecting both the subset of variables and optimal parameters within a single cross-validation (CV) loop introduces significant

bias to the selection process and leads to overfitting and generalization errors [83]. In order to prevent such bias, the variable subset selection and testing has to be independent of the parameter tuning process for the learning algorithm. This independence can be achieved by embedding the parameter tuning process with its own (inner) CV loop for finding the best parameter values for a given subset of environmental variables inside an outer or wrapper CV loop that computes the error estimate for the model trained with the optimized parameters in the inner CV loop. The wrapper CV loop uses test data that has been withheld from the inner CV loop so that this data is not used at any step in the model training process, ensuring that testing is independent of the parameter tuning process. This approach of nesting the parameter tuning CV loop within the variable selection CV loop is called *nested cross-validation* and has been shown to be superior to other selection methods for numerous real-world and artificial datasets [84].

Another method to ensure the validity of the selection process is the introduction of a number of randomly generated, non-physical variables and entering them into the variable selection process alongside the actual variables. The variable selection process is expected to eliminate these random, or noise, variables as they are independent of the output value to be predicted, and the inclusion of any such variable in the final selected subset indicates the failure of the learning algorithm used in the selection process.

The flowchart of the algorithm for selecting the most relevant environmental variables or features using nested CV from a corrosion database that consists of $N_V$ environmental input variables (T, pH, RH, etc.) is presented in Figure 27. The algorithm is repeated for each learning algorithm (also repeated for each SVR kernel and $g_H$ for ANN) and is outlined as follows:

1. $N_R$ "Random" or "Noisy" features ( $R_1, R_2, ..., R_{N_R}$ ) generated by a random number generator, are combined with the $N_V$ input variables of the corrosion database, producing a "Noisy Dataset" that consists of $N_V + N_R$ inputs and the associated corrosion rate values (for the $N_V$ real input variables).
2. The Wrapper CV Loop is the external loop that performs 10-fold CV on the Noisy Dataset. The dataset is split into 10 mutually exclusive partitions (folds) of equal size. At each iteration, 90% of the data (L1) is passed to the inner feature selection block, and the remaining 10% (T1) is withheld from the inner block for subsequent testing of models trained with different subsets of features. In the flowchart, this first level of partitioning is denoted by L1 for training data and T1 for test data. A new training set L1 is passed to the Feature Selection block for each of the 10 folds of the wrapper CV loop. After ten iterations, mean error values (RMSE and MAE) are calculated for all possible subsets of features. The feature subset with the lowest mean RMSE of the 10 CV folds is selected as the optimal feature subset for the learning algorithm currently used and returned as the final output of the feature selection algorithm, along with the associated error values for each CV fold.
3. The Feature Selection Block first generates feature subsets from all possible combinations of the $N_V + N_R$ input parameters ( $N_V$ real and $N_R$ random). Next, a set of tuning parameters (e.g., $\gamma, d, c_0$ for SVR with the polynomial kernel) are generated and passed on to the Inner CV loop along with L1 and the current subset of inputs (e.g. $R_1$, T, RH). The inner CV loop performs 10-fold CV and returns the mean error for the current parameter values and feature subset back to the Feature Selection Block. Following this, the returned error value is

compared against two termination criteria: (a) returned error is below the convergence error; (b) no improvements occurred in the last 1000 parameter set generations. If neither termination criterion is met, a new parameter set is generated using grid-search for discrete and evolutionary computation for continuous parameters. The new set of parameters is passed to the Inner CV loop, and the parameter generation process is repeated until either one of the termination criteria is met. The parameter set at termination is then accepted as the optimal one for the current feature subset. The Feature Selection Block is repeated for each feature subset combination until all feature subset combinations have been considered. Finally, all feature subsets and their optimal parameter sets are passed back to the outer Wrapper CV loop.

4. The Inner Cross-validation Loop receives the current subset of inputs, a set of parameters, and an already partitioned training set L1. First, L1, which consists of 90% of the samples from the initial Noisy Dataset, is further partitioned into 10-folds of equal size; 90% of L1, or in other words, 81% of the Noisy Dataset is used for training (L2). The remaining 10% of L1 (9% of the Noisy Dataset) is retained as the test set (T2). After ten iterations of training and testing with every fold of data, the mean error values are returned to the Feature Selection Block to guide the search for the optimal parameter set for the current feature subset.

It is important to emphasize that the outputs of the feature selection algorithm are (i) the optimal feature subset for a specific learning algorithm and (ii) the associated errors obtained from the outer or wrapper CV loop. In addition to the mean errors (RMSE and MAE), 10 individual error values for each CV fold are also retained and will be used to evaluate the stability of the learning algorithm

for the feature subset selection process. Generally speaking, different optimal values are obtained for the tuning parameters at each fold of the outer CV loop. Since iteration of CV uses a training set L1 that is only slightly different than any other (only 11.1% of the training data is different between two training sets L1), the expectation is that all 10 predictive models trained during 10-fold CV using the same learning algorithm should be similar. If a learning algorithm is too sensitive to the changes in tuning parameters, it may train wildly dissimilar models – an undesirable trait that implies instability. The coefficient of variation (COV), defined as the ratio of the standard deviation to the mean, is a strong metric in assessing the stability of a learning algorithm on a particular dataset. COV of the errors from the outer CV loop can be calculated for each learning algorithm with its associated optimal feature subset from the retained error values for each fold. A low COV value, generally defined as COV<1, is indicative of low-variance and is a strong indicator of a learning algorithm's stability on the dataset used.

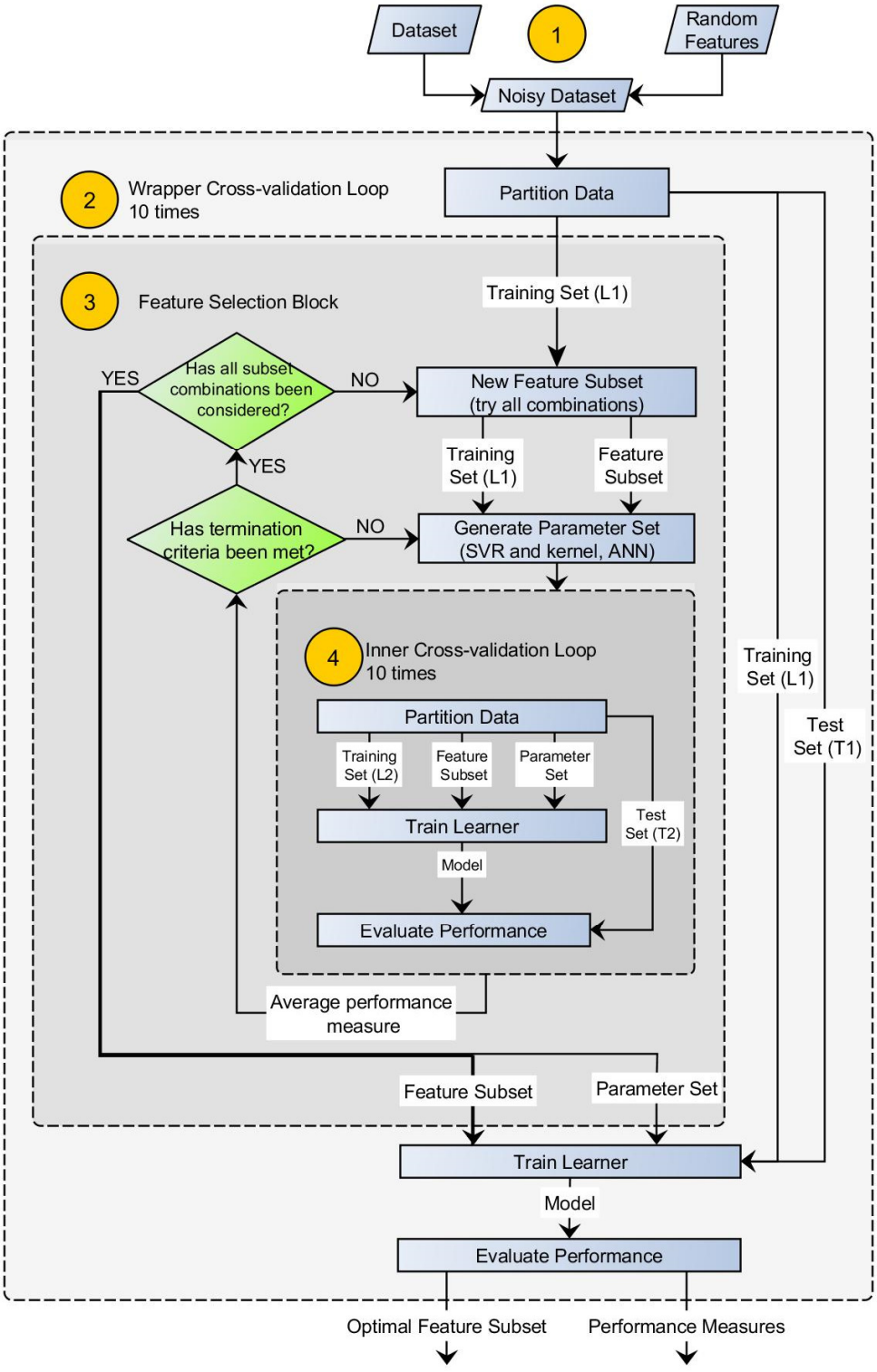


Figure 27: Flow chart of the Feature Selection algorithm

At the end of the feature selection process, the best subset of environmental variables is chosen for each learning algorithm by the feature subset selection process. The best performing environmental variable subset and learning algorithm pair is then selected by comparing learning algorithms by their prediction accuracy, stability, and by their ability to eliminate the random features introduced at the beginning of the selection process. Next, the chosen environmental variable subset and learning algorithm pair will be used to develop the model for estimating the annual corrosion rate of carbon steel for any new set of values of the environmental variables.

## Model Development

At this point, a model to estimate the annual corrosion rate of carbon steel can be trained from a corrosion database that consists of measured environmental variables and the corresponding annual corrosion rates, using the learning algorithm selected in the feature selection process.

Figure 28 displays the algorithm for obtaining the corrosion rate prediction model from a corrosion database using the selected learning algorithm. The database contains only the environmental variables selected by the feature selection algorithm (Figure 27) as inputs and associated corrosion rate measurement values as the output. 10-fold CV block is again used to determine the optimal tuning parameters for the learning algorithm. Upon completion of this search, the optimal parameter set and the mean CV error are obtained. The common practice is to create the final model by training on the entire dataset using the optimal tuning parameters since a larger dataset used in training generally improves the prediction accuracy of a model [85,86]. The mean error observed over all 10 folds of CV provides an estimate of the prediction accuracy of the model trained on the

entire dataset [87]. The true prediction accuracy of the model trained on the entire dataset is expected to be better than this estimate since a larger dataset is used in training (100% of the data is used compared to 90% used in each run of the 10-fold CV). The output of the algorithm is the annual corrosion rate model that predicts the corrosion rate for the previously selected set of environmental inputs.

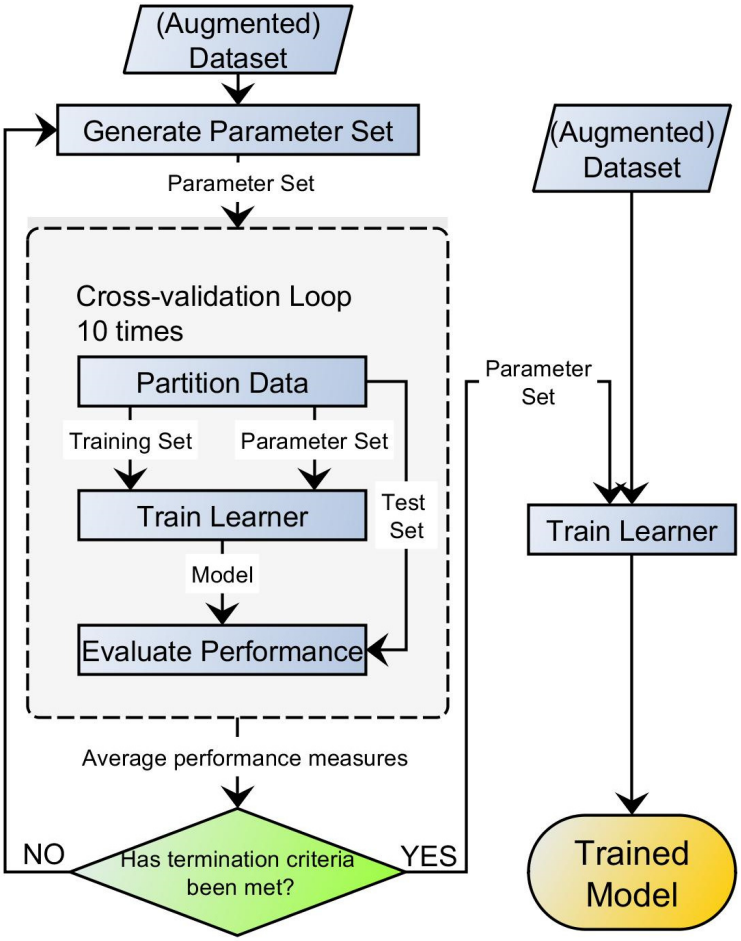


Figure 28: Flow chart for obtaining the predictive corrosion rate model

The data-based methodology to develop a model that predicts the annual corrosion rate of carbon steel is dependent upon the selection of the most relevant environmental variables and training the final predictive model using the selected variables. Subsequently, implementation of the aforementioned methodology requires the selection of an adequate corrosion database in order to develop a model with high prediction accuracy.

## Compiling the Dataset

### Data from Atmospheric Corrosion Tests

A multitude of atmospheric corrosion tests performed on carbon steel worldwide is available in literature, providing extensive corrosion rate data for a broad range of environmental inputs. Atmospheric corrosion data from over 250 test sites in 33 countries was compiled from 14 unique references to establish the "worldwide" database. The reader is referred to Appendix A for the list of references employed, classified according to the countries from which the data was collected. In these tests, carbon steel specimens were exposed to varying atmospheric conditions for a year. The database has a total of 309 records for the measured annual corrosion rate versus six recorded environmental variables: temperature, relative humidity (%), time of wetness (period of time during which a surface layer of moisture is present on a metal, %), annual rain precipitation (mm), pH of rainwater, and chloride ion concentration (mg/L). Table 7 shows the basic statistical information associated with the compiled database.

Table 7: Basic statistical information on the worldwide atmospheric corrosion database

| Variable | Mean | Minimum | Maximum |
|---|---|---|---|
| Temperature (°C) | 15.23 | -3.10 | 29.82 |
| RH (%) | 68.70 | 33.33 | 91.10 |
| TOW (%) | 46 | 0 | 98 |
| Precipitation (mm) | 882 | 13 | 3677 |
| pH | 4.99 | 3.45 | 7.37 |
| $Cl^-$ (mg/L) | 12.35 | 0.01 | 192.7 |
| Annual Corrosion rate (μm/year) | 38.5 | 3.3 | 376.7 |

The worldwide dataset compiled from tests on carbon steel is extensive, yet, the data is not specific to bridge wires. On the other hand, carbon steels such as the bridge wire are not highly alloyed, and most grades exhibit similar corrosion rates [88]. The composition of carbon steel does not play an appreciable role on the corrosion rate unless the steel has high Cr content (Cr>12%) or is a high Si or Ni iron alloy [32]. Alloying elements such as Cu, Ni, Cr, and P that slow down the corrosion rate are either non-existent or only present in negligible quantities in carbon steels. Specifically, the bridge wire contains minimal alloying elements of around 0.7% Mn, 0.2% Si, and only trace amounts of P and S. Thus, the compiled dataset can be considered representative of the corrosion behavior of bridge wires.

The worldwide dataset is used to select the most relevant variables—out of the six available—that would affect the corrosion rate. This dataset will be complemented with bridge wire-specific data obtained in Chapter 2 from cyclic corrosion testing at different levels of the selected environmental variables. The final predictive model will then be developed using this augmented dataset.

## Selection of the Most Relevant Variables

The feature selection algorithm shown in Figure 27 is applied to the worldwide dataset to select the most relevant environmental variables out of the six available. In order to eliminate the scale bias introduced by the relative magnitudes of parameters, all input variables are scaled into the [-1,1] range by linear range transformation. In this linear transformation, the lower and upper bounds of each environmental input from Table 7 are used.

Table 8 presents the performance statistics for the investigated learning methods obtained from the feature selection process on the worldwide corrosion dataset. From these results, it is clear that SVR algorithms with RBF and polynomial kernels outperform the other learning methods due to their superior performance in all three metrics considered. Despite the fact that RBF and polynomial kernels yield virtually identical error statistics over the dataset, the RBF kernel is the better choice due to computational considerations: in fact, while polynomial type kernels require the selection of three kernel parameters, RBF type kernels only require the determination of a single parameter (see Table 6). With the addition of the two extra parameters for the SVR algorithm, the optimal parameter search for polynomial kernels becomes computationally expensive and prone to local minima. For this reason, the simpler of the two kernels that are performing equally well, RBF, is selected for corrosion rate modeling.

Table 8: Performance comparison of learning methods

| Learning Method | RMSE (μm/year) | | MAE (μm/year) | | $R^2$ | |
|---|---|---|---|---|---|---|
| | μ | σ | μ | σ | μ | σ |
| Linear Regression | 30.018 | 13.09 | 16.694 | 3.867 | 0.526 | 0.167 |
| MLP (Neural Network) | 27.198 | 11.56 | 16.223 | 4.952 | 0.721 | 0.161 |
| SVR | | | | | | |
| Linear | 31.15 | 15.341 | 16.205 | 6.111 | 0.513 | 0.193 |
| RBF | 13.958 | 4.888 | 9.153 | 2.521 | 0.836 | 0.106 |
| Sigmoid | 30.971 | 21.13 | 14.918 | 8.99 | 0.543 | 0.105 |
| Polynomial | 13.58 | 4.2 | 9.248 | 2.329 | 0.82 | 0.115 |

The model trained using SVR with RBF has a mean absolute error (MAE) of 9.153 μm/year. This error value represents 23.8% of the mean value of annual corrosion rates of the training dataset (38.5 μm/year). It should be emphasized, however, that the MAE is not the true expected error around the mean value as it (and also the RMSE) includes errors due to inherent scatter in the training data that can be attributed to measurement errors and different methods used to collect data from multiple sources.

The prediction accuracy of the trained model using SVR with RBF can be reviewed by comparing the $R^2$ value obtained with the ones reported in similar studies. Cai et al. [89] and Feliu et al. [90] performed modeling studies on atmospheric corrosion of carbon steel. Both studies use corrosion databases like the one used in this study, consisting of data collected from multiple countries. Cai et al. consider T, TOW, $Cl^-$, and sulfur dioxide ($SO_2$) concentration as inputs and use ANN in training

whereas Feliu et al. consider RH, TOW, T, $Cl^-$, and $SO_2$ as inputs and use linear regression. The $R^2$ value achieved using SVR with RBF of 0.836 indicates a better fit than 0.74 reported by Cai et al. and 0.62 by Feliu et al. It should be noted that this is not a direct comparison as each study uses different datasets and sets of environmental inputs.

Next, we turn our attention to the set of environmental inputs selected by each learning algorithm (Table 9). The top performing learners, SVR with RBF and polynomial kernels, chose [T, RH, pH, $Cl^-$] as the optimal feature subset. The coefficients of variation (COV) for RMSE and MAE errors recorded during feature selection using SVR with RBF are 0.35 and 0.27, respectively. Both values are well below 1 and point to the stability of the feature selection process. Therefore, the subset [T, RH, pH, $Cl^-$] is adopted as the relevant feature set for the corrosion rate modeling problem.

Table 9: Features selected for each learning algorithm

| Learning Method | Selected Features |
|---|---|
| Linear Regression* | [T, RH, TOW, Prec, pH, $Cl^-$] |
| MLP (Neural Network) | [T, RH, TOW, pH, $Cl^-$] |
| SVR | |
| Linear* | [T, RH, TOW, Prec, pH, $Cl^-$] |
| RBF | [T, RH, pH, $Cl^-$] |
| Sigmoid | [T, RH, TOW, pH, $Cl^-$] |
| Polynomial | [T, RH, pH, $Cl^-$] |

Features were selected from the set of variables: temperature [T], relative humidity [RH], time of wetness [TOW], annual precipitation [Prec], pH of rainwater [pH], and chloride concentration [Cl-]. Three features generated from random noise were also added to the feature set for validation purposes.

* Learning method failed to eliminate all three noise attributes.

At this point, the final corrosion rate model can be trained using the selected subset of environmental variables from an augmented dataset that is created by joining the worldwide data outlined in Table 7 with cyclic corrosion test data specific to bridge wires.

## Augmented Dataset for Bridge Wires

### Cyclic Corrosion Tests

The data available in the literature do not specifically refer to bridge wires; therefore, it was decided to augment this worldwide dataset with the data collected from cyclic tests on bridge wires. Thus, information particular to bridge wires could also be included in the database. The testing program and the associated corrosion dataset is given in Table 2.

### Input Scaling for Cyclic Test Data

In order to accelerate the corrosion process in the laboratory environment, the cyclic tests were run in environments harsher than typical atmospheric conditions. Hence, to combine the data from cyclic tests with the compiled worldwide atmospheric corrosion data, all input parameters—temperature, relative humidity, pH, and chloride content—have to be scaled into ranges typical of atmospheric conditions and suspension bridge cable environment. Consequently, the corrosion depth values measured after the 48-cycles long tests also have to be converted into annual corrosion rate values.

In order to convert values estimated in cyclic tests into annual corrosion rates, a scaling factor needs to be established between corrosion depth after 48-cycles of testing and that after one year of ambient exposure. The conversion is achieved by comparing the average values of lower, mean and upper corrosion rates estimated by Eiselstein and Caligiuri [15] for bridge wires in service to the rates measured in cyclic tests that represent the mildest, average, and harshest conditions, respectively. Among the 18 cyclic tests, 4 of them were chosen as representative of the cable's interior environmental conditions. Test 1, performed at the lowest temperature (T=30˚C), the lowest $Cl^-$ concentration ($Cl^-$ concentration=100ppm) and the most neutral pH (pH=6), was chosen to represent the mildest conditions. Similarly, Test 18, performed at the opposite extremes (T=45˚C, $Cl^-$ concentration=500ppm, pH=3), was chosen to represent the harshest conditions. Tests 5 and 14 were performed at intermediate values of temperature (T=35˚C) and pH (pH=4) and $Cl^-$ concentrations of 100 and 500 ppm, respectively and were chosen as representative of average conditions. Table 10 shows the scaling factors calculated by dividing annual corrosion rate estimates by the corrosion depth estimated after 48-cycles of testing for each representative condition. Since the four scaling factors calculated for the three representative conditions are within 10% of each other, an average scaling factor of 1.92 is applied to the corrosion depths for all 18 tests to bring the corrosion rates from cyclic tests to annual corrosion rates. This conversion estimates each 48-cycle test to be equivalent to 0.52 years in service.

Table 10: Scaling factors for corrosion depth values in cyclic corrosion tests

| Cyclic test | Representative condition | Corrosion depth after 48-cycles (μm) | Annual corrosion rate estimate[a] (μm/year) | Scaling factor | Scaled Annual Corrosion Rate (μm/year) |
|---|---|---|---|---|---|
| Test 1 | Mildest | 14.87 | 28 | 1.88 | 28.71 |
| Test 5 | Average | 19.56 | 40 | 2.04 | 37.77 |
| Test 14 | | 21.20 | | 1.89 | 40.93 |
| Test 18 | Harshest | 28.00 | 52 | 1.86 | 54.06 |
| Mean Value | | | | 1.92 | |

a Average corrosion rates estimated by Eiselstein and Caligiuri [15] for mild, average, and harsh conditions.

For the other variables, the overall relative humidity for all tests is calculated as 80% while the range of pH values of the solution sprayed on specimens is within the range of field conditions, and does not need scaling. The only parameters that need to be scaled are the temperature and the $Cl^-$ content. In fact, in the cyclic tests, temperature values of 30, 35, 45˚C and solutions with $Cl^-$ contents of 100 and 500 ppm were used to accelerate corrosion reactions. These ranges correspond to higher temperatures and $Cl^-$ concentration values than the ones that occur in bridges (usual temperature range: from 0 - 35˚C, $Cl^-$ content: 0 – 20 ppm).

The scaling of temperature and $Cl^-$ values from cyclic tests is performed by taking advantage of the corrosion model developed from the compiled worldwide corrosion dataset of Table 7. First, by setting the RH to 80% used in all tests and the pH to the corresponding value used in Tests 1, 5, 14, and 18, temperature and $Cl^-$ values are varied to estimate the annual corrosion rate from the model. Then, curves of constant annual corrosion rate that is equal to the values given in Table 10 for each of the four tests are plotted. Figure 29 displays the plotted curves, where each plotted point

corresponds to the temperature and $Cl^-$ value pair that, along with the corresponding pH and RH values, produces the estimated annual corrosion rate that matches the scaled annual corrosion rate value for the particular test. Next, constraints of the scaling procedure are established by observing that the four tests shared the following common input values for temperature and $Cl^-$ content:

- Test 1 and Test 5 are carried out at the same $Cl^-$ content (100 ppm)
- Test 5 and Test 14 are carried out at the same temperature (35˚C)
- Test 14 and Test 18 are carried out at the same $Cl^-$ content (500 ppm)

It then follows that by enforcing the scaled temperature and $Cl^-$ content values to be the same for the test pairs above (e.g. Test 1 and Test 5 should have the same scaled input $Cl^-$ content value), a unique set of scaled temperature and $Cl^-$ content can be obtained. This is achieved by drawing lines of constant $Cl^-$ content between Tests 1 and 5, constant temperature between Tests 5 and 14, and constant $Cl^-$ content between Tests 14 and 18 (lines 1, 2, and 3 in Figure 29) and sweeping the lines until they intersect at the unique, scaled values of temperature and $Cl^-$. In this way, the tests that share original input values end up with the same scaled input values. For example, Tests 1 and 5 were both carried out with solutions of $Cl^-$ content equal to 100ppm; therefore, the corresponding scaled $Cl^-$ content values for both tests has to be equal (0.5 ppm). Figure 29 shows the scaled temperature inputs of 16.5, 20, and 29˚C that correspond to test temperatures of 30, 35, and 45˚C, respectively. Similarly, $Cl^-$ content of 0.5 and 2.5 ppm correspond to test values of 100 and 500 ppm.

Table 11 shows the scaled experiment data that will be combined with the worldwide atmospheric corrosion data to train the final annual corrosion rate ( $A$ ) model.

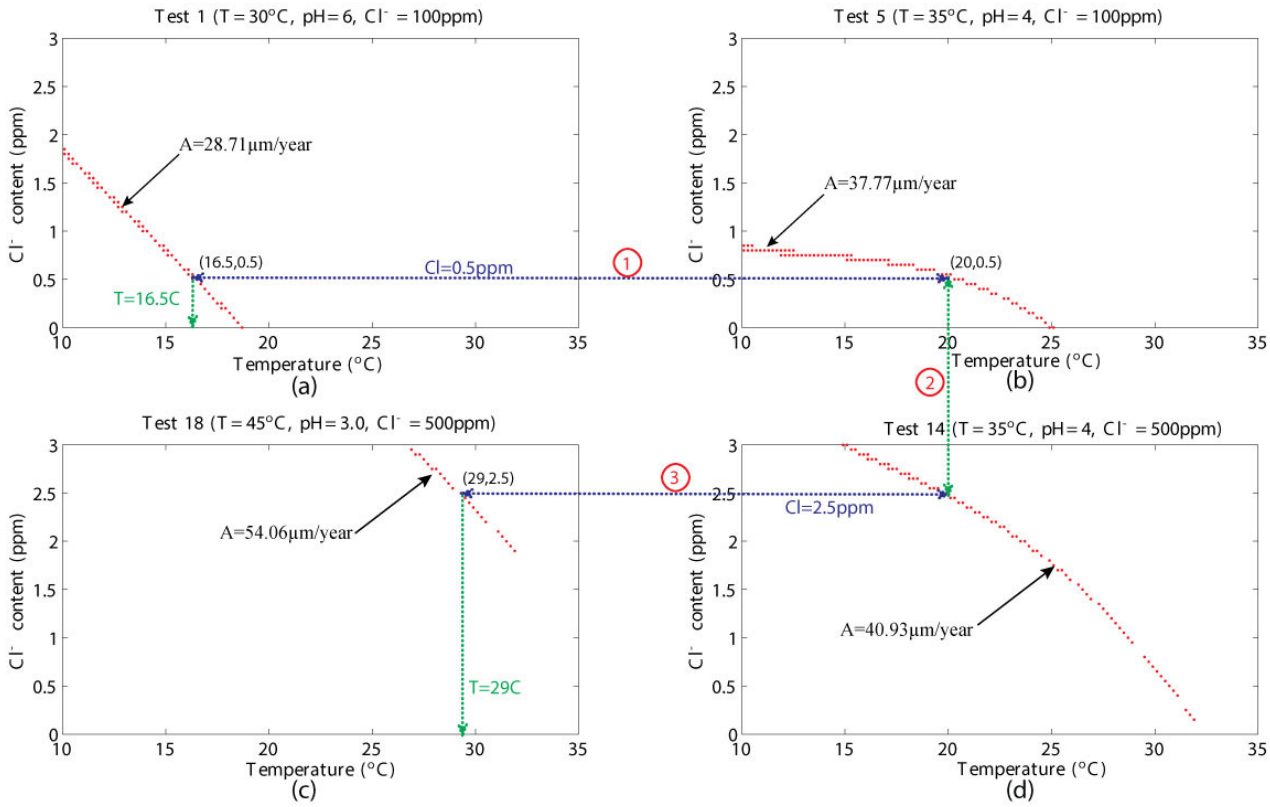


Figure 29: Scaling of Temperature and $Cl^-$ content inputs

Table 11: Scaled inputs and corrosion rates for cyclic tests

| Test No. | Temperature (°C) | RH (%) | pH | $Cl^-$ (mg/L) | Scaled Annual Corrosion Rate (μm/year) |
|---|---|---|---|---|---|
| 1 | 16.5 | 80 | 6 | 0.5 | 28.71 |
| 2 | 20 | 80 | 6 | 0.5 | 32.19 |
| 3 | 29 | 80 | 6 | 0.5 | 34.62 |
| 4 | 16.5 | 80 | 4 | 0.5 | 34.14 |
| 5 | 20 | 80 | 4 | 0.5 | 37.77 |
| 6 | 29 | 80 | 4 | 0.5 | 40.91 |
| 7 | 16.5 | 80 | 3 | 0.5 | 37.73 |
| 8 | 20 | 80 | 3 | 0.5 | 40.08 |
| 9 | 29 | 80 | 3 | 0.5 | 47.02 |
| 10 | 16.5 | 80 | 6 | 2.5 | 30.14 |
| 11 | 20 | 80 | 6 | 2.5 | 33.54 |
| 12 | 29 | 80 | 6 | 2.5 | 42.92 |
| 13 | 16.5 | 80 | 4 | 2.5 | 36.22 |
| 14 | 20 | 80 | 4 | 2.5 | 40.93 |
| 15 | 29 | 80 | 4 | 2.5 | 46.73 |
| 16 | 16.5 | 80 | 3 | 2.5 | 39.93 |
| 17 | 20 | 80 | 3 | 2.5 | 45.76 |
| 18 | 29 | 80 | 3 | 2.5 | 54.06 |

# Results and Discussion

## Corrosion Rate Model from Augmented Dataset

The final annual corrosion rate model is trained on the augmented dataset that is created by joining the worldwide data and the scaled cyclic corrosion test data. SVR with an RBF kernel is used along with the feature subset [T, RH, pH, $Cl^-$], following the flowchart shown in Figure 28.

## Trained model and performance

Once the data from cyclic testing has been scaled, it is combined with the data set obtained from the available literature to form an augmented database that is then used to determine a proper corrosion rate model suitable for bridge wires. The final corrosion rate model is defined by support vectors $\mathbf{x}_j$ containing [T, RH, pH, $Cl^-$], optimization constants $\nu_j$, constant $b$ from Eq. (18) and RBF kernel parameter $\gamma$ from Eq. (21). Appendix B lists the complete set of 175 support vectors $\mathbf{x}_j$ and their associated constants $\nu_j$. The optimization process based on the 10-fold CV shown in Figure 28 estimated the optimal SVR parameters $C, \varepsilon$ as 45.0 and 6.1, respectively. $\gamma = 0.091$ was obtained as the optimal RBF kernel parameter and constant $b$ was calculated as 85.95.

These parameters can be substituted in Eq. (18) to yield the predictive function to estimate the annual corrosion rate $A$ as:

$$A(\mathbf{x}) = \sum_{i=1}^{175} \nu_i \exp\left(-0.091 \left\| \mathbf{x}_i - \mathbf{x} \right\|^2\right) + 85.95 \tag{24}$$

In Eq.(24), all environmental inputs should be linearly scaled into the [-1,1] range as a preprocessing step, the same way as the environmental inputs were transformed in the selection and model training processes previously. In this linear transformation, the lower and upper bounds of each environmental input used in training from Table 7 shall be used. The corrosion rate model in Eq. (24) produces non-negative corrosion rate values for all inputs in the range of variables used in training the model. For inputs outside of these ranges, there is no guarantee that the model will

produce realistic or non-negative rates. Therefore, it is recommended that any input value outside of these ranges be mapped to the appropriate minimum or maximum value for that variable given in Table 7 (e.g. an RH value of 30% would be mapped to the lower bound of RH inputs used in training: 33.33%)

Table 12 shows the performance measures obtained for the corrosion rate model on the augmented dataset. These values are in line with the ones reported for the SVR model with RBF kernel on the data set obtained from the literature reported in Table 8, and the same analysis of results applies here.

Table 12: Evaluation of model's generalization performance. Performance measures used are root mean squared error (RMSE), mean absolute error (MAE), and squared correlation coefficient ($R^2$)

| Learning Method | RMSE | MAE | $R^2$ |
|---|---|---|---|
| SVR (RBF kernel) | 19.80 | 10.96 | 0.805 |

## Discussion of Corrosion Rate Model

The results of a sensitivity analysis conducted on the trained SVR model help shed some light on the nonlinear interactions between the corrosion rate and the relevant subset of environmental variables: temperature, relative humidity, pH, and chloride concentration. These interactions can be clearly seen in Figure 30, where the corrosion rate is plotted against one of the chosen environmental variables, while the three remaining variables are prescribed around their mean values in the augmented corrosion database.

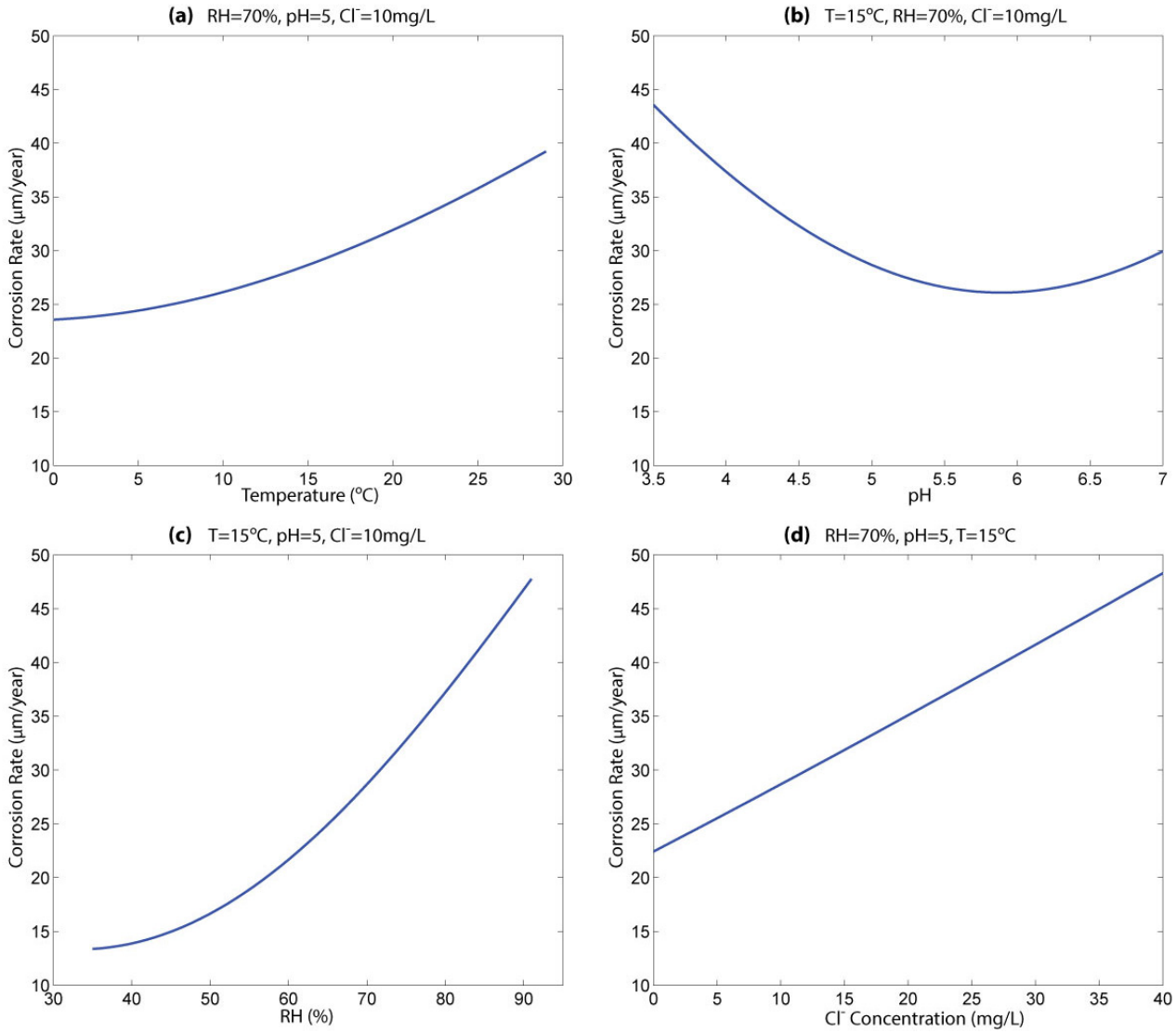


Figure 30: Corrosion rate vs. each environmental variable

Figure 30a shows the variation of corrosion rate with respect to temperature. The observed trend is an exponential increase at lower temperatures that approaches a more linear increase at higher temperatures. This trend at higher temperatures is in agreement with the corrosion rate dependence observed in the cyclic tests presented in Chapter 2. While the corrosion rate follows the exponential trend as suggested in literature for metal corrosion at lower temperatures, the interaction of temperature with the other variables causes a departure from the exponential relationship at higher

temperatures, perhaps due to metal surfaces drying more quickly at higher temperatures. Figure 31 shows surfaces showing corrosion rate values plotted against the full range of $Cl^-$ and RH values at pH=5.0 for T=15, 21, 27°C. It can be seen that the corrosion rate increases with temperature over the full range of $Cl^-$ and RH. Additionally, the increase in the separation between surfaces at higher $Cl^-$ and RH values point to the accelerating effect of these two variables on the corrosion rate, with this effect being most pronounced when both $Cl^-$ and RH values are at their highest.

Figure 30b shows the variation of corrosion rate with respect to the pH of the solution. In agreement with the literature [75] and the results of cyclic corrosion tests used in this study, corrosion rate increases at lower pH values. In near-neutral conditions (5<pH<8), extensive studies on carbon steel corrosion show that the pH no longer plays a direct role in the corrosion process [75,77]. It can be observed from Figure 30b that the variation in corrosion rate in the pH=5 to 7 range is much smaller compared to the variation at lower pH values. While alkaline conditions are not typical of bridge cable environment, the corrosion rate of carbon steel typically decreases when pH>8 due to the catalyzing effect of pH on the formation of an oxidation layer that blocks the transport of electrons [33].

Figure 30c shows the variation of corrosion rate with respect to RH. An exponential relationship is observed between RH and corrosion rate when the other variables are kept at levels close to mean values. This result agrees with Suzumura et al.'s [12] findings for tests performed at the same $Cl^-$ concentration [12]. Figure 32 shows surface plots representing corrosion rate values plotted against the full range of pH and temperature values at a $Cl^-$ concentration of 1 mg/L for three different values of the RH. The annual mean corrosion rates, $A$, for the three plotted surfaces corresponding

to RH=35, 65, and 85% are 14.45, 25.10, and 41.56 µm/year, respectively, suggesting a substantial increase in the corrosion rate with increasing RH.

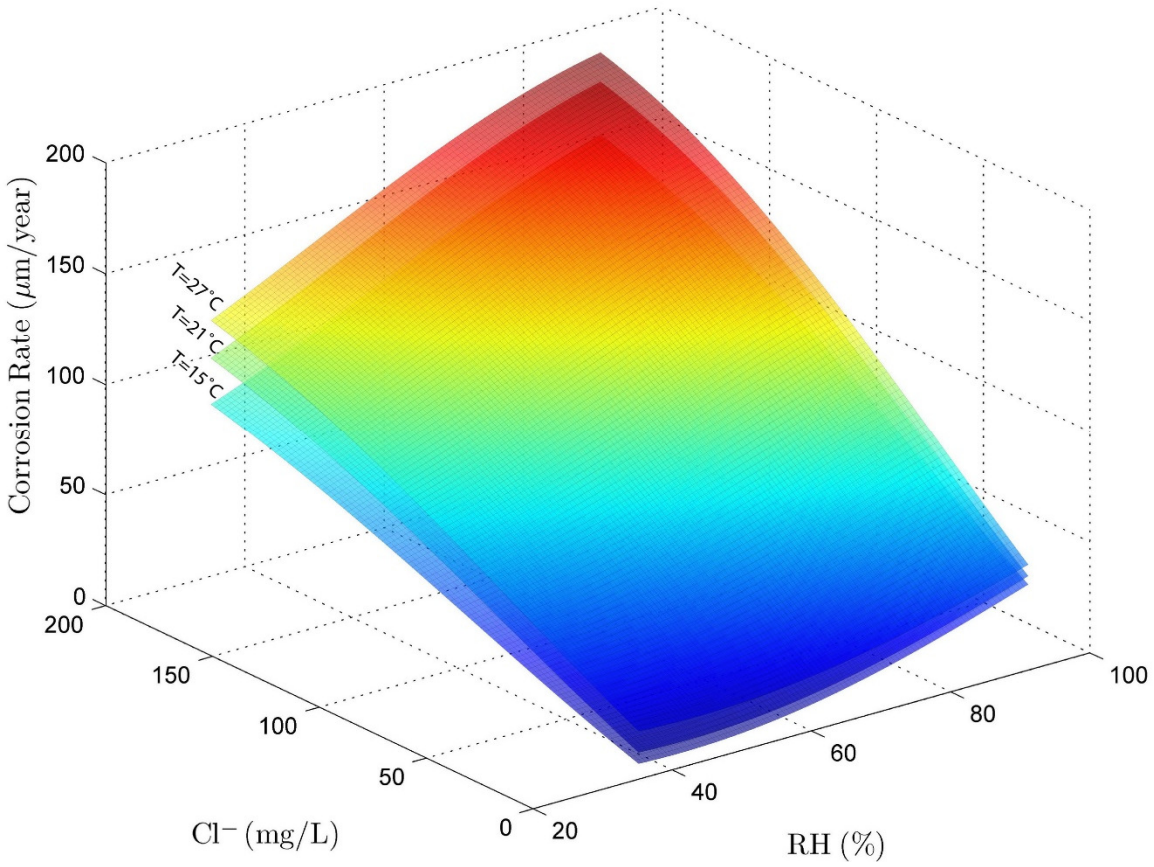


Figure 31: RH & $Cl^-$ vs. Corrosion Rate for different levels of Temperature, constant pH=5.0

Lastly, Figure 30d shows the change in corrosion rate with respect to $Cl^-$ concentration as the other variables are kept at a constant value near their mean values. The relationship in this environment appears to be almost perfectly linear. However, by inspecting the changing slopes of the plotted surfaces in Figure 31, it can be concluded that the relationship is not linear over the entire domain of

inputs and the rate of increase in corrosion rate due to $Cl^-$ decreases at higher RH values. This effect is likely due to the washing away of $Cl^-$ deposits from the metal surface at higher RH values.

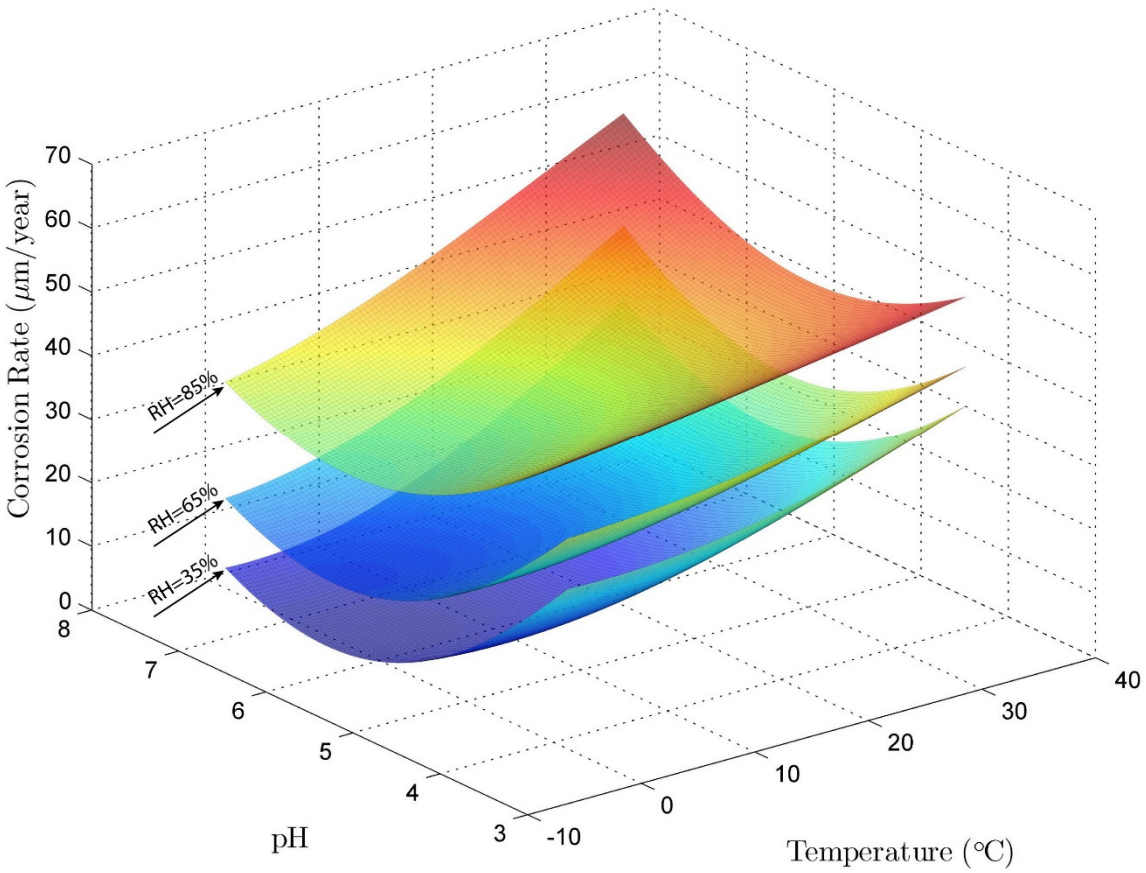


Figure 32: Temperature & pH vs. Corrosion Rate for different levels of RH, constant $Cl^-$=1 mg/L

## Summary and Conclusions

In this chapter, we proposed a time-dependent corrosion rate prediction model for bridge wires that also depends on environmental variables monitored within the cable. According to this model, the

cumulative corrosion depth for a bridge wire $C$ at any specific time during the service life of a cable is described by the equation

$$C(t, T, pH, RH, Cl^-) = A(T, pH, RH, Cl^-)t^n .$$

Due to the complexity of the interactions between environmental variables and the corrosion rate, data-based methods were used in this chapter to develop a model that predicts the annual corrosion rate $A$. The first step in the development of this model was the selection of the set of environmental variables that leads to the highest prediction accuracy. A feature selection algorithm using the wrapper cross-validation approach was applied to a corrosion database compiled from worldwide atmospheric tests that consisted of numerous environmental variables. Temperature, RH, pH, and $Cl^-$ were determined to be the environmental variables that lead to the highest corrosion rate prediction accuracy.

In order to improve the prediction accuracy of the model, cyclic test data presented in Chapter 2 was used to augment the worldwide corrosion database. The predictive model, trained using the augmented database, estimates the annual corrosion rate based on environmental inputs and captures the nonlinear nature of the corrosion process.

In the next chapter, the annual corrosion rate model developed in this chapter is extended to a full-fledged time-dependent model, completing the predictive model for estimating the corrosion rate of bridge wires.

# CHAPTER 4. LONG-TERM CORROSION AND ESTIMATION OF REMAINING CABLE STRENGTH

## Introduction

Given the harsh conditions to which suspension bridges are exposed, bridge main cables comprised of high-strength steel wires are inherently susceptible to corrosion. Recent inspections of this vital infrastructure have revealed wide-spread corrosion problems, raising concern regarding the safety of these deteriorated suspension bridge main cables. Determining the remaining strength of such bridge cables in their deteriorated state poses a critical challenge to inspection agencies during bridge safety assessments. The current practice of cable strength estimation uses data from a limited number of wires removed for tensile testing and visual gradation of wires into various stages of corrosion ranked according to severity (i.e. Stage 1 to Stage 4). Despite providing a straightforward means to organize corrosion data, this practice does not capture the condition of the wires across the cross-section of the cable nor along the entire length of the cable. Moreover, statistical approaches currently used in cable strength estimation [7] or random-field based methods that are built upon such statistical methods [52] also fail to estimate the decline in cable strength as corrosion occurs and provide a snapshot of the cable only at the time of an inspection. Given the substantial cost and lack of completeness associated with the current methods, an improved technique is needed to help bridge owners make better informed maintenance decisions. Predominantly, in order to estimate the decline in cable strength with time due to ongoing corrosion, a relationship between the cumulative corrosion of bridge wires—as induced by environmental conditions—and the remaining wire strength must be established.

As a first step to address this challenge, a framework for modeling the time-dependent corrosion rate of bridge wires was introduced in Chapter 3. This framework, as will be explored in further detail later in this chapter, relates the cumulative corrosion, $C$, after $t$ number of years to the annual corrosion rate, $A$, which is a function of the environmental conditions to which the cable is exposed, employing a relation of type $C(t) = At^n$. The missing piece of the puzzle in Chapter 3 was the exponent $n$, an exponential constant that is a function of the type of corroding metal and the environmental conditions to which the metal is subjected.

This chapter will complete this previously proposed framework, in an effort to develop a generic methodology for estimating the remaining strength of a suspension bridge cable. Specifically, an approach to determine the exponential constant $n$ is developed and used in the estimation of the remaining cable strength over time. Finally, two numerical examples are provided to demonstrate the strength of the proposed approach, focusing on the evolution of cable strength of the Williamsburg Bridge in New York City, and of a hypothetical, new bridge constructed with modern cable materials.

# METHODOLOGY

## Overview of the Strategy

The most straightforward way of finding $n$ would be to compare the initial and final area of several individual wires exposed to monitored environmental variables for the duration of $t$ years. However, information regarding the physical changes in bridge wires as a function of time is hard to come by due to various practical and technical difficulties. In most cases, data from two well-defined points within the lifetime of a wire—a minimum requirement to determine $n$ —is not available. Thus, a novel strategy that circumvents these limitations is required. In order to illustrate this strategy, it is first necessary to set the stage by briefly revisiting the fundamental expression of the framework proposed in Chapter 3.

In Chapter 3, the long-term corrosion of bridge wires is described in terms of section or thickness loss by the exponential expression

$$\begin{gathered} C(t,T,pH,RH,Cl^-) = A(T,pH,RH,Cl^-)t^n \\ or, \\ C(t,\mathbf{x}) = A(\mathbf{x})t^n \end{gathered} \tag{25}$$

where $C(t,T,pH,RH,Cl^-)$ is the cumulative corrosion after *t* years, usually measured in micrometers (μm), and $A(T,pH,RH,Cl^-)$ is the annual corrosion rate for a metal free of corrosion products, measured in μm per year, as a function of the environmental conditions— temperature (T), relative humidity (RH), pH, and chloride ion concentration ($Cl^-$)—to which the cable is

exposed. The selection process for the four environmental inputs (T, RH, pH, $Cl^-$) used in Eq. (25) is outlined in the previous chapter. The vector containing the four environmental inputs selected is expressed as $\mathbf{x}$ in short. Lastly, *n* is typically in the range [0-1].

A predictive model to estimate the annual corrosion rate $A(\mathbf{x})$ in Eq. (25) according to these four environmental input parameters is established in Chapter 3 using machine learning methods and an experimental corrosion database as:

$$A(\mathbf{x}) = \sum_{j=1}^{N_{SV}} \nu_j \exp\left(-0.091\left\|\mathbf{x}_j - \mathbf{x}\right\|^2\right) + 85.95 \tag{26}$$

where, $\nu_j$ are optimization constants, $\mathbf{x}_j$ are support vectors, and $N_{SV}$ is the number of support vectors. These variables are further defined and provided in Chapter 3 and Appendix B.

Expanding on the predictive model defined above, we propose that given the strength data for wires from a bridge known after $t$ years in service, the value of $n$, and hence the remaining strength of a bridge wire, can be determined in a six-step methodology. Before discussing the steps of the methodology, note that there are two main factors that have the potential to affect $n$: 1) the type of metal, and 2) the surrounding environmental conditions. In regards to the corrosion process, the chemical composition of a metal plays the most important role in dictating the rate of corrosion [88]. Since bridge wires are made from high-carbon steel grades with minimal additional alloying elements [88], similar corrosion rates are expected even across a range of wires installed in various suspension bridges. This leads to the key conclusion that for the majority of suspension bridge main cables (i.e. excluding those in bridges that experience atypical environmental conditions such as arctic or tropical environments), *n* may be considered a quasi-universal parameter. Consequently,

assuming that one has access to critical mechanical property data, i.e. the strength test data of bridge wires after $t$ years in service, $n$ needs to be determined for only a single, representative case. Using this information, it is possible to estimate the remaining strength of any bridge cable via the following steps, as summarized in Figure 33:

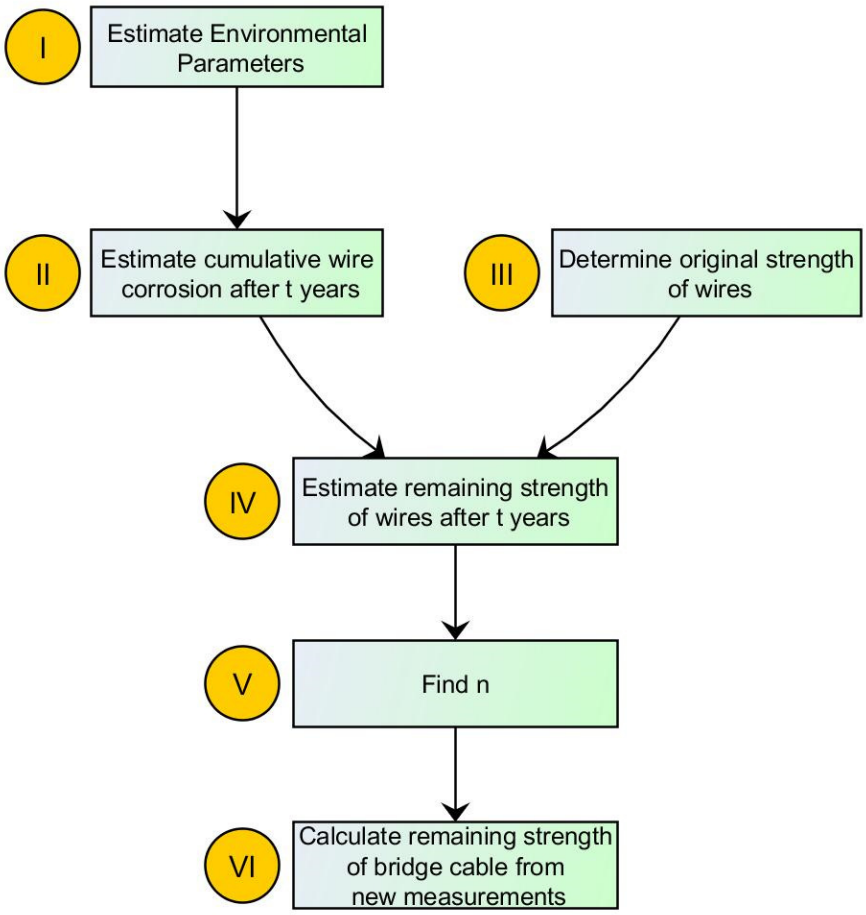


Figure 33: Six-Step Methodology

Step-I. Estimate the relevant environmental parameters (T, RH, pH, $Cl^-$, as discussed in the companion paper) that represent the environmental conditions to which each wire is subjected for the duration of $t$ years;

Step-II. Starting with hypothetical new (thus uncorroded) wires matching the cross section of the bridge under consideration, estimate the cumulative individual wire corrosion and remaining wire area after $t$ years using Eq. (25) and (26) for values of $n$ between [0-1];

Step-III. Based on strength data of uncorroded wire samples taken from the particular bridge in question, determine the original strength of individual wires and subsequently, calculate the initial strength of an entire cable;

Step-IV. Using the reduced individual wire areas calculated in Step-II, estimate the remaining strength of individual wires and ultimately, of the entire cable after $t$ years in service for the corresponding range of $n$ values;

Step-V. By means of comparison, find the value of $n$ that captures the in-situ corrosion behavior by matching the remaining cable strength after $t$ years in service—estimated in Step-IV—to the in-situ remaining cable strength estimated at the same time;

Step-VI. Once the $n$ value is determined, calculate the remaining strength of a bridge cable at any instant in time using measured environmental parameters.

As stated previously, this methodology relies on bridge cable strength data to provide a quasi-universal *n* value that can be used to estimate the remaining strength of a bridge cable at any point in time. To this end, the Williamsburg Bridge investigation program of 1988 is an excellent source of information [48]. It provides extensive tensile test data on bridge wires exhibiting various levels of corrosion after 85 years in service as well as uncorroded wires classified as brand new. The wires in the uncorroded condition are of particular importance as they can be considered to be representative of wires in the original condition when the bridge opened to service in 1903. It is thus clear that this valuable data set provides an invaluable benchmark, furnishing the additional data point required to establish the relationship between ongoing corrosion and reduction in cable strength over time. Accordingly, after establishing the environmental data for the region in Step-I to Step-II, the tensile test data taken from Williamsburg Bridge is used in Step-III to Step-V to set the basis for continuous estimation of remaining bridge cable strength in Step-VI.

In Step-IV and Step-V, the $n$ value is established by comparing the entire cable strength computed at two different points in time, as opposed to performing the same comparison for an individual wire. In this study, computation of the *n* value is restricted to this process due to the available data from the Williamsburg Bridge investigation: while tensile test data available for a sampling of individual wires from the time of the investigation lends itself to estimating the distribution of the strengths of individual wires within a cable section (described in detail later in this section in Step-III), it offers neither the wire area nor the tensile strength of a specific wire sample at two different points in time. Additionally, even though the environmental conditions at

the cable interior can be estimated for different areas of the cross-section (Step-I), the actual environmental inputs to which a specific wire is exposed during the considered time span is not known. The absence of these two vital pieces of information—test data from two different points in time and the actual environmental inputs at a given wire—precludes the determination of the *n* value for each individual wire since the calculated extents of corrosion (calculated using Eq. (25) ) need to be compared to the computed change between two test data points, corresponding to the same duration of time as well as the same environmental conditions. For this reason, the presented methodology estimates the *n* value by ensemble averaging the representations of a large collection of wires from all parts of the cable cross-section, exposed to environmental inputs estimated at their respective locations. This large collection of wires is chosen as the entire cable composed of the same number of wires as the Williamsburg Bridge for convenience and allowing direct comparisons to be drawn between the cable strength estimated at different times by the presented methodology and research published by others.

In the rest of the Methodology section, Step-I to Step-IV are described in detail. Specific emphasis is placed on Step-I—the estimation of relevant environmental parameters—, and Step-IV—the estimation of cable strength—, both of which required the development of dedicated sub-methodology. Step-V, a single step calculation, and Step-VI, the application of the method, are discussed in the Results section.

## Environmental Parameters at the Cable Interior (Step-I)

As shown in Chapter 3, T, RH, pH, and $Cl^-$ concentration are the environmental inputs most relevant for predicting the corrosion rate of bridge wires using Eq. (26) [91]. However, applying these inputs is complicated due to the fact that these parameters vary significantly across the cross-section of a cable [8,11,12]. For instance, Furuya et al. [11] observed that the T measured at the sides of the cable interior started lower than the external T in the morning, eventually surpassing it in the afternoon, while the interior T at the upper section of the cable interior was consistently higher than the external T. Sloane et al. [8] measured elevated RH levels near the cable surface, whereas lower RH levels were measured near the center. In order to calculate the corrosion rate of a specific wire within the cable cross-section, one needs to determine the environmental parameters at or in the vicinity of that wire. While continuous records of environmental data are readily available for the cable exterior from programs such as the National Atmospheric Deposition Program (NADP), there are no records of monitored data from within the interior of a cable, thereby complicating efforts to track cable corrosion rates over time.

In an effort to improve the prevailing bridge cable health monitoring practices, the Federal Highway Administration (FHWA) is aiming to implement monitoring systems capable of reading data from bridge cable interiors [92]. One such system is presented in Sloane et al. [8] and will soon become available for permanent installation in the interior of bridge cables. In this work, we use the results of a project in the FHWA research program [8], that specifically focused on collecting data from sensors installed at various locations inside a full-scale mock-up cable that

was exposed to cyclic T and humidity conditions. The mock-up cable represents a typical panel segment—the portion between consecutive cable bands—of a typical suspension bridge main cable. The core of the cable was composed of 61 hexagonal strands, each containing 127 high-strength steel wires of 5 mm diameter. Additional wires from 12 more strands were added around the circumference to complete a circular cross-section—producing a cable 50.8 cm in diameter and 6.10 m (20 ft) in length. T and RH sensors were placed throughout the cross-section of the mock-up cable, widely distributed by installing the sensors at various depths (outer, middle, and inner locations) along three directions inclined at 60° with respect to one another (Figure 34). Following the installation of the sensors, the mock-up cable was wrapped with aluminum foil tape, which served as a protective wrapping, preventing direct contact of the wires to the atmosphere and thus resembling the exposure conditions of a realistic suspension bridge main cable. The cable specimen was then enclosed within an atmospheric chamber designed to accelerate corrosion. During testing the cable was exposed to cyclic conditions that consisted of various combinations of humidity and temperature. The T and RH sensor data from the 50.8 cm diameter mock-up cable was recorded at 5 min intervals for the entire duration of each testing period.

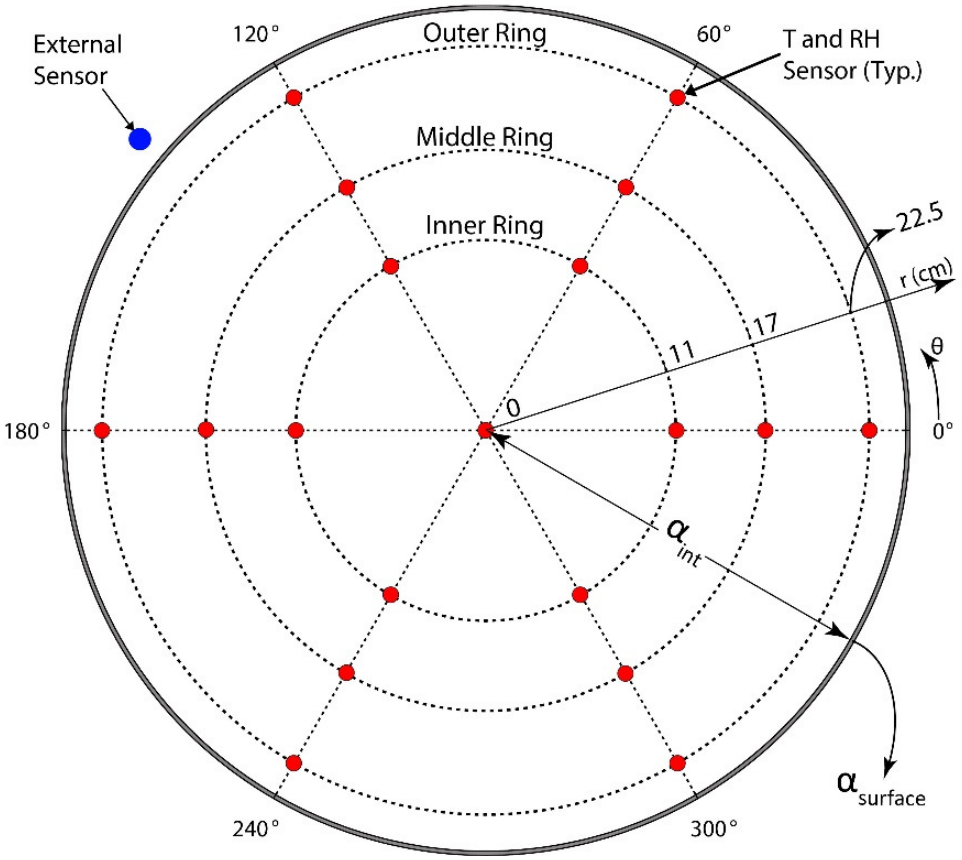


Figure 34: Mock-up Cable Cross-section [8]

In order to determine the T distribution within the cable cross-section as a function of the outside temperature, the heat equation given below in Eq. (27) is used together with data from one of the experimental tests from the study described above (Test 1, May 23, 2009 performed by Sloane et al. [8]) to relate the external temperature recordings to the measured temperature values at the sensors installed within the cable interior. The heat equation is a partial differential equation (PDE) that describes the variation of temperature in a given region over time: for the cable in question, this can be formulated as a 2-D problem in polar coordinates with origin at the center of the cable, resulting in the following expression for the heat equation:

$$T_t(r,\theta,t) = \alpha(r)\cdot(\mathrm{T}_{rr} + \frac{1}{r}T_r + \frac{1}{r^2}T_{\theta\theta}) \tag{27}$$

In Eq. (27), $T_t(r,\theta,t)$ is the partial derivative of the temperature at a given time, $t$, at a location characterized by radial distance, $r$, and polar angle, $\theta$ with respect to $t$. $\alpha(r)$ is the thermal diffusivity that measures the ability of a medium to conduct thermal energy relative to its ability to store it, as a function of $r$. $(T_r, T_{rr}, T_{\theta\theta})$ denotes the partial derivative of $T$ with respect to $r$, the second partial derivative of $T$ with respect to $r$, and the second partial derivative of $T$ with respect to $\theta$, respectively.

Given that a bridge cable is composed of axi-symmetrically distributed parallel wires of identical thermal properties, the thermal diffusivity, $\alpha(r)$, can be taken as a constant value over the cable cross-section. However, as described in Sloane et al. [8], the surface of the cable used in the study was covered with aluminum wrapping having different material properties than the cable interior. In order to account for this variation in thermal properties, the aluminum wrapping is modeled as a 0.5 cm thick exterior boundary layer with a different thermal diffusivity, described by the value $\alpha_{surface}$, and replaces $\alpha(r)$ in Eq. (27) for values of *r* that fall within the thickness of the exterior boundary layer. Similarly, the constant thermal diffusivity value at the interior of the cable is denoted by $\alpha_{\text{int}}$ (see Figure 34) and replaces $\alpha(r)$ at the cable interior.

Turning our attention now to the solution of the PDE given in Eq. (27), the boundary conditions imposed for the specific problem are defined as:

$$T(r = 25.4\,cm, 0 \le \theta < 360^{\circ}, t) = T_{ext}(t) \tag{28}$$

$$T_r(r = 0, 0 \le \theta < 360^{\circ}, t) = 0 \tag{29}$$

$$T(r = 25.4\,cm, \theta = 0^{\circ}, t) = T(r = 25.4\,cm, \theta = 360^{\circ}, t) \tag{30}$$

$$T_\theta(r = 25.4\,cm, \theta = 0^\circ, t) = T_\theta(r = 25.4\,cm, \theta = 360^\circ, t) \quad (31)$$

The first boundary condition in Eq. (28) sets the temperature at the cable surface to be equal to the actual temperature measured by the external sensor, $T_{ext}$ . Here it is assumed that the distribution of the surface temperature is uniform around the cable; in-situ cables deviate from this assumption due to various factors including exposure to the sun, however, given the monitored test conditions, a uniform distribution is a reasonable assumption for analyzing our test data. The second boundary condition specified in Eq. (29) indicates that zero heat flow is reached at the center of the cable, a boundary condition that is commonly used for transient heat conduction in circular, cylindrical and spherical media [93]. The final two boundary conditions in Eq. (30) and (31) are the periodicity conditions; $\theta = 0^\circ$ corresponds to the same point as $\theta = 360^\circ$ at $r = 25.4\,cm$ where the temperature is the same and the heat flow in the $\theta$ direction is continuous.

The finite difference method—a commonly used technique for numerically solving partial differential equations—is used to solve Eq. (27) [94]. In this technique, the circular cross-section is discretized into a mesh of $\Delta r$ and $\Delta\theta$ node spacings, while time is discretized into steps of $\Delta t$. For the problem at hand, $\Delta\theta$ =60$^\circ$ spacing is chosen in the tangential direction to match the distribution of sensors installed within the cable cross-section in Sloane et al.'s tests [8]. Similarly, a time-step of $\Delta t$ =5 min is used, which is equal to the data gathering interval applied in the same tests. In order to capture the temperature variation along the depth of the cable cross-section, a finer spacing of $\Delta r$=0.43 cm is chosen in the radial direction.

At this point, $\alpha_{\text{int}}$ and $\alpha_{surface}$ that define the thermal diffusivity characteristics of the bridge cable can be obtained by solving Eq. (27) for the available test data from Sloane et al. [8] by imposing the boundary conditions given in Eqs. (28)-(31). Once $\alpha_{\text{int}}$ and $\alpha_{surface}$ are obtained, the temperature distribution within any bridge cable can be approximated using Eq. (27) by setting $T_{ext}$ in Eq. (28) equal to the monitored external temperature.

Next, we shift our attention to determining the distribution of RH within a cable cross-section, a challenging task to complete. In fact, RH depends on multiple factors including, but not limited to, the change in T, the dew point temperature, the water vapor pressure, the equilibrium vapor pressure, and the location where water infiltrates the cable. As a result of these complex interactions, the RH distribution cannot be modeled through a set of differential equations as was done for the temperature distribution. Instead, a simplified estimation model has been developed based on experimental test data [8]. The mean value of all sensor measurements recorded during these tests are compiled in Table 13, categorized into various regions of the cable cross-section.

Table 13: Average RH (%) values measured during tests [8]

| | All | Top Half | Bottom Half | Top Half (Middle Column) | Top Half (Sides) | Bottom Half (Middle Column) | Bottom Half (Sides) | External |
|---|---|---|---|---|---|---|---|---|
| Cable Center[b] | 57.7 | - | - | - | - | - | - | |
| Inner Ring[b] | 60.4 | 61.6 | 59.2 | 58.3 | 63.3 | 36.7 | 70.4 | |
| Middle Ring[b] | 71.8 | 59.3 | 84.3 | N/A | 59.3 | N/A | 84.3 | |
| Outer Ring[b] | 78.9 | 77.5 | 83.3 | 59.2 | 86.6 | 83.3 | N/A | |
| Mean | 68.2 | 66.0 | 69.6 | 58.8 | 69.7 | 60.0 | 77.3 | 67.3[a] |

[a]External RH value is available for 4 tests between the dates May 23, 2009 and September 15, 2009.

[b]Figure 34 shows the location of sensors used in Sloane et al.'s tests.

Reviewing the presented data, it becomes apparent that RH increases with radial distance, yielding the lowest readings at the center of the cable and an increased reading as the location approaches the surface. In addition, it can be observed that RH is ~10% higher in the bottom portion of the cable compared with the top portion, due to the tendency of water to accumulate in the lower portion of the cross-section. Lastly, RH measurements are symmetric about the cable centroid in the horizontal direction. From the analysis of this data, it appears that the average reading from the sensor that recorded the external RH shows a good match with the mean value of all sensor recordings from within the cable. A linear relationship for establishing the internal RH value at a given location within the cable cross-section based on a recorded external RH value is obtained by minimizing the mean squared error (MSE) between the measured and the estimated RH values at all sensor locations. In this regression, MSE is expressed as:

$$MSE = \frac{\sum_{i=1}^{N_s} \left[ RH(y_i, r_i) - RH_{mea}(y_i, r_i) \right]^2}{N_s} \tag{32}$$

where $N_s$ is the number of RH sensors, $y_i$ is the vertical distance of sensor $i$ from the cable centroid in cm (positive values are in the up direction), $r_i$ is the radial distance of sensor $i$ from the cable centroid in cm, $RH(y_i, r_i)$ is the estimated RH value at the location of sensor $i$, and $RH_{mea}(y_i, r_i)$ is the RH value measured by sensor $i$ during testing. Using this technique, the following equation was obtained which enables the estimation of the RH value at any location $(y, r)$ within the cable cross-section based solely on the measured external RH value:

$$RH(y, r) = RH_{ext} - 0.13y + 0.81r - 10 \tag{33}$$

where $RH_{ext}$ is the external RH. As can be seen from the linear relation in Eq. (33), the RH at the cable centroid (y=0, r=0) is 10% lower than the value of the RH measured outside the cable, agreeing with the observations stated above.

The remaining environmental input parameters used in this study, pH and $Cl^-$ concentration, are estimated based on weekly local precipitation records from various stations in New York State between 1978-2008 [95]. Since the relationship between the internal distribution of pH and $Cl^-$ concentration and the externally measured values is unknown, it is assumed that the internal pH and $Cl^-$ concentration values at each wire match the externally recorded measurements.

## Cumulative Wire Corrosion (Step-II)

Using only external measurements and the techniques outlined in Step-I, we are able to establish the anticipated distribution of T, RH, pH, and $Cl^-$ concentration within a cable's cross-section at a given point in time. Once this information is provided, it is possible to calculate the long-term corrosion rate of a particular wire under the assumption of constant environmental variables. However, in practice these environmental inputs are not constant over time but continuously fluctuate within the cable. As a result, to account for the changing values of T, RH, pH, and $Cl^-$ concentration, the incremental corrosion of a wire must be calculated for each interval between consecutive measurements, assuming that the variables stay constant within the interval. The incremental corrosion depth, $\Delta C$, in μm that occurs during the time increment $\Delta t$ is calculated from Eq. (25) and (26) as:

$$\Delta C(\mathbf{x}, t, \Delta t) = C(\mathbf{x}, t) - C(\mathbf{x}, (t - \Delta t)) = A(\mathbf{x})(t^n - (t - \Delta t)^n) \tag{34}$$

where $\mathbf{x}$ is the input vector of T, RH, pH, and $Cl^-$ concentration, $t$ is the time elapsed since the start of steel corrosion in years (assumed to be the initial time of construction), $\Delta t$ is the time increment in *year* units (e.g. if parameters are measured hourly: $\Delta t$ is 1/8760 years), and $A(\mathbf{x})$ is the annual corrosion rate of an uncorroded wire from Eq. (26) in μm/year. Ultimately, the cumulative corrosion depth in μm after $t_{end}$ years, $C_{tot}(\mathbf{x},t)$, is obtained for each individual wire by summing the calculated incremental corrosion depths, using an increment equal to $\Delta t$:

$$C_{tot}(\mathbf{x},t) = \sum_{\substack{t=0 \\ increment=\Delta t}}^{t=t_{end}} \Delta C(\mathbf{x},t,\Delta t) \tag{35}$$

## Original Strength of Cable (Step-III)

The strength of a bridge cable may be estimated from tensile test data for a representative sample of individual bridge wires. During a cable inspection, it is common practice for wire samples of different lengths to be removed from the cable, cut into specimens of unit length, and tested for ultimate tensile strength (UTS—indicates stress, not force). From the UTS values of the unit length wire segments, a probability distribution function (pdf) is obtained and used in the calculation of the overall UTS of each individual wire. The strength of a wire of prescribed length is the minimum strength of the $N_{ul}$ unit-length segments (i.e. the weakest link model). In the UTS calculation of an individual bridge wire, the prescribed length is established as the *clamping length* of the wire. This is due to the fact that when a wire breaks (as a result of a defect or corrosion), friction forces enable the broken wire to regain its load carrying capacity after a certain redevelopment or clamping length (18.3 m or 60 ft) [48,51,52]). These friction forces arise due to the clamping force at each cable band and compaction force due to the outer wire

wrapping around the cable. Beyond the clamping length, the strength of a broken wire can be considered to be redeveloped in its entirety and will contribute fully to the cable strength.

Two approaches that have been used extensively in the estimation of cable strength are the one based on a Type I asymptotic distribution of the smallest value (Type I EVD) and the one based on Monte Carlo simulations of Independent and Identically Distributed Random Variables (IID R.V.) [48,50–52]. In these approaches, the strengths of successive unit-length segments along a wire of prescribed length are assumed to be uncorrelated. Recently, a contrasting approach known as the Random-Field based Method (RFM) has been developed by Shi et al. [52]. In this novel method, spatial correlation of the wire strength over a wire's length—an experimentally measured property of steel wires that is disregarded in the Type I EVD and IID R.V. methods—is also captured in the calculation of the cable's strength. Hence, the strength of a wire along its length is modeled as a random field of which the minimum strength value along the prescribed length of the field (the bridge wire) represents the overall wire strength.

For the samples investigated in this work (i.e. a representative panel from one of the main cables of the Williamsburg Bridge), all three methods of estimation, (Type I EVD, IID R.V., and RFM), are employed. As a first step, the available experimental data is analyzed, considering 19 long wire samples removed during the 1988 inspection that were assigned a corrosion rating of *grade 0* (*i.e.* "no visible corrosion; the wire appears to be in its original condition") along the entire sample length [48]. In this study, these samples are considered to represent the original wire condition in 1903. Given that the composition of a new bridge cable is assumed to be entirely undeteriorated wires, no correlation exists between the strength of a new wire and its position

along the length or across the cross-section of the main cable. Taking advantage of this observation, statistical sampling requirements can be relaxed for the grade 0 samples such that these 19 long wire samples are assumed to be representative of the entire cable cross-section—regardless of the position within the cross-section from which they were removed. In the Steinman study [48], these wires were segmented into 130 unit-length segments of 30.5 cm length each—the same unit-length used by Shi et al. [52]—and were tested to determine the UTS of each segment. Moreover, the location of each segment along the wire length was recorded, making it possible to estimate the correlation structure of the UTS along the length of the wires. It is assumed here that the 19 wire samples are realizations of a random field modeling the wire UTS for every wire in the cable's cross-section. The mean $\mu_{130}$ and standard deviation $\sigma_{130}$ of the UTS obtained from these 130 segments are $\mu_{130} = 1{,}548 MPa$ and $\sigma_{130} = 42.8 MPa$, respectively. The standardized UTS of the unit-length wire segments, $\bar{z}_i$, where $i = 1,\ 2,\ \ldots,\ 130$, can be determined from the individual segment UTS values $z_i$ as $\bar{z}_i = \frac{z_i - \mu_{130}}{\sigma_{130}}$. A number of common statistical distributions are fitted to the 130 $\bar{z}_i$ values and the best-fit distribution is chosen based on the Anderson-Darling (AD) statistic. This approach gives more weight to fitting the tails of the distribution (of which the left tail ultimately controls the UTS over a prescribed length of wire) compared to other statistical measures such as the chi-square and Kolmogorov-Smirnov goodness-of-fit tests [96]. Ultimately, the generalized extreme value (GEV) distribution with the following probability density function (pdf) is determined to be the best fit for the data:

$$f(\bar{z}) = \frac{1}{\sigma} e^{-(1+k\bar{z})^{-1/k}} (1 + k\bar{z})^{(-1-1/k)} \tag{36}$$

where $\bar{z} = (z - b)/a$ , while $k$ , $a$ , and $b$ are the shape, scale, and location parameters, respectively. The values of these three parameters are estimated as $k$ =-0.46, $a$ =1.08, and $b$=-0.27 using the MATLAB Statistics Toolbox [97]. It should be noted that the procedure used in fitting preserves the zero mean and unit standard deviation of the underlying standardized data. The skewness and kurtosis coefficients for this GEV distribution are -0.53 and 3.06, respectively, indicating a mild skew with respect to the standardized Gaussian distribution. The three strength estimation methods outlined in this paper employ these sample statistics to determine the original strength of Williamsburg Bridge wires: the mean and standard deviation of the samples are used in the Type I EVD method with an assumed Gaussian distribution while the GEV distribution is used in the IID R.V. and RFM.

## Type I EVD

Type I EVD (Type I asymptotic distribution of the smallest value) is an extreme value distribution often used to model the limiting distribution of the minimum values of a collection of random observations from an arbitrary distribution. Type I EVD has been used to represent the minimum strength values of bridge wires from tensile test data as a means of establishing the UTS of a bridge wire [51,52]. It is assumed that the standardized UTS of a 30.5 cm wire segment follows a standardized Gaussian distribution. The cumulative distribution function (CDF) is then given by

$$F_{\bar{Z}}(\bar{z}) = 1 - \exp\left(-\exp(\gamma_1(\bar{z} - u_1))\right) \tag{37}$$

where $\bar{Z}$ indicates the random variable representing the standardized UTS of a wire of length equal to the chosen clamping length of 18.3 m and $\bar{z}$ is the standardized UTS of individual wire

segments. The parameters $u_1$ and $\gamma_1$ are determined from $F(u_1) = 1/N_s$ and $\gamma_1 = N_s \cdot f(u_1)$, where $F(.)$ and $f(.)$ are the CDF and pdf of the standardized Gaussian distribution, respectively. Here, the value of $N_s$ is taken as 60, denoting the number of unit length (30.5 cm) wire segment UTS values within the clamping length. The mean and variance of $\overline{Z}$ are available in closed form as

$$\mu_{\overline{Z}} = u_1 - \frac{0.57721}{\gamma_1}$$
$$Var[\overline{Z}] = \frac{\pi^2}{6\gamma_1^{\,2}} \tag{38}$$

It has been shown by Shi et al. [52] that the mean $\mu_{F_{cable}}$ and standard deviation $\sigma_{F_{cable}}$ of the cable's strength $F_{cable}$ can be computed using the following equations:

$$\mu_{F_{cable}} = Area \sum_{i=1}^{N_c} \mu(x_i, y_i) + N_c \cdot Area \cdot \sigma_{130} \cdot \mu_{\overline{Z}} \tag{39}$$

$$\sigma_Y^{\,2} = N_c \cdot \sigma_{130}^{\,2} \cdot Area^2 \cdot Var[\overline{Z}] \tag{40}$$

where *Area* is the area of a single wire, $N_c$ is the total number of wires making up the cable. The values of *Area* and $N_c$ for the Williamsburg Bridge cables are 18.71 mm$^2$ and 7,696, respectively. $x_i$ and $y_i$ are the horizontal and vertical coordinates of the *i*-th wire within the cable's cross-section, and $\mu(x_i, y_i)$ denotes the mean UTS of wires based on the wire's location within the cable's cross-section. Since the goal is to determine the original strength of the cable composed entirely of brand new wires, in the absence of corrosion induced variations in the wire properties across the cable cross-section, there is no dependence of the UTS with the $x$ and $y$ coordinates. Accordingly, $\mu(x_i, y_i)$ can be replaced by the sample mean $\mu_{130}$ and the computation of the cable's mean strength given in Eq. (39) is reduced to

$$\mu_{F_{cable}} = N_c \cdot Area \cdot (\mu_{130} + \sigma_{130} \cdot E[\bar{Z}]) \tag{41}$$

**Simulation of Independent and Identically Distributed Random Variables (IID R.V.)**

In this Monte Carlo simulation based approach, a wire of prescribed length is modeled with $N_s$ uncorrelated random variables, each describing the UTS of a unit-length wire segment. The standardized UTS of 30.5 cm wire segments, $\bar{z}$, is assumed to follow the GEV distribution with the pdf given in Eq. (36). Subsequently, 60 UTS values for the wire segments are generated from the prescribed GEV distribution to simulate a wire of the chosen clamping length. The UTS of the 18.3 m long wire is determined as the smallest of the 60 generated UTS values. By generating a large number of 18.3 m long wire realizations, the mean and variance of wire UTS are established. Finally, the mean and standard deviation of the cable's strength are calculated through the use of Eq. (40) and (41).

**Random Field Method (RFM)**

In RFM, the UTS of a wire is modeled as a random field, $\bar{z}(x)$, that consists of UTS values of individual wire segments, each at the positional variable, $x$, that denotes the location or index of a wire segment along the wire length. As shown first by Shi et al. [52] and again later in this chapter, the data from the inspection program of the Williamsburg Bridge [98] indicates that this random field is a non-Gaussian one. The autocorrelation function of the non-Gaussian random field, $\bar{z}(x)$, is determined from the UTS values considering the sequence of the unit-length wire segments in each of the 19 sample wires. In the study we conducted, several forms of correlation

functions were tested, and the one that yielded the minimum sum of square errors compared to the empirical autocorrelation function was selected:

$$R_{\bar{z}}(\xi) = e^{-\left(\xi/294\right)^2} \tag{42}$$

where ξ represents the separation distance between segments. Substantial correlation of the wire UTS along the wire length is found with a correlation value above 0.75 at a separation distance of 244 cm. The corresponding spectral density function (SDF) can be computed from Eq. (42) using the Wiener-Khinchin transform as:

$$S_{\bar{z}}(\kappa) = 82.95 \cdot e^{-21615\kappa^2} \tag{43}$$

where κ indicates the wave number in the frequency domain. The compatible non-Gaussian SDF and the underlying Gaussian SDF are next determined by ensemble averaging 400 samples generated using Shi et al.'s methodology [52]. Having established this compatible SDF pair, 100,000 sample functions of the standardized field $\bar{z}(x)$ are generated for the clamping length of 18.3 m. For each "simulated" wire *i*, the smallest value of $\bar{z}(x)$ along its length can be considered as the UTS of the that wire and is denoted by the random variable $\bar{Z}_{(i)}, (i = 1,2,...,N_{samples} = 100,000)$. It is important to note the difference between the random variable $\bar{Z}_{(i)}$ and the random variable $\bar{Z}$ used in Type I EVD (Eq. (37)). In fact, while both random variables model the UTS of an 18.3 m long wire, only $\bar{Z}_{(i)}$ considers the correlation of UTS along the wire's length. In a similar manner to Eq. (40) and (41), after computing the mean $\mu_{\bar{Z}_{(i)}}$ and variance $Var[\bar{Z}_{(i)}]$ of the random variable, the mean and standard deviation of the cable's strength, $\mu_{F_{cable}}$ and $\sigma_{F_{cable}}$ can be computed using the following equations:

$$\mu_{F_{cable}} = N_c \cdot Area \cdot (\mu_{130} + \sigma_{130} \cdot \mu_{\bar{Z}_{(i)}}) \tag{44}$$

$$\sigma_{F_{cable}}{}^2 = N_c \cdot \sigma_{130}{}^2 \cdot Area^2 \cdot Var[\bar{Z}_{(i)}] \tag{45}$$

## Overall Cable Strength

Following the calculation of the tensile strength of a single bridge wire, one of several strength models proposed in the literature for main cables of suspension bridges can be used to calculate the overall cable strength: these models are the ductile-wire model, brittle-wire model, brittle-ductile model, BTC method, to name a few [7,44,55]. The ductile-wire model—the approach employed by Shi et al. [52], which, for the sake of consistency, is also used in this work—assumes that all the wires in a cable share the cable force until each wire reaches its capacity and the entire cable fails as a unit. The cable strength is simply calculated as the sum of individual wire strengths:

$$F_{cable}(t) = \sum_{i=1}^{N_c} F_i(t) \tag{46}$$

where $F_{cable}(t)$ is the strength of the entire cable consisting of $N_c$ wires at time *t,* and $F_i(t)$ denotes the strength of wire *i* at time *t,* where both $F_{cable}$ and $F$ are in force units. The strength of an uncorroded wire segment *i* of cross-sectional area $Area_{new}$ and UTS $\bar{Z}_{(i)}$ can be calculated as:

$$F_{new(i)} = \bar{Z}_{(i)} \times Area_{new} \tag{47}$$

Accordingly, by replacing $F_i(t)$ in Eq. (46) with $F_i(t=0) = \bar{Z}_{(i)} \times Area_{new}$, the original strength of a cable can be calculated.

## Remaining Strength of Cable After t Years in Service (Step-IV)

In order to establish the strength of a deteriorated bridge wire, remaining wire strength can be related to the cross-sectional area loss due to corrosion. It has been shown by various researchers that for a given wire, the UTS, defined as the ultimate load divided by the cross-sectional area, does not change with an increasing level of corrosion [9,10,15,37,99]. For this reason, the reduction in the ultimate strength of a wire can be directly related to the reduction in the wire's cross-sectional area, yielding the following expression for the strength of a deteriorated bridge wire:

$$F_{corr}(\mathbf{x},t) = F_{new} \times Area_{corr}(\mathbf{x},t) / Area_{new} \tag{48}$$

In this equation, $F_{corr}(\mathbf{x},t)$ is the strength of a wire at time $t$, $F_{new}$ is the strength of an uncorroded wire given in Eq. (47) and computed in Step-III, both in force units. $Area_{corr}(\mathbf{x},t)$ represents the remaining steel area of a corroded wire at time $t$, calculated using the cumulative corrosion depth, $C_{tot}(\mathbf{x},t)$, computed in Step-II, and the radius of the uncorroded wire, $r_{new}$, as:

$$Area_{corr}(\mathbf{x},t) = \pi(r_{new} - C_{tot}(\mathbf{x},t))^2 \tag{49}$$

Since $C_{tot}(\mathbf{x},t)$ is a function of the environmental inputs, $\mathbf{x}$, to which a wire is exposed up to time $t$, it follows from Eq. (49) that $Area_{corr}(\mathbf{x},t)$ is also a function of $\mathbf{x}$; as environmental conditions vary within the cable, the reduction in cross-sectional area of a specific wire depends on its position within the cable section.

Following the calculation of $Area_{corr}(t)$ and $F_{new}$, the strength of each individual wire within the cable can be determined through Eq. (48). Finally, the remaining strength of the corroded cable can be calculated from Eq. (46).

# RESULTS

In the following section, the results obtained using the method developed for cable strength calculation outlined in detail above are presented in two parts. First, the long-term exponent *n* is determined using available data collected during the 1988 inspection of the Williamsburg Bridge. Second, the calculated *n* value is applied to different case studies.

## Application of the developed methodology to determine *n*

In Step-I of the proposed method, the environmental conditions to which each Williamsburg Bridge wire is subjected are estimated over the 85-year service life (from the completion of the bridge in 1903 (t=0 years) to the 1988 inspection (t=85 years)). This is achieved by using historical records of external pH, $Cl^-$ concentration, temperature, and RH, and applying the techniques explained in Step-I to estimate the internal distribution of these parameters for each wire inside the cable cross-section.

Internal pH and $Cl^-$ concentration are estimated using precipitation data from various stations in New York State between the years 1978-2008 [95]. From the precipitation data, the best-fit to pH values recorded is found to be a generalized logistic (GL) distribution with the pdf:

$$f(z_{pH}) = \frac{(1+k\bar{z}_{pH})^{-1-1/k}}{a\left(1+(1+k\bar{z}_{pH})^{-1/k}\right)^2} \quad \text{for} \quad k \neq 0 \text{ where } \bar{z}_{pH} = \frac{z_{pH}-b}{a} \tag{50}$$

where $z_{pH}$ denotes the pH value and the variables that minimize the Anderson-Darling (AD) statistic for the best-fit are obtained as $k$=0.149 (shape parameter), $a$=0.203 (scale parameter), and $b$=4.39 (location parameter). Similarly, for $Cl^-$ concentration, a generalized extreme value (GEV) distribution with the pdf given in Eq. (36) ($z$ replaced with $z_{Cl^-}$, k=0.63448, a=0.08559, and b=0.10037) yielded the best-fit to $Cl^-$ concentration records based on the AD statistic. Hourly pH and $Cl^-$ concentration values are sampled from these fitted distributions, generating hourly data for the duration of the 85-year period. Note that since data is not available regarding the variation of environmental inputs along the 18.3 m clamping length, T, RH, pH, and $Cl^-$ inputs at each 30.5 cm wire segment are assumed to be constant along the wire length, while varying hourly and across the cross-section.

Continuing the methodology discussed in Step-I, thermal diffusivity values for the bridge cable are computed to estimate the internal temperature distribution. In this computation, the temperature data used was collected from a full-size mock-up cable specimen that was exposed to varying environmental conditions as discussed in Step-I [8]. Using the compiled test data, the bridge cable thermal diffusivity values are computed as $\alpha_{\text{int}} = 8.49\times10^{-7}\ m^2/s$ and $\alpha_{surface} = 1.82\times10^{-7}\ m^2/s$ by numerically solving Eq. (27) and minimizing the root mean squared error (RMSE) between the measured and numerically calculated temperature values at each

sensor location. Figure 35 displays the average of measured (solid lines) and estimated (dashed lines) T values for sensors at the same radial distance from the cable's center for a 4-cycle test. The plots show a strong correspondence between the recorded and predicted results, a promising result given the large number of parameters that have the potential to introduce random or systematic uncertainties.

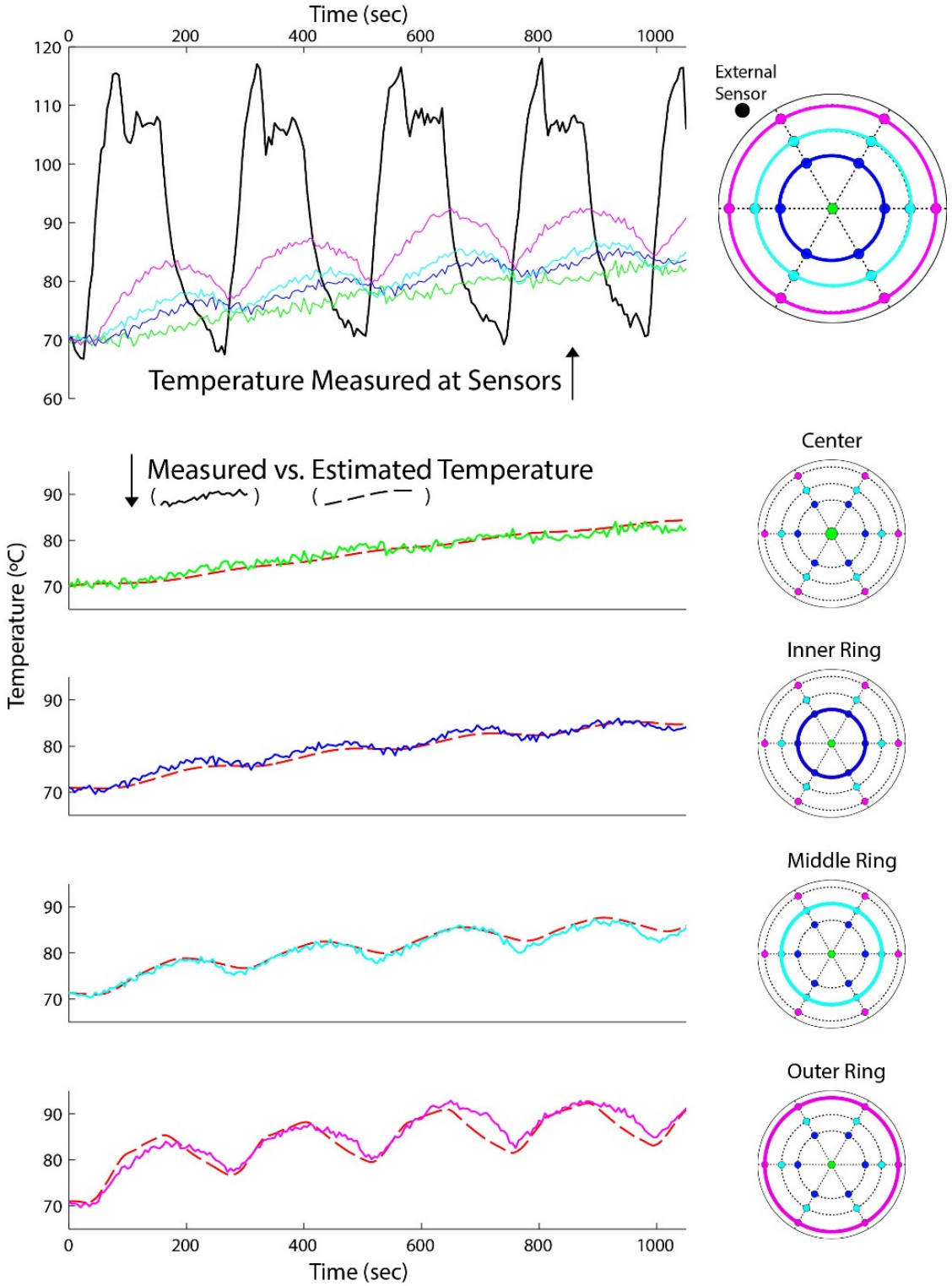


Figure 35: Measured vs. estimated average T at various distances from the cable center

Internal T and RH inputs within the cross-section are estimated using historical T and RH records and the methods developed in Step-I for determining the internal distribution of these variables according to these externally measured records. Using hourly T and RH data measured at the La Guardia Airport Station (New York City) between the 1984 and 1997 by the National Climatic Data Center [100], the hourly external T and RH inputs for the period spanning 1903 until 1988 are extrapolated by repeating the 14-year long records. The heat equation provided in Eq. (27) and the internal RH distribution represented by Eq. (33) are then applied to this data to estimate the internal T and RH values, respectively, at each wire within the cable cross-section.

Having established the applicable environmental variables, in Step-II, the cumulative corrosion depth values after 85 years are calculated by inputting these values into Eq. (34) and (35) for each wire within the cable cross-section.

The three methods introduced in Step-III—Type I EVD, IID R.V., and RFM—are next used to determine the original strength of the Williamsburg Bridge cable. Based on the statistical approach applied, each method produces a representation of the bridge cable in its original state in 1903 (t=0 years), thereby yielding different estimations of the original cable strength. The results are illustrated below in Table 2. Comparing the original cable strength estimated using Type I EVD and IID R.V. to the result from RFM, we see that while the results produced by Type I EVD and IID R.V. are approximately equal, the RFM yields a value for the original cable strength that is 4-5% higher —in agreement with the findings of Shi et al. [52] for estimated strengths in 1988. The difference in strength between the standard approaches and RFM, while

not as pronounced as in the 1988 results, is an indicator of significant correlation of the wire strength over its length.

Table 14. Mean and Standard Deviation of Cable Strength (in kN): Comparison of Original Strength Results in 1903 and 1988

| Method | Cable strength | | | | | |
|---|---|---|---|---|---|---|
| | Original Strength in 1903 | | | Strength in 1988[a] | | |
| | Distribution Type[b] | $\mu_Y$ (kN) | $\sigma_Y$ (kN) | Distribution Type[b] | $\mu_Y$ (kN) | $\sigma_Y$ (kN) |
| Type I EVD | Gaussian | 208,295 | 35 | Gaussian | 184,948 | 74 |
| IID R.V. | GEV | 206,926 | 39 | Beta | 179,745 | 91 |
| RFM | GEV | 216,800 | 52 | Beta | 203,022 | 135 |

a Results from Shi et al. [52].

b Distribution of 30.5 cm wire segments

Subsequently, in Step-IV, the predicted remaining strength of each wire after 85 years of corrosion (i.e. in 1988) is calculated from Eq. (47) and (48) for $n$ values ranging from [0-1], where $\overline{Z}_{(i)}$ in Eq. (47) for each wire sample is the generated UTS value in Step-III. For each value of $n$ considered, the remaining cable strength after 85 years is calculated by summing up the individual wire strengths (in kN) per Eq. (46).

Next, in Step-V, the long-term exponential constant, $n$, for each of the three methods is obtained by selecting the corresponding value that equates the same remaining cable strength in 1988 calculated in Step-IV with the benchmark values previously estimated by Shi et al. [52] (shown in Table 14). The resulting values of $n$ are summarized in Table 15.

Table 15. Long-term exponential constant *n*: Comparison of Results Between the Three Methods Used

| Method | Loss in cable strength in 85 years | Long-term exponential constant *n* |
|---|---|---|
| Type I EVD | 11.2% | 0.45 |
| IID R.V. | 13.1% | 0.48 |
| RFM | 6.4% | 0.38 |

Reviewing the results in Table 15, it is interesting to observe that all three estimated *n* values fall within the range of values reported by Briggs (*n*=0.25-0.41) and Feliu et al. (*n*=0.59) for industrial and rural-industrial atmospheres [40,41]. Note that, *n* could be seen as an index on the presence of the corrosion product layer, and on the physicochemical reactions of this layer with various environmental factors [101]. Once the corrosion process has begun, the rate of corrosion is controlled by three characteristics of the corrosion products layer: the thickness, the porosity, and the chemical composition. $n = 0.5$ is a special case of the so-called ideal diffusion-controlled corrosion mechanism in which all corrosion products remain on the metallic surface as an unperturbed layer. If the metal surface is exposed to mechanisms that result in the removal of this layer of corrosion products—specifically, erosion, dissolution, and cracking—the diffusion process is accelerated, and the value of the exponent *n* exceeds 0.5, ranging up to a limiting value of 1.0. In contrast, when *n* assumes a value lower than 0.5, it implies that the diffusion rate is decreasing with time. Accordingly, the results suggest that within a bridge cable, a corrosion layer is formed on the surface of the wires that decelerates the rate of corrosion and there is minimal removal of this rust layer by erosion or dissolution processes.

Finally, in Step-VI, the remaining cable strength may be continuously estimated using new measurements of the monitored variables (T, pH, RH, and $Cl^-$ concentration) by utilizing the obtained values of *n*, without having to perform any physical inspection.

## Case studies of cable strength estimation

In this section, the estimated values of the long-term exponential constant, *n*, are used to simulate the evolution of the remaining cable strength for two cases: (i) the Williamsburg Bridge main cable following the 1988 inspection; (ii) a hypothetical, new bridge cable identical to the one of the Williamsburg Bridge. In both instances, the hourly environmental inputs for T, RH, pH, and $Cl^-$ concentration prepared in Step-I for a bridge cable in the New York City region are used. Similar to the previous section, historical records for T and RH are used to estimate the internal distribution of these variables [95]. These inputs are then repeated as many times as necessary to make up the duration of each simulation. Additionally, for the duration of each simulation, pH and $Cl^-$ concentration inputs are generated by means of sampling from the previously established distributions.

**(i)** Williamsburg Bridge cable: Completed in 1903, the Williamsburg Bridge connects the boroughs of Manhattan and Brooklyn. The 488 m main span of the bridge is supported by four main cables, draped in two pairs and each 49 cm in diameter. Each cable is composed of 7,696 ungalvanized high-strength bridge wires of 4.9 mm diameter.

Based on data gathered during a 1988 inspection, Shi et al. [52] estimated the remaining strength at the time of investigation of a Williamsburg Bridge cable using two standard approaches (Type I EVD and IID R.V.) as well as the RFM. Utilizing this estimation of the remaining strength as the starting point and in conjunction with the *n* values calculated previously, the subsequent evolution of the cable strength is estimated. In order to accomplish this, 7,696 sample wires—representative of the 1988 condition of the Williamsburg Bridge wires—are subjected to the generated environmental inputs from the year 1988 to 2100. The progression of remaining strength is then simulated three times; once for each of the three methods discussed above by using the corresponding *n* value presented in Table 15. It is important to note that the simulation starts at t=85-years (as opposed to at t=0-years) since the ungalvanized wires of the Williamsburg Bridge had already been in service for 85-years at the time of the inspection.

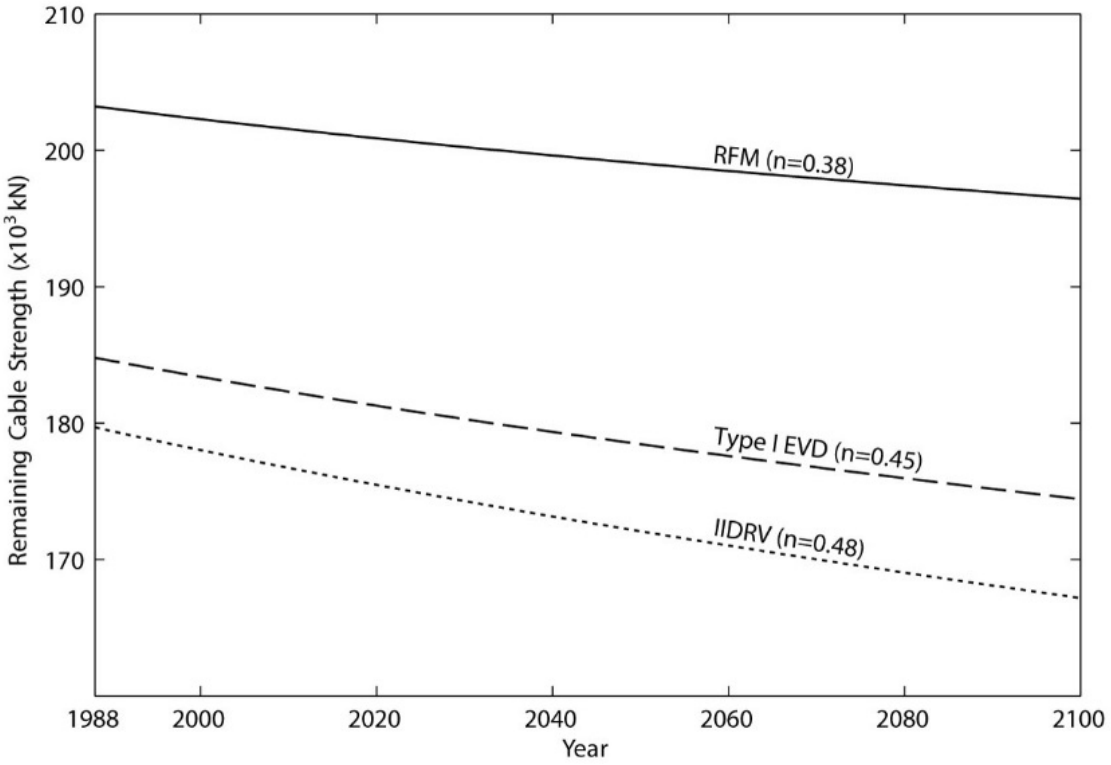


Figure 36: Williamsburg Bridge Cable - Evolution of the remaining cable strength

Figure 36 shows the estimated evolution of the remaining cable strength for each of the three methods considered. The reduction in cable strength from 1988 to 2100 is calculated as 5.69% (184,948kN to 174,428kN) for Type I EVD, 6.99% (179,745kN to 167,180kN) for IID R.V, and 3.24% (203,022kN to 196,451kN) for RFM. As a comparison, the calculated reduction in cable strength for all three methods is significantly smaller than the cable strength reduction forecasted by Eiselstein & Caligiuri [15] that employed a corrosion damage model based on a constant pit growth rate. While some aspects of this corrosion damage model are not published in full detail, it is evident that the work extrapolates long-term corrosion rates based on initial corrosion rates determined through cyclic testing. This assumption led to an apparent overestimation of the long-term corrosion rate of wires as compared to the rates forecasted in this study. In fact, Eiselstein & Caligiuri estimated a cable strength of approximately 125,000 kN in 1988, dropping to 87,000 kN in 2005. This corresponds to a reduction in strength of 45% by 1988 and 62% by 2005 from their initial strength estimate of 227,000kN. Finally, extrapolation of the strength deterioration curve from the Eiselstein & Caligiuri study yields a remaining cable strength of roughly 56,000kN in 2016, a capacity that would equate to a safety factor of only 1.1 based on the research of Haight et al. [50] and represents less than a third of the strength predicted by any of the methods used in this study.

The predicted evolution of the strength of a Williamsburg Bridge cable captures both general and localized (pitting, embrittlement, stress-corrosion cracking, etc.) corrosion effects since the wire strength data used in the estimation of the long-term exponent $n$ in Eq. (25) already reflects the contributions of each corrosion mechanism. It should be noted that this study uses the ductile-wire model for the calculation of cable strength, which assumes that all wires are ductile and capable

of elongating plastically under the cable load until the entire cable fails as a unit. This model was selected for two reasons: (i) to be consistent with Shi et al. [52] in order to estimate *n*, and, (ii) for its simplicity, as the focus of this study is the long-term corrosion model for bridge wires as opposed to the cable strength estimation method itself. It is important to recall that the NCHRP Report 534 [7] also presents additional models—such as the limited ductility and brittle-ductile models—that take into account that wires might fail at low strains and recommends the use of these models for strength estimation of bridge cables. Following the same procedure presented, an alternative cable strength estimation method can easily be used in lieu of the ductile-wire model and this will imply a slight variation in the estimated *n* value.

**(ii) Hypothetical Bridge:** In contrast with the Williamsburg Bridge, almost all suspension bridges use galvanized bridge wires in their main cables for corrosion protection. As a result, it is of particular interest to study the evolution of cable strength for a hypothetical bridge cable composed of galvanized wires. For the sake of comparison, the hypothetical cable considered in this study is identical in diameter and number of wires to the Williamsburg Bridge cable and is subjected to environmental conditions identical to the previous case.

The primary difference between the previously worked numerical example on the Williamsburg Bridge cable and the hypothetical cable studied here is the presence of a galvanized layer surrounding each wire; this zinc layer protects the steel core of the wire so that corrosion and the associated loss of cross-sectional area begins only after the zinc layer is depleted. With some exceptions, long-span suspension bridges are typically constructed with wires protected by a Class A coating with a weight of 300 g/m$^2$ [24,29]. ASTM publication STP 435 [40] indicates that in

most environments, the corrosion rate of zinc is, at least, ten times lower than that of steel. A power curve fitted (with a coefficient of determination, $R^2$, of 0.65) to the steel versus zinc corrosion data presented in STP 435 yields:

$$A_{zinc}(\mathbf{x}) = 0.392 \times A_{steel}(\mathbf{x})^{0.561} \tag{51}$$

where $A_{zinc}(\mathbf{x})$ and $A_{steel}(\mathbf{x})$ are the annual corrosion rate of zinc and steel, respectively. The long-term exponent value of $n = 0.92$ reported by Feliu et al. [41] for the corrosion of zinc in urban-industrial atmospheres will be used to calculate the cumulative zinc corrosion, $C_{zinc}(t, \mathbf{x})$, by substituting the zinc corrosion rate estimated in Eq. (51) into Eq. (25):

$$C_{zinc}(t, \mathbf{x}) = A_{zinc}(\mathbf{x}) \times t^{0.92} = 0.392 \times A_{steel}(\mathbf{x})^{0.561} \times t^{0.92} \tag{52}$$

In this case study, an initial zinc coating thickness of 42 μm is used for all wires—this value corresponds to the thickness required to achieve the Class A minimum coating weight of 300 g/m$^2$ for the uncoated steel wire of 4.9 mm diameter used here. Hence, only the corrosion of zinc needs to be considered until the cumulative zinc corrosion depth reaches 42 μm, after which corrosion of the steel wires will begin. It is important to point out that since the internal distribution of the environmental parameters (T, RH, pH, $Cl^-$, etc.) varies across the cable's cross-section, the depletion of the zinc layer, and thus the initiation of steel corrosion, will not occur uniformly across the cable. Following the onset of steel corrosion, the method for estimating the remaining cable strength is per the procedure presented in this chapter: (i) the cumulative steel corrosion depths are calculated by summing the incremental corrosion values; (ii) subsequently, the remaining wire strengths are calculated using Eq. (47) and (48); (iii) finally, the remaining cable strength is obtained by summing the individual wire strengths (in kN) using Eq. (46). By applying this process, the corrosion model developed for the

Williamsburg Bridge can be adapted to capture the impact of the galvanization layer on the bridge wire corrosion.

Another distinction from the Williamsburg Bridge example arises from variations in the properties of fabricated bridge wires. Modern wires are fabricated with advanced technology yielding a higher degree of precision along with better control over the raw material inputs as compared to the fabrication of the original wires used in the Williamsburg Bridge. As a result, the variation in strength is minimal for brand new wires, both along the length of a single wire and across samples taken from random locations and different reels of wire. For instance, three 457.2 cm long segments of wire were removed from two new reels of galvanized bridge wire supplied by Wirerope Works, Inc. of Williamsport, PA, cut into ten consecutive 45.7 cm long wire segments (30.5 cm length between grips) and tested for their UTS. The resulting mean and standard deviation of the UTS of these sixty 30.5 cm segments are $\mu_{60} = 1{,}807 MPa$ and $\sigma_{60} = 9.8 MPa$, respectively. Comparing these results to the mean and standard deviation of the UTS of the 130 wire segments representative of the original condition of the Williamsburg Bridge wires ($\mu_{130} = 1{,}548 MPa$ and $\sigma_{130} = 42.8 MPa$), we see that the coefficient of variation (COV) of the UTS of the modern bridge wire, $\frac{\sigma_{60}}{\mu_{60}} = 0.0054$, is approximately one-fifth of the corresponding COV for the Williamsburg Bridge wires, $\frac{\sigma_{130}}{\mu_{130}} = 0.0276$.

Following identical steps to those taken to calculate the original strength of the Williamsburg Bridge cable, Type I EVD, IID R.V., and RFM approaches are used to compute the strength of this hypothetical bridge cable. For the new wire datasets, the best-fit for the distribution of

30.5 cm wire UTS is determined as the Generalized Logistic (GL) distribution with the pdf given in Eq. (50) and $k$=0.02, $\sigma$=0.54, and $\mu$=-0.02. The skewness and kurtosis coefficients for this GL distribution are 0.18 and 4.28, respectively—indicative of a mildly skewed non-Gaussian distribution. The autocorrelation function $R_{\bar{z}}(\xi)$ and the corresponding SDF, $S_{\bar{z}}(\kappa)$, are determined as:

$$R_{\bar{z}}(\xi) = e^{-\xi/37} \tag{53}$$

$$S_{\bar{z}}(\kappa) = \frac{37}{\pi(1+37^2\kappa^2)} \tag{54}$$

In the strength simulation of the hypothetical cable, the UTS values of representative wires in the uncorroded condition are calculated using the Type I EVD by sampling from a Gaussian distribution with $\mu = 1{,}807 MPa$ and $\sigma = 9.8 MPa$ calculated above, the IID R.V. method using the GL distribution given in Eq. (50) with k=0.02, a=0.54, and b=-0.02, and lastly, the RFM, by generating samples from the GL distribution given in Eq. (50) and the target SDF given in Eq. (54) using the approach proposed by Shi et al. [52].

Table 16: Mean and Standard Deviation of Initial Strength of a Hypothetical New Bridge Cable Composed of 7,696 Wires (in kN).

| Method | Distribution of 30.5 cm wire segments | $\mu_Y$ (kN) | $\sigma_Y$ (kN) |
|---|---|---|---|
| Type I EVD | Gaussian | 256,464 | 8.28 |
| IID R.V. | Generalized Logistic (GL) | 256,790 | 10.02 |
| RFM | Generalized Logistic (GL) | 257,222 | 11.21 |

The resulting values of $\mu_{F_{cable}}$ and $\sigma_{F_{cable}}$ representing the strength of the new cable calculated using each of the three approaches are shown in Table 16. In comparison to the Williamsburg Bridge where the initial cable strength calculated using RFM is 4.6% and 3.9% higher than those calculated using IID R.V. and Type I EVD, respectively, the initial cable strength calculated for the modern bridge cable shows less than 0.3% variation between the three methods. This disparity can be attributed to the variation in the material properties—particularly of the carbon content—of the billets from which the Williamsburg Bridge wires were manufactured; the investigation report by Steinman et al. [48] states that wires from the Williamsburg Bridge showed a wide range of carbon content between 0.6% to 1.1%, confirmed by chemical tests of wire samples extracted during the 1988 investigation. Consequently, Williamsburg Bridge wire samples in the new condition show minor strength variations along their length, but significant variations across different wire samples given the variability of material properties between different billets. This observation is substantiated by comparing the mean COV of the UTS of unit-length wire segments originating from the same wire sample, 0.0057, to the COV of the UTS of the entire population of unit-length wire segments, 0.0276; the variation of the UTS across all wire samples is almost five times greater than the variation observed in segments from a common wire. In contrast, the UTS data for the modern bridge wires tested in this study reveals a COV of 0.0054 for the entire population as compared to a mean COV of 0.0040 for unit-length wire segments taken from the same wire. The coincidence of the strength values for the modern bridge cable calculated using the three methods is attributable to the greater degree of precision prevalent today in bridge wire fabrication. Unlike the results of the Williamsburg Bridge cable study, since the variability of wire strength between wires is minimal for the modern bridge cable

considered in this case, the RFM—which considers this variation—yielded almost identical results with the two standard approaches.

Next, for each of the three methods considered, the new and galvanized bridge wires that comprise the cable are subjected to the previously established hourly environmental inputs for a 100-year period. Figure 37 displays the evolution of the remaining cable strength for each of the three methods considered. Since the estimated initial cable strength is nearly equal and the zinc corrosion rate is the same for all three methods given identical environmental conditions, it follows that the predicted cable strength is essentially the same for all three methods until depletion of the zinc layer (approximately 20 years). Beyond the 20-year mark, depletion of the galvanization layer results in the initiation of steel corrosion in an increasing number of wires and the predictions of the methods begin to diverge. As the wires continue to deteriorate, the reduction in cable strength after 100 years in service is estimated as 10.32% (256,464kN to 229,994kN) for Type I EVD ($n$=0.45), 11.83% (256,790kN to 226,415kN) for IID R.V. ($n$=0.48), and 7.93% (257,222kN to 236,833kN) for RFM ($n$=0.38).

Furthermore, Figure 37 illustrates the estimated corrosion depth using the RFM method ($n$=0.38) for each wire across the cable cross-section after 25, 50, and 100 years in service. It can be observed that after 25 years in service, the simulation predicts that steel corrosion will have initiated at the bottom and on the sides of the cable cross-section, whereas no steel corrosion is observed in the remainder of the cable. This observed behavior is consistent with the expected distribution of the environmental variables RH and T within the cable cross-section. The simulated distribution of RH within the cable determined by Eq. (33) predicts that the cable's bottom and sides are subjected

to higher values of RH, therefore zinc depletion occurs faster in these areas than at the top or in the core of the cable [91]. Similarly, looking at the simulated temperature distribution, the core of the cable undergoes more moderate fluctuations in temperature than the external T due to the delay caused by the thermal inertia of the cable. For this reason, higher peak temperatures and consequently, higher corrosion rates, are experienced in the areas closer to the cable surface. In the simulation, pH and $Cl^-$ concentrations are assumed to be constant across the cross-section, thereby isolating the roles of the distribution in RH and T on the variation of corrosion depth across the cable. An inspection of the corrosion depth distribution after year 50 shows a clear trend of increasing wire cumulative corrosion with radial distance from the center of the cable, as well as a bias in the downward direction for wires that are equidistant from the cable centroid. Consequently, at the 50-year mark, the core of the cable still consists mainly of wires protected by intact zinc galvanization layers. After 100 years in service, we observe significant disparities in the corrosion depth observed at different parts of the cross-section: corrosion depth at the bottom of the cable is around 50% greater than at the top, 22% higher than at the sides, and more than 200% higher than at the core of the cable.

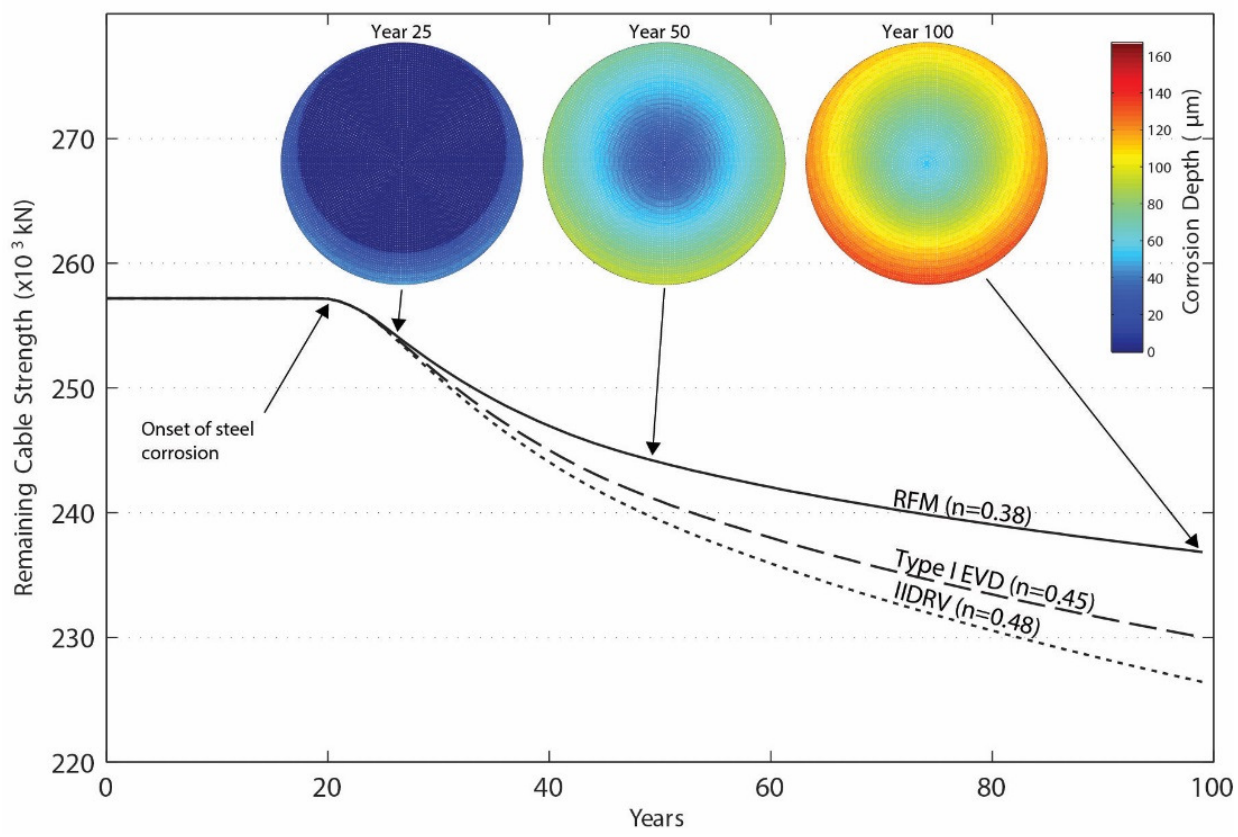


Figure 37: New Bridge Cable - Evolution of the remaining cable strength

The predicted distribution of corrosion depth values across the cross-section correspond well with inspection findings from several suspension bridges. The 1986 inspection of the Mid-Hudson Bridge (opened to traffic in 1930) noted that the outer perimeter wires, particularly at the bottom and side portions, exhibited severe (Stage 4) level of corrosion while the upper portions were reported to be in substantially better condition (Stages 1-2) [102]. Steinman et al. [98] reported that the 1991 inspection of the main cable of the Bear Mountain Bridge, NY (opened to service in 1924) uncovered more heavily corroded wires along the bottom of the cable than at the remainder of the cable. In addition, beyond the outermost 4-5 layers of wires that displayed significant corrosion, the inner wires were in good condition. In the 1992 inspection of the George Washington Bridge (opened to service in 1931), it was found that while

the interior wires were generally in good condition, the outermost 10-15 cm of the cross-section displayed Stage 3 corrosion, with the outer 2.5 cm of the bottom third of the cable exhibiting more severe (Stage 4) corrosion [70]. Ultimately, these reported conditions from three distinct bridges in the NYC metropolitan area correlate well to the estimated corrosion distribution shown in Figure 37 for a cable with a service life of over 50-years.

# CONCLUSIONS

Assessment of the remaining cable capacity is essential for bridge authorities in making maintenance and rehabilitation decisions concerning suspension bridges. An accurate and complete assessment requires estimating the strength reduction of bridge wires due to ongoing corrosion. It was shown in Chapter 3 that the long-term corrosion of bridge wires are heavily influenced by T, RH, pH and $Cl^-$ concentration and may be estimated by continuously monitoring these environmental parameters. In this chapter, the proposed time-dependent corrosion model for bridge wires that depends on monitored environmental variables is completed by extending the annual corrosion rate model developed in Chapter 3 to consider the long-term corrosion of bridge wires.

The exponent $n$ in $C(t) = At^n$ has previously been determined for carbon steel by a number of researchers [40,41,89]. The values for exponent $n$ obtained in this chapter are in the ranges reported by these other studies. Our findings indicate that the oxidation layer formed on the

surface of bridge wires decelerates the long-term corrosion rate and does not dissolve and erode at a significant rate.

The numerical study performed on the cable strength of the Williamsburg Bridge revealed significantly less reduction in cable reduction than the study Eiselstein & Caligiuri [15]. This finding was expected as the forecast model used by Eiselstein & Caligiuri ignored the protective nature of the oxide layer formed on the surface of wires and instead extrapolated initial corrosion rates linearly for the entire duration of their simulation.

The distribution of corrosion depth values across the cable cross-section of the hypothetical bridge main cable consisting of new galvanized wires matched well with inspection data gathered from several long-span suspension bridges. The two numerical case studies presented demonstrate that as long as the relevant environmental variables are continously monitored within the cable cross-section, the procedure to estimate the long-term corrosion of wires and the remaining cable strength is straight-forward and can be applied to any suspension main cable constructed in the typical fashion.

# CHAPTER 5. CONCLUSIONS AND FUTURE RESEARCH

Given the increasing age of the world's suspension bridges and ever increasing demands from traffic, the need to accurately determine the condition of the main cables of these bridges has become a priority. Inspections have uncovered extensive corrosion of the high strength bridge wires—a condition universally recognized as the biggest threat to the wellbeing of long span suspension bridges. Bridge owners face difficult maintenance and repair decisions in their constant battle to ensure the safety of public, while trying to adhere to limited maintenance budgets. Main cable inspections play a crucial role in deciding when repair, maintenance, rehabilitation, and even replacement of parts or the entirety of the bridge takes place. In these inspections, evaluation of the bridge cable is based on visually classified deterioration of bridge wires, supplemented with mechanical test results of a limited number of wire samples removed from the bridge. These inspections are infrequent, costly, intrusive, highly localized and limited in terms of the area of the main cable they manage to cover. Safety of a main cable is determined by calculating the remaining strength of bridge wires in their deteriorated state using the data collected from such inspections. Logically, any shortcomings in the quality and completeness of the data used raises questions on the reliability of this assessment. Another key limitation is the inability to estimate the declining cable strength between inspections.

## Contributions

In this dissertation, we strove to develop a more reliable and less intrusive method to assess the safety of suspension bridge main cables. The main idea stemmed from developments in sensing

systems and research of Sloane et al. [8] that demonstrated the ability to monitor internal cable conditions using sensors installed inside main cables. A natural progression of the monitoring idea is to develop a framework that uses the monitored environmental parameters in the safety assessment of suspension bridge main cables. This thesis tackled the development of such a framework. This framework investigated (i) the link between the corrosion rate of bridge wires and the monitored environmental parameters, and (ii) a methodology to estimate the remaining strength of a main cable using monitored environmental inputs.

The initial question in relating measured environmental parameters to wire corrosion rate was to find which parameters were relevant to the prediction of bridge wire corrosion rate. This exploration began in Chapter 2 in which basic relationships between various environmental parameters and wire corrosion rate were studied through a suite of cyclic corrosion tests performed at various levels of pH, T, and Cl- concentration. The observed effects of these environmental variables were in agreement with metallic corrosion theory and corroborated the findings from a number of similar studies [10,12,75,77,78]. The dataset collected during the cyclic tests was later used in establishing the model that created the link between environmental parameters and the corrosion rate.

Due to the complexity of the interactions between environmental variables and the corrosion rate, we used data-based machine learning methods to select the most relevant variables for the prediction of corrosion rate and to develop a model that predicts the annual corrosion rate from these selected variables. In Chapter 3, [T, RH, pH, and Cl-] were determined to be the four environmental variables that led to the highest prediction accuracy of the corrosion rate. To

arrive at this finding, a large dataset of corrosion data on carbon steel that considered the environmental variables [T, RH, TOW, Prec, pH, Cl-] was analyzed with a novel feature selection algorithm using the wrapper cross validation approach. Monitoring of the two of the four selected variables, T and RH, have already been demonstrated by Sloane et al. [8]. While pH and Cl- monitoring have not yet been demonstrated within a cable environment, predicting the corrosion rate of bridge wires from as little as four variables can prove an invaluable tool for bridge owners in locating problem areas and detecting damage to corrosion protection systems.

Using the selected relevant variables, we next shifted our attention to the prediction of the annual (short term) corrosion rate of bridge wires. We assessed a number of machine learning algorithms and found SVR using an RBF kernel to produce the highest prediction accuracy. A sensitivity study performed on the trained SVR model displayed the nonlinear relationships between the corrosion rate and the environmental variables. The annual corrosion rate model can be used as a standalone instrument to predict short term corrosion rates of new bridge wires.

The final step in the development of the time dependent corrosion rate model involves extending the annual corrosion rate model to a long term model that can be used to estimate corrosion rate of bridge wires over the course of their lifetimes. Chapter 4 introduces a general methodology for the calculation of the remaining strength of a main cable at any point in time that considers the long term corrosion of bridge wires. This methodology was applied to Williamsburg Bridge inspection data to determine the exponential constant *n* in the long-term corrosion expression $C(t) = At^n$. The values of exponent n values for carbon steel found in the literature compare well with the values obtained in this study for each of the three cable strength estimation methods

considered. It is worth noting that the estimated values are slightly lower than 0.5, suggesting that the corrosion layer formed on a deteriorated bridge wire is not completely porous and provides a certain degree of protection, thereby slowing down the corrosion rate as the degradation progresses.

It was noted that the long term corrosion of bridge wires is predominantly influenced by the temperature, relative humidity, pH, and Cl- concentration to which the wires are subjected and may be estimated by continuously monitoring these environmental parameters. This is particularly useful as it provides a non-intrusive technique for determining the strength of bridge cables in their deteriorated state. The method presented in this thesis offers a straightforward means of estimating the long-term loss of wire cross sectional area due to corrosion using only the aforementioned monitored environmental inputs. Estimating the remaining cable strength from monitored parameters provides a more complete picture of the cable condition, thereby augmenting the currently used cable inspection methods that reveal the condition of wires only at the time of the inspection and at a few designated locations.

Using the calculated value of the exponent n, numerical examples on a Williamsburg Bridge cable and a hypothetical new bridge cable composed of galvanized wires demonstrated how the evolution of cable strength can be predicted over the long term from monitored environmental inputs. While the examples outlined herein are performed for cable segments delimited to a length equal to the cable's clamping length and rely on the use of the ductile wire model in the

strength estimation for simplicity, the presented procedure can readily be extended to cover the entire length of a cable and to the use of any cable strength estimation model available.

## Future Research

One of the outstanding concerns relating to the accuracy of the presented method poses the question as to how closely the long-term cumulative corrosion of bridge wires follows the exponential trend defined by the equation $C = At^n$ throughout the service life of a suspension bridge. As future inspections of the Williamsburg Bridge and other long-span suspension bridges are conducted, results should be reviewed to provide additional data points for the verification of the estimated *n* value.

Complementary studies could explore the dependency of the exponent *n* on specific suspension bridge properties—such as size and usage—and the impact of significantly different climates. We suggest that *n* values be calculated for different bridges as inspection data becomes available to verify the universality of the proposed model.

At the time of this work, environmental sensor data from an actual bridge main cable or a scale mock-up cable for an extended duration of time was not available. Now that these systems are becoming a reality, the proposed long-term corrosion model can be improved by collecting additional data points from monitored sensor data and measuring mass loss due to corrosion from bridge wires.

# REFERENCES


[1] T. Wilder, *The Bridge of San Luis Rey*, New York: Grosset and Dunlap, 1927.

[2] T. Kawada, *History of the modern suspension bridge : solving the dilemma between economy and stiffness*, Reston, VA: American Society of Civil Engineers, 2010.

[3] N. Gimsing, *Cable supported bridges : concept and design*, Chichester, West Sussex: John Wiley & Sons, 2012.

[4] M. Buchholz, "The Menacing of the East River Bridge," 2013.

[5] J.E. Harding, G. Parke, M.J. Ryall, and others, *Bridge Management: Inspection, Maintenance, Assessment, and Repair*, Elsevier Applied Science, 1993.

[6] J.E. Harding, *Bridge management 3 : inspection, maintenance, assessment, and repair*, London New York: E & FN Spon, 1996.

[7] R.M. Mayrbaurl and S. Camo, *NCHRP Report 534: Guidelines for Inspection and Strength Evaluation of Suspension Bridge Parallel-wire Cables*, Transportation Research Board, 2004.

[8] M. Sloane, R. Betti, G. Marconi, A. Hong, and D. Khazem, "Experimental Analysis of a Nondestructive Corrosion Monitoring System for Main Cables of Suspension Bridges," *J. Bridge Eng.*, vol. 18, 2012, pp. 653–662.

[9] S.C. Barton, G.W. Vermaas, P.F. Duby, A.C. West, and R. Betti, "Accelerated corrosion and embrittlement of high-strength bridge wire," *Journal of Materials in Civil Engineering*, vol. 12, 2000, pp. 33–38.

[10] Y. Cao, G.W. Vermaas, R. Betti, A.C. West, and P.F. Duby, "Corrosion and Degradation of High-Strength Steel Bridge Wire," *Corrosion*, vol. 59, 2003, pp. 547–554.

[11] K. Furuya, M. Kitagawa, S.-I. Nakamura, and K. Suzumura, "Corrosion mechanism and protection methods for suspension bridge cables," *Structural Engineering International: Journal of the International Association for Bridge and Structural Engineering (IABSE)*, vol. 10, 2000, pp. 189–193.

[12] K. Suzumura and S.-I. Nakamura, "Environmental factors affecting corrosion of galvanized steel wires," *Journal of Materials in Civil Engineering*, vol. 16, 2004, pp. 1–7.

[13] R. Betti and B. Yanev, "Conditions of Suspension Bridge Cables: New York City Case Study," *Transportation research record*, Jan. 1999, pp. 105–112.

[14] M. Bieniek and Betti, *Cable Conditions for New York City Bridges*, NYCDOT, 1998.

[15] L.E. Eiselstein and R.D. Caligiuri, "Atmospheric corrosion of the suspension cables on the Williamsburg Bridge," *ASTM Special Technical Publication*, Philadelphia, PA, USA: Publ by ASTM, Philadelphia, PA, USA, 1988, pp. 78–95.

[16] R. Kohavi, "A Study of Cross-Validation and Bootstrap for Accuracy Estimation and Model Selection," *IJCAI*, 1995, pp. 1137–1145.

[17] I. Witten, *Data Mining*, San Francisco: Morgan Kaufman, 2011.

[18] J. Hyslop, *The Inka road system*, Orlando Fla.: Academic Press, 1984.

[19] J.A. Roebling, "Specification (27 March, 1841) Patent Application for 'New and Improved Mode of Manufacturing Wire Ropes' (patent not granted–perhaps not submitted)," Mar. 1841.

[20] I. Hopwood, J.H. Havens, and others, *Corrosion of cable suspension bridges*, Kentucky Transportation Center, 1984.
[21] S. Alampalli, *Inspection, evaluation and maintenance of suspension bridges*, Boca Raton: CRC Press, 2016.
[22] W.-F. Chen and L. Duan, *Bridge engineering handbook*, Boca Raton: CRC Press, 2014.
[23] B.R. Colford and C.P.E. Cocksedge, "Forth Road Bridge – first internal inspection, strength evaluation, acoustic monitoring and dehumidification of the main cables," *5th International Cable-Supported Bridge Operators' Conference*, Bridge Engineering Association, 2006.
[24] F.L. Stahl, *Cable corrosion in bridges and other structures : causes and solutions*, New York: ASCE Press, 1996.
[25] I. Hopwood, J.H. Havens, and others, *Introduction to Cable Suspension Bridges, Research Report. 690*, Kentucky Transportation Center, 1984.
[26] P.A. Schweitzer and others, *Fundamentals of corrosion: mechanisms, causes, and preventative methods*, CRC Press, 2009.
[27] R.M. Mayrbaurl, *Wire test results for three suspension bridge cables*, Taylor & Francis; London, 2006.
[28] A. Lang, "Current and Future-Bridge Cable Options," *Proceedings of the International Bridge Conference: Bridges into the 21st Century*, 1995.
[29] ASTM, *A586-04a(2009)e1 Standard Specification for Zinc-Coated Parallel and Helical Steel Wire Structural Strand*, ASTM, 2009.
[30] X.G. Zhang, *Corrosion and electrochemistry of zinc*, New York: Plenum Press, 1996.
[31] I.O. Wallinder, C. Leygraf, C. Karlen, D. Heijerick, and C. Janssen, "Atmospheric corrosion of zinc-based materials: runoff rates, chemical speciation and ecotoxicity effects," *Corrosion Science*, vol. 43, 2001, pp. 809–816.
[32] R. Revie, *Corrosion and corrosion control : an introduction to corrosion science and engineering*, Hoboken, N.J: Wiley-Interscience, 2008.
[33] X.G. Zhang, "Uhlig's Corrosion Handbook," *Uhlig's corrosion handbook*, R.W. Revie, ed., New York: Wiley, 2000, pp. 887–904.
[34] E. Bardal, *Corrosion and protection*, London New York: Springer, 2004.
[35] P. Roberge, *Corrosion engineering : principles and practice*, New York: McGraw-Hill, 2008.
[36] J. Saha, *Corrosion of constructional steels in marine and industrial environment frontier work in atmospheric corrosion*, India New York: Springer, 2013.
[37] R. Betti, A.C. West, G. Vermaas, and Y. Cao, "Corrosion and embrittlement in high-strength wires of suspension bridge cables," *Journal of Bridge Engineering*, vol. 10, 2005, pp. 151–162.
[38] S. Nakamura and K. Suzumura, "Experimental Study on Repair Methods of Corroded Bridge Cables," *Journal of Bridge Engineering*, vol. 17, 2012, pp. 720–727.
[39] S. Nakamura and K. Suzumura, "Corrosion assessment of bridge cables," *Proceedings of the 5th International Conference on Bridge Management*, vol. 1, 2005, pp. 28–36.
[40] C. Briggs, "Atmospheric Corrosion of Carbon and Low Alloy Cast Steels, STP435," W.H. Ailor and S.K. Coburn, eds., ASTM, 1968, pp. 271–284.
[41] S. Feliu, M. Morcillo, and J.S. Feliu, "The prediction of atmospheric corrosion from meteorological and pollution parameters–II. Long-term forecasts," *Corrosion Science*, vol. 34, 1993, pp. 415–422.

[42] M.L. and Bloomstine and O. Soerensen, “State-Of-The-Art Main Cable Corrosion Protection by Dehumidification,” *3rd New York City Bridge Conference*, Bridge Engineering Association, 2005.
[43] M.L. Bloomstine, O. Soerensen, and J.V. Thomsen, “Main cable corrosion protection by dehumidification,” *Conference on Operation, Maintenance and Rehabilitation of Large Infrastructure Projects, Bridges and Tunnels*, Copenhagen, Denmark: 2006, p. 90.
[44] B.W. Chavel, B.J. Leshko, and others, *Primer for the Inspection and Strength Evaluation of Suspension Bridge Cables*, Government Printing Office, 2012.
[45] N.Y.S.D. of Transportation, *2017 Bridge Inspection Manual*, 2017.
[46] R.A. Hartle and F.H. Administration, *Bridge Inspector’s Reference Manual*, U.S. Government Printing Office, 2004.
[47] I. Hopwood, J.H. Havens, and others, *Inspection, prevention, and remedy of suspension bridge cable corrosion problems, Research Report. 690*, Kentucky Transportation Center, 1984.
[48] Steinman, Boynton, Gronquist, and Birdsall, *Williamsburg bridge cable investigation program: Final report*, New York State Department of Transportation, 1988.
[49] J. Cheng, C.S. Cai, and R.-C. Xiao, “Estimation of cable safety factors of suspension bridges using artificial neural network-based inverse reliability method,” *International Journal for Numerical Methods in Engineering*, vol. 70, 2007, pp. 1112–1133.
[50] R.Q. Haight, D.P. Billington, and D. Khazem, “Cable safety factors for four suspension bridges,” *Journal of Bridge Engineering*, vol. 2, 1997, pp. 157–167.
[51] J. Matteo, G. Deodatis, and D.P. Billington, “Safety analysis of suspension-bridge cables: Williamsburg Bridge,” *Journal of Structural Engineering*, vol. 120, 1994, pp. 3197–3211.
[52] Y.W. Shi, G. Deodatis, and R. Betti, “Random field-based approach for strength evaluation of suspension bridge cables,” *Journal Of Structural Engineering-Asce*, vol. 133, 2007, pp. 1690–1699.
[53] A. Montoya, H. Waisman, and R. Betti, “A simplified contact-friction methodology for modeling wire breaks in parallel wire strands,” *Computers & Structures*, vol. 100, 2012, pp. 39–53.
[54] H. Waisman, A. Montoya, R. Betti, and I.C. Noyan, “Load Transfer and Recovery Length in Parallel Wires of Suspension Bridge Cables,” *Journal of Engineering Mechanics*, vol. 137, Apr. 2011, pp. 227–237.
[55] R.J. Perry, “Estimating Strength of the Williamsburg Bridge Suspension Cables,” *The american statistician*, vol. 52, 1998, pp. 211–218.
[56] R. Betti, D. Khazem, M. Carlos, R. Gostautas, and Y.P. Virmani, *Corrosion Monitoring Research for New York City Bridges*, FHWA, 2013.
[57] F. Corvo, N. Betancourt, and A. Mendoza, “The influence of airborne salinity on the atmospheric corrosion of steel,” *Corrosion Science*, vol. 37, 1995, pp. 1889–1901.
[58] F. Corvo, J. Minotas, J. Delgado, and C. Arroyave, “Changes in atmospheric corrosion rate caused by chloride ions depending on rain regime,” *Corrosion Science*, vol. 47, 2005, pp. 883–892.
[59] L.-G. Johansson and N.G. Vannerberg, “The atmospheric corrosion of unprotected carbon steel - a comparison between field study and laboratory test,” *Materials and Corrosion*, vol. 32, 1981, pp. 265–268.

[60] H. Katayama, K. Noda, H. Masuda, M. Nagasawa, M. Itagaki, and K. Watanabe, "Corrosion simulation of carbon steels in atmospheric environment," *Corrosion Science*, vol. 47, 2005, pp. 2599–2606.
[61] D. Knotkova, "Atmospheric Corrosion-Research, Testing, and Standardization," *Corrosion*, vol. 61, 2005, p. 723.
[62] D. Knotkova, V. Kucera, S.W. Dean, and P. Boschek, "Classification of the Corrosivity of the Atmosphere-Standardized Classification System and Approach for Adjustment, STP1421," *ASTM Special Technical Publication*, vol. 1421, 2002, p. 109.
[63] J. Kobus, "Long-term atmospheric corrosion monitoring," *Materials and Corrosion*, vol. 51, 2000, pp. 104–108.
[64] T.T.N. Lan, N.T.P. Thoa, R. Nishimura, Y. Tsujino, M. Yokoi, and Y. Maeda, "Atmospheric corrosion of carbon steel under field exposure in the southern part of Vietnam," *Corrosion Science*, vol. 48, 2006, pp. 179–192.
[65] A.R. Mendoza and F. Corvo, "Outdoor and indoor atmospheric corrosion of carbon steel," *Corrosion Science*, vol. 41, 1999, pp. 75–86.
[66] A.L. Morales, D. Cartagena, J.L. Rendón, and A. Valencia, "The Relation between Corrosion Rate and Corrosion Products from Low Carbon Steel," *physica status solidi (b)*, vol. 220, 2000, pp. 351–356.
[67] B. Mosayebi, M. Kazemeini, A. Badakhshan, and A. Safekordi, "Modelling of the effect of operational parameters and concentration of some corrosion inhibitors on the corrosion of carbon steel," *Anti-Corrosion Methods and Materials*, vol. 49, 2002, pp. 426–432.
[68] S.J. Oh, D.C. Cook, and H.E. Townsend, "Atmospheric corrosion of different steels in marine, rural and industrial environments," *Corrosion Science*, vol. 41, 1999, pp. 1687–1702.
[69] J.J.S. Rodriguez, F.J.S. Hernandez, and J.E.G. Gonzalez, "The effect of environmental and meteorological variables on atmospheric corrosion of carbon steel, copper, zinc and aluminium in a limited geographic zone with different types of environment," *Corrosion Science*, vol. 45, 2003, pp. 799–815.
[70] J.J.S. Rodriguez and H. Patel, *Main cable inspection program for the George Washington Bridge*, Engineers' Society of Wester Pennsylvania, Pittsburg, 1993.
[71] J.W. Spence, F.H. Haynie, and F.W. Lipfert, "Atmospheric Corrosion Model for Galvanized Steel Structures," *Corrosion*, vol. 48, 1992, pp. 1009–1019.
[72] Y. Wan, C. Yan, C. Cao, and J. Tan, "Atmospheric corrosion of carbon steels pre-corroded by different pollutants," *Materials and Corrosion*, vol. 55, 2004, pp. 119–123.
[73] J.H. Wang, F.I. Wei, Y.S. Chang, and H.C. Shih, "The corrosion mechanisms of carbon steel and weathering steel in SO2 polluted atmospheres," *Materials Chemistry and Physics*, vol. 47, 1997, pp. 1–8.
[74] ASTM, *Standard Practice for Modified Salt Spray (Fog) Testing, ASTM G 85-02, v03.02x*, ASTM International, 2011.
[75] ASM, ed., *Metals Handbook Ninth Edition*, Metals Park, Ohio: ASM International, 1987.
[76] D.A. Jones, *Principles and Prevention of Corrosion*, Prentice Hall, 1996.
[77] M. Fischer, "Possible Models of the Reaction Mechanism and Discussion of the Functions of Passivating Additions during the Chemical Passivation of Iron in Weakly Acid, Neutral and Basic pH Ranges right bracket .," *Werkstoffe und Korrosion*, vol. 29, 1978, pp. 188–198.

[78] I. Sekine and K. Senoo, "The corrosion behaviour of SS 41 steel in formic and acetic acids," *Corrosion Science*, vol. 24, 1984, pp. 439–448.
[79] C. Bishop, *Pattern recognition and machine learning*, New York: Springer, 2006.
[80] R.-E. Fan, P.-H. Chen, and C.-J. Lin, "Working Set Selection Using Second Order Information for Training Support Vector Machines," *J. Mach. Learn. Res.*, vol. 6, Dec. 2005, pp. 1889–1918.
[81] C.-C. Chang and C.-J. Lin, "LIBSVM: A library for support vector machines," *ACM Transactions on Intelligent Systems and Technology*, vol. 2, 2011, pp. 27:1–27:27.
[82] T. Bäck and H.-P. Schwefel, "An overview of evolutionary algorithms for parameter optimization," *Evol. Comput.*, vol. 1, 1993, pp. 1–23.
[83] S. Varma and R. Simon, "Bias in error estimation when using cross-validation for model selection," *BMC Bioinformatics*, vol. 7, Feb. 2006, pp. 91–91.
[84] R. Kohavi and G.H. John, "Wrappers for Feature Subset Selection," *Artificial Intelligence*, vol. 97, 1997, pp. 273–324.
[85] F. Harrell, *Regression Modeling Strategies With Applications to Linear Models, Logistic Regression, and Survival Analysis*, New York, NY: Springer New York, 2001.
[86] D.M. Hawkins and J. Kraker, "Deterministic fallacies and model validation," *J. Chemometrics*, vol. 24, Mar. 2010, pp. 188–193.
[87] G. Cawley and N. Talbot, "On Over-fitting in Model Selection and Subsequent Selection Bias in Performance Evaluation," *Journal of machine learning research*, vol. 11, Jul. 2010, pp. 2079–2107.
[88] J.R. Davis, *Alloying understanding the basics*, Materials Park, OH: ASM International, 2001.
[89] J. Cai, R.A. Cottis, and S.B. Lyon, "Phenomenological modelling of atmospheric corrosion using an artificial neural network," *Corrosion Science*, vol. 41, 1999, pp. 2001–2030.
[90] S. Feliu, M. Morcillo, and J.S. Feliu, "The prediction of atmospheric corrosion from meteorological and pollution parameters–I. Annual corrosion," *Corrosion Science*, vol. 34, 1993, pp. 403–414.
[91] E. Karanci and R. Betti, "Corrosion in Suspension Bridge Main Cables I: Experiments and Corrosion Rate Model Development," *Journal of Bridge Engineering*, 2016.
[92] R. Gostautas, M. Carlos, R. Betti, and D. Khazem, "Corrosion Monitoring Research Study of New York City Suspension Bridges," *CINDE Journal*, vol. 31, 2010, pp. 12–15.
[93] J.P. Holman, *Heat transfer*, Boston Mass: McGraw Hill Higher Education, 2010.
[94] W. Ames, *Numerical methods for partial differential equations*, Boston: Academic Press, 1992.
[95] NADP, *Monthly precipitation-weighted mean concentrations data for New York State monitoring locations*, NADP Program Office, Illinois State Water Survey, 2204 Griffith Dr., Champaign, IL 61820: National Atmospheric Deposition Program (NRSP-3), 2008.
[96] C. Carol, *Goodness-of-fit tests and model validity*, Boston: Birkhauser, 2002.
[97] MATLAB, *version 8.3 (R2014a)*, Natick, Massachusetts: The MathWorks Inc., 2014.
[98] Steinman, Boynton, Gronquist, and Birdsall, *Cable Investigation Report*, New York, 1991.
[99] S.-I. Nakamura, K. Suzumura, and T. Tarui, "Mechanical Properties and Remaining Strength of Corroded Bridge Wires," *Structural Engineering International: Journal of the*

*International Association for Bridge and Structural Engineering (IABSE)*, vol. 14, 2004, pp. 50–54.
[100] NCDC, *Hourly temperature and relative humidity data for New York City*, National Climatic Data Center, NOAA, 2015.
[101] M. Benarie and F.L. Lipfert, "A general corrosion function in terms of atmospheric pollutant concentrations and rain pH," *Atmospheric Environment (1967)*, vol. 20, 1986, pp. 1947–1958.
[102] Modjeski and Masters, *Mid-Hudson Bridge - Main cable investigation*, Report, Harrisburg, PA, 1987.
[103] W.W. Kirk and H. Lawson, eds., *Atmospheric Corrosion, ASTM STP 1239*, ASTM, 1995.
[104] H. Guttman, "Atmospheric Corrosion," W.H. Ailor, ed., Wiley, 1982, p. 51.
[105] W.H. Ailor and S.K. Coburn, eds., *Metal Corrosion in the Atmosphere, ASTM STP 435*, ASTM, 1968.
[106] W.H. Ailor and F.H. S.W. Haynie Dean, eds., *Corrosion in Natural Environments, ASTM STP 558*, ASTM, 1973.
[107] W. Hou, J. Yu, and C. Lian, "Atmospheric corrosion of carbon steel and low alloy steels," *Journal of Chinese Society of Corrosion and Protection*, vol. 13, 1993, p. 291.
[108] K.S. Rajagopalan and P.L. Annamalai, *International Congress on Metallic Corrosion*, 1969.
[109] S.W. Dean, ed., *Degradation of Metals in the Atmosphere, ASTM STP 965*, ASTM, 1986.
[110] V. Kucera, L. Haagenrud, L. Attereaas, and J. Gullman, "Corrosion of Steel and Zinc in Scandinavia with Respect to the Classification of the Corrosivity of AAtmosphere, STP965," W. Dean and T.S. Lee, eds., ASTM, Philadelphia, 1986, p. 264.
[111] F.H. Haynie and J.P. Upham, "Materials protection and performance," *National Association of Corrosion Engineers*, vol. 9, 1970, p. 10.
[112] J.S. Feliu and M. Morcillo, "Atmospheric Corrosion," *British Corrosion Journal*, vol. 22, 1987, p. 99.
[113] Y.-N. Chang and F.-I. Wei, "High temperature chlorine corrosion of metals and alloys.," *Journal of materials science*, vol. 26, 1991, p. 3693.
[114] F.H. Haynie and J.P. Upham, "Materials protection and performance," *National Association of Corrosion Engineers*, vol. 10, 1971, p. 18.
[115] F. Mansfeld and R. Vijayakumar, "Atmospheric corrosion behavior in Southern California," *Corrosion Science*, vol. 28, 1988, pp. 939–946.
[116] D.M. Drazic and V. Vasciz, "The correlation between accelerated laboratory corrosion tests and atmospheric corrosion station tests on steels," *Corrosion Science*, vol. 29, 1989, pp. 1197–1204.

# APPENDIX A. DATABASE COMPILED FROM WORLD-WIDE ATMOSPHERIC CORROSION TESTS

Table A-1 shows the references used in forming the database, classified according the countries from which the data was collected.

Table A-1: References used to form the corrosion database

| Country | References |
|---|---|
| Argentina | [103] |
| Australia | [104] |
| Brazil | [103,104] |
| Canada | [103–106] |
| Chile | [103] |
| China | [107] |
| Colombia | [103] |
| Costa Rica | [103] |
| Czechoslovakia | [103,104,106] |
| Cuba | [103,104] |
| Ecuador | [103] |
| France | [103] |
| Germany | [103] |
| Hungary | [104] |
| India | [108] |
| Japan | [103] |
| Mexico | [103] |
| New Zealand | [103,109] |
| Norway | [104,110] |

| | |
|---|---|
| Panama | [103–105] |
| Peru | [111] |
| Poland | [104] |
| Portugal | [103] |
| Russia | [103,104] |
| Spain | [103,104,112] |
| South Africa | [104] |
| Sweden | [103,104,110] |
| Taiwan | [113] |
| U.K. | [103,104] |
| Uruguay | [103] |
| U.S.A. | [103–106,109,111,114,115] |
| Venezuela | [103] |
| Yugoslavia | [116] |

The database has a total of 309 records for corrosion rate versus six recorded environmental variables: temperature, relative humidity (%), time of wetness (%), annual precipitation (mm), pH of rainwater, and chloride concentration (mg/L). Some pH and chloride data were estimated from chemical composition of rainfall data and chloride deposition rates. Table A-2 displays the compiled database.

Table A-2: References used to form the corrosion database

| Record No. | Temperature (°C) | RH (%) | TOW (%) | Precipitation (mm) | pH | Cl (mg/L) | Corrosion (μm) |
|---|---|---|---|---|---|---|---|
| 1 | 17.88 | 66% | 78.1 | 610 | 3.89 | 0.54 | 92.9 |
| 2 | 24.24 | 49% | 76.3 | 950 | 3.91 | 3.69 | 50.8 |
| 3 | 27.2 | 56% | 68 | 2593 | 4.74 | 2.1 | 25.7 |
| 4 | 26.83 | 98% | 89.8 | 936 | 6.88 | 10.14 | 67 |

| Record No. | Temperature (°C) | RH (%) | TOW (%) | Precipitation (mm) | pH | Cl (mg/L) | Corrosion (µm) |
|---|---|---|---|---|---|---|---|
| 5 | -2.9 | 30% | 84.5 | 240 | 4.85 | 5.4 | 41.1 |
| 6 | 27.27 | 65% | 77.3 | 944 | 4.09 | 2.91 | 45.4 |
| 7 | 26.97 | 60% | 77.3 | 1154 | 4.45 | 2.18 | 34.8 |
| 8 | 5.76 | 33% | 69.2 | 316 | 5.1 | 2.54 | 15 |
| 9 | 26.06 | 58% | 76.3 | 1396 | 5.11 | 0.01 | 19.9 |
| 10 | -2.59 | 56% | 90.6 | 797 | 3.65 | 0.03 | 44 |
| 11 | 3.94 | 40% | 69.2 | 258 | 5.2 | 1.63 | 17 |
| 12 | 27.2 | 56% | 70.3 | 1739 | 4.657 | 2.3 | 23 |
| 13 | 6.97 | 42% | 69.2 | 356 | 4.58 | 2.91 | 34.8 |
| 14 | 12.43 | 57% | 76.3 | 928 | 5.4 | 0.01 | 38.4 |
| 15 | 21 | 21% | 56 | 1724 | 4.971 | 0.8 | 11.4 |
| 16 | 26.73 | 67% | 66 | 1223 | 3.55 | 70.97 | 145 |
| 17 | 17 | 30% | 62.8 | 521 | 4.946 | 0.8 | 19.4 |
| 18 | 16.97 | 59% | 76.3 | 777 | 4.37 | 38.13 | 49.9 |
| 19 | 27 | 58% | 77 | 792 | 4.632 | 4.3 | 24.8 |
| 20 | -2.76 | 71% | 89.2 | 1178 | 5.05 | 0.03 | 26 |
| 21 | 14.34 | 53% | 64.1 | 773 | 3.54 | 0.02 | 41 |
| 22 | 26.5 | 56% | 69.2 | 1686 | 4.365 | 1.6 | 25.6 |
| 23 | 27.3 | 35% | 48.3 | 997 | 6.806 | 8.6 | 27.9 |
| 24 | -2.49 | 74% | 36.2 | 1274 | 4.89 | 9.75 | 10 |
| 25 | 12.84 | 24% | 62.7 | 540 | 3.99 | 0.01 | 30.8 |
| 26 | 26.97 | 45% | 75.2 | 1307 | 4.82 | 3.92 | 30.2 |
| 27 | 12.76 | 40% | 69.2 | 665 | 5.14 | 0.01 | 16.5 |
| 28 | 13.03 | 49% | 76.3 | 945 | 5.56 | 0.01 | 21.3 |
| 29 | -2.14 | 55% | 66.9 | 1486 | 6.82 | 71.32 | 30 |
| 30 | 25.3 | 47% | 79.4 | 1447 | 4.626 | 2.7 | 29 |
| 31 | 26.28 | 42% | 63.8 | 1467 | 3.58 | 0.03 | 48 |
| 32 | 14.85 | 31% | 69.2 | 735 | 5.32 | 0.01 | 10.8 |
| 33 | 7.58 | 43% | 73.1 | 402 | 4.28 | 4.97 | 30.7 |

| Record No. | Temperature (°C) | RH (%) | TOW (%) | Precipitation (mm) | pH | Cl (mg/L) | Corrosion (µm) |
|---|---|---|---|---|---|---|---|
| 34 | 7.58 | 37% | 69.2 | 395 | 5.2 | 3.14 | 20.5 |
| 35 | 6.67 | 37% | 69.2 | 364 | 5.33 | 5.33 | 21.6 |
| 36 | 13.03 | 80% | 83 | 950 | 5.12 | 0.01 | 19.9 |
| 37 | 13.34 | 24% | 62.7 | 537 | 3.72 | 0.01 | 34.8 |
| 38 | 17.2 | 0% | 33.3 | 89 | 4.629 | 0.8 | 16.5 |
| 39 | 16.97 | 32% | 69.2 | 777 | 4.13 | 4.14 | 26.8 |
| 40 | 27.6 | 56% | 80.2 | 1598 | 5.227 | 8.2 | 61.6 |
| 41 | 10.91 | 29% | 69.2 | 531 | 4.55 | 0.01 | 19.9 |
| 42 | -2.3 | 35% | 90 | 473 | 5.194 | 5.4 | 56 |
| 43 | 16.06 | 19% | 61.1 | 562 | 4.57 | 2.18 | 19.9 |
| 44 | -2.03 | 40% | 34 | 1368 | 3.52 | 0.01 | 9 |
| 45 | -1.3 | 54% | 35.4 | 1425 | 6.96 | 8.64 | 12 |
| 46 | 17.1 | 48% | 71.5 | 983 | 5.146 | 2.5 | 16.1 |
| 47 | 10 | 29% | 35.2 | 498 | 5.57 | 0.01 | 7.8 |
| 48 | 16.97 | 35% | 69.2 | 779 | 3.96 | 21.69 | 90.8 |
| 49 | 23.9 | 57% | 81 | 1488 | 4.752 | 1.5 | 34.1 |
| 50 | 13.34 | 16% | 61.1 | 557 | 3.59 | 5.58 | 47.1 |
| 51 | 19.4 | 65% | 75.2 | 1034 | 4.401 | 0.8 | 24.2 |
| 52 | 7.28 | 37% | 69.2 | 401 | 5.12 | 18.21 | 66.8 |
| 53 | 23.9 | 57% | 81 | 1488 | 4.735 | 3 | 32.5 |
| 54 | 20 | 10% | 49.3 | 111 | 4.674 | 0.8 | 4.5 |
| 55 | 24.85 | 60% | 77.3 | 1047 | 5.1 | 65 | 171.2 |
| 56 | 10.91 | 59% | 84.3 | 905 | 6.67 | 0.01 | 31.3 |
| 57 | 18.8 | 76% | 83.5 | 13 | 3.448 | 3.9 | 34 |
| 58 | 6.37 | 35% | 69.2 | 341 | 4.98 | 5.1 | 49 |
| 59 | 13.34 | 16% | 61.1 | 631 | 4.38 | 47.62 | 48.1 |
| 60 | 14.85 | 24% | 62.7 | 536 | 5.14 | 0.01 | 11.1 |
| 61 | 13.91 | 51% | 34.2 | 525 | 6.83 | 73.1 | 20 |
| 62 | 3.49 | 26% | 67.7 | 262 | 4.9 | 0.01 | 13.7 |

| Record No. | Temperature (°C) | RH (%) | TOW (%) | Precipitation (mm) | pH | Cl (mg/L) | Corrosion (µm) |
|---|---|---|---|---|---|---|---|
| 63 | 14.1 | 68% | 79.2 | 817 | 5.104 | 5.3 | 24.9 |
| 64 | 13.34 | 16% | 61.1 | 428 | 5.01 | 0.92 | 25.6 |
| 65 | 26.5 | 68% | 84 | 807 | 5.643 | 3 | 37.3 |
| 66 | 16.3 | 15% | 59.3 | 416 | 4.67 | 0.8 | 12.3 |
| 67 | -2.3 | 26% | 85 | 114 | 4.717 | 3.2 | 24.1 |
| 68 | 13.64 | 49% | 76.3 | 1049 | 6 | 0.01 | 32.6 |
| 69 | 7.28 | 46% | 75.2 | 502 | 5.2 | 3.59 | 28 |
| 70 | 6.97 | 46% | 75.2 | 505 | 5.32 | 3.59 | 34.8 |
| 71 | 17.1 | 48% | 76.2 | 1036 | 4.654 | 2.1 | 37.6 |
| 72 | 14.38 | 57% | 66.6 | 1312 | 6.98 | 0.03 | 24 |
| 73 | 5.17 | 39% | 69.2 | 295 | 5.12 | 0.5 | 13.7 |
| 74 | 13.03 | 41% | 69.2 | 685 | 5.11 | 2.18 | 9.9 |
| 75 | 12.43 | 49% | 76.3 | 691 | 4.59 | 5.58 | 30.2 |
| 76 | 26.6 | 57% | 77.1 | 362 | 5.06 | 5.7 | 16.6 |
| 77 | 29.82 | 53% | 35.1 | 1457 | 4.82 | 70.24 | 56 |
| 78 | 6.14 | 38% | 69.2 | 328 | 4.4 | 2.06 | 25.9 |
| 79 | 19.1 | 84% | 86 | 14 | 3.694 | 8 | 35.2 |
| 80 | 17 | 59% | 77.5 | 1178 | 5.098 | 0.8 | 25.3 |
| 81 | 16.97 | 69% | 81.4 | 1286 | 5.49 | 2.37 | 49.9 |
| 82 | 22.12 | 60% | 77.3 | 1155 | 6.92 | 97.62 | 221.2 |
| 83 | 16.97 | 60% | 77.3 | 1123 | 5.12 | 0.01 | 30.2 |
| 84 | 6.37 | 38% | 69.2 | 335 | 4.9 | 1.63 | 21 |
| 85 | -2.71 | 57% | 88.5 | 724 | 6.87 | 8.72 | 44 |
| 86 | 23.03 | 82% | 83 | 1034 | 4.92 | 4.5 | 90.8 |
| 87 | 26.12 | 49% | 89.2 | 963 | 7.02 | 0.03 | 48 |
| 88 | -2.54 | 44% | 88.1 | 888 | 5.03 | 74.23 | 64 |
| 89 | 26.37 | 56% | 64.4 | 1308 | 4.93 | 0.02 | 22 |
| 90 | 22.73 | 54% | 76.3 | 1185 | 4.64 | 0.58 | 60.4 |
| 91 | 16 | 27% | 62 | 747 | 4.613 | 0.8 | 15.4 |

| Record No. | Temperature (°C) | RH (%) | TOW (%) | Precipitation (mm) | pH | Cl (mg/L) | Corrosion (µm) |
|---|---|---|---|---|---|---|---|
| 92 | 17.88 | 31% | 69.2 | 882 | 5.1 | 0.01 | 24.9 |
| 93 | 16.97 | 60% | 77.3 | 1239 | 5.5 | 2.18 | 10 |
| 94 | 18.1 | 39% | 65.2 | 554 | 4.825 | 0.8 | 20.3 |
| 95 | 13.64 | 31% | 69.2 | 671 | 5.13 | 0.01 | 9.5 |
| 96 | 17.2 | 35% | 71.3 | 685 | 4.804 | 2 | 27.1 |
| 97 | 26.32 | 50% | 89 | 1110 | 7.027 | 80.86 | 228.2 |
| 98 | 5.76 | 40% | 69.2 | 317 | 5.03 | 3.01 | 16.6 |
| 99 | 20 | 10% | 61.1 | 522 | 6.08 | 0.01 | 7.9 |
| 100 | 16.97 | 47% | 76.3 | 804 | 4.16 | 5.1 | 39.7 |
| 101 | 26.67 | 87% | 87.1 | 513 | 4.1 | 181.98 | 376.7 |
| 102 | -1.78 | 67% | 90.7 | 970 | 3.59 | 75.1 | 78 |
| 103 | 13 | 42% | 62.8 | 359 | 4.845 | 1.4 | 10.6 |
| 104 | 2.8 | 10% | 72 | 738 | 4.815 | 0.87 | 3.3 |
| 105 | 15.8 | 13% | 57.7 | 239 | 4.813 | 0.8 | 6.8 |
| 106 | 25.7 | 40% | 66.4 | 1419 | 3.73 | 0.01 | 41.7 |
| 107 | 14.31 | 57% | 89.8 | 704 | 3.53 | 0.03 | 53 |
| 108 | 13.96 | 35% | 66.6 | 766 | 6.9 | 67.37 | 61 |
| 109 | 26.97 | 52% | 76.3 | 1310 | 4.92 | 12.02 | 39.7 |
| 110 | 26.91 | 45% | 75.2 | 1402 | 5.42 | 0.01 | 28.4 |
| 111 | 13.34 | 16% | 61.1 | 483 | 4.39 | 0.92 | 22.2 |
| 112 | 1.21 | 18% | 61.1 | 203 | 5.13 | 0.28 | 6 |
| 113 | 17.27 | 27% | 67.7 | 785 | 5.27 | 0.01 | 11.3 |
| 114 | 13.34 | 16% | 61.1 | 500 | 4.41 | 5.58 | 29.7 |
| 115 | 6.37 | 41% | 69.2 | 332 | 4.52 | 1.4 | 33.1 |
| 116 | 16.4 | 0% | 37 | 17 | 4.267 | 0.8 | 15 |
| 117 | 18 | 11% | 50.6 | 35 | 4.435 | 0.8 | 4.6 |
| 118 | 26.5 | 57% | 77 | 608 | 5.527 | 4.3 | 53 |
| 119 | 20.2 | 60% | 83.6 | 1229 | 4.477 | 3.1 | 73.1 |
| 120 | 21 | 19% | 56 | 1352 | 5.08 | 0.8 | 15.2 |

| Record No. | Temperature (°C) | RH (%) | TOW (%) | Precipitation (mm) | pH | Cl (mg/L) | Corrosion (μm) |
|---|---|---|---|---|---|---|---|
| 121 | 27.51 | 77% | 34.7 | 1142 | 4.98 | 0.02 | 18 |
| 122 | 14.5 | 74% | 80.3 | 1226 | 5.182 | 13.6 | 66 |
| 123 | 23.94 | 30% | 51.2 | 1106 | 5.26 | 0.01 | 20.9 |
| 124 | 6.06 | 31% | 69.2 | 351 | 4.31 | 1.63 | 34.8 |
| 125 | 14.55 | 52% | 76.3 | 752 | 4.41 | 1.15 | 26.8 |
| 126 | 28.16 | 46% | 34.1 | 1208 | 6.85 | 9.18 | 33 |
| 127 | 26.04 | 49% | 63.6 | 648 | 7.02 | 0.03 | 35 |
| 128 | 18.18 | 16% | 61.1 | 536 | 7.37 | 0.01 | 13.7 |
| 129 | 16.1 | 35% | 66 | 685 | 4.898 | 1.7 | 24.5 |
| 130 | 4.66 | 10% | 41.8 | 338 | 4.83 | 1.63 | 5 |
| 131 | 22.42 | 60% | 77.3 | 1381 | 5.33 | 13.27 | 52.4 |
| 132 | 14.12 | 58% | 63.5 | 1041 | 3.54 | 8.75 | 43 |
| 133 | 19.6 | 65% | 76 | 1910 | 4.537 | 0.8 | 23.4 |
| 134 | 11 | 45% | 77 | 510 | 5.14 | 2.6 | 12.8 |
| 135 | 27.24 | 68% | 34.8 | 1513 | 7.01 | 66.13 | 61 |
| 136 | 6.06 | 35% | 69.2 | 635 | 5.03 | 192.73 | 86.7 |
| 137 | 6.37 | 33% | 69.2 | 354 | 3.92 | 0.92 | 35.9 |
| 138 | 16.9 | 37% | 71.5 | 1828 | 4.416 | 2.8 | 27 |
| 139 | 13.88 | 44% | 65.7 | 1182 | 4.98 | 65.49 | 81.1 |
| 140 | 23.94 | 59% | 76.3 | 1409 | 5.33 | 3.69 | 30.2 |
| 141 | 7.28 | 46% | 75.2 | 507 | 5.22 | 2.54 | 24.9 |
| 142 | 17 | 49% | 73.6 | 1420 | 5.222 | 2.4 | 12.4 |
| 143 | 13.03 | 52% | 76.3 | 865 | 5.11 | 0.01 | 36.5 |
| 144 | 17.88 | 49% | 76.3 | 947 | 4.81 | 47.62 | 37.7 |
| 145 | -2.81 | 67% | 65.8 | 1158 | 6.92 | 9.5 | 17 |
| 146 | 6.06 | 43% | 73.1 | 351 | 4.26 | 8.22 | 44.8 |
| 147 | 14.3 | 34% | 69 | 271 | 4.966 | 2.6 | 14.1 |
| 148 | -2.45 | 43% | 88.4 | 917 | 6.86 | 73.78 | 72 |
| 149 | 6.97 | 36% | 69.2 | 382 | 5.5 | 3.27 | 35.9 |

| Record No. | Temperature (°C) | RH (%) | TOW (%) | Precipitation (mm) | pH | Cl (mg/L) | Corrosion (µm) |
|---|---|---|---|---|---|---|---|
| 150 | 8.18 | 51% | 76.3 | 526 | 4.87 | 2.06 | 19.7 |
| 151 | 18.9 | 70% | 83.4 | 1845 | 5.381 | 3.3 | 16.6 |
| 152 | 26.58 | 81% | 84 | 1033 | 5.22 | 84.34 | 237.4 |
| 153 | -2.24 | 69% | 66.8 | 1102 | 3.64 | 0.03 | 35 |
| 154 | 14.1 | 80% | 81.4 | 1800 | 5.267 | 0.8 | 13.6 |
| 155 | 12.9 | 41% | 66 | 554 | 5.711 | 0.3 | 7.7 |
| 156 | 20.91 | 45% | 75.2 | 1234 | 5.12 | 0.01 | 19.9 |
| 157 | 13.03 | 41% | 69.2 | 691 | 5.2 | 3.92 | 19.9 |
| 158 | 23.94 | 69% | 81.4 | 1511 | 5.84 | 3.01 | 50.8 |
| 159 | 4.86 | 37% | 69.2 | 291 | 5.33 | 0.92 | 14.9 |
| 160 | 7.58 | 43% | 73.1 | 415 | 4.52 | 4.23 | 32.1 |
| 161 | 26.67 | 82% | 83 | 615 | 3.88 | 154.47 | 376.7 |
| 162 | 15.9 | 38% | 62.1 | 1129 | 4.05 | 41.2 | 78.9 |
| 163 | 15.9 | 17% | 63 | 705 | 4.544 | 1.5 | 16.1 |
| 164 | 4.85 | 47% | 76.3 | 353 | 4.81 | 3.27 | 35.9 |
| 165 | 17.84 | 50% | 76.3 | 833 | 4.34 | 93.18 | 198.5 |
| 166 | 26.1 | 49% | 76.3 | 1211 | 4.87 | 53.31 | 154.5 |
| 167 | 15.1 | 25% | 69.6 | 1312 | 4.267 | 5 | 28.1 |
| 168 | 10.31 | 28% | 38.2 | 503 | 5.26 | 0.01 | 10.7 |
| 169 | 19.09 | 80% | 83 | 692 | 4.34 | 3.92 | 30.2 |
| 170 | 23.9 | 57% | 81 | 1488 | 5.005 | 1.8 | 28.6 |
| 171 | 7.28 | 46% | 75.2 | 410 | 4.46 | 4.23 | 34.2 |
| 172 | 13.34 | 16% | 61.1 | 535 | 3.98 | 5.58 | 33.7 |
| 173 | 12 | 38% | 68.8 | 652 | 4.557 | 0.8 | 19.3 |
| 174 | -2.87 | 79% | 35.2 | 797 | 3.54 | 70.8 | 36 |
| 175 | -2.02 | 44% | 35.4 | 1180 | 7 | 119.33 | 26 |
| 176 | 14.2 | 13% | 71 | 355 | 4.317 | 1.5 | 29.3 |
| 177 | 24.24 | 71% | 81.4 | 1540 | 6.53 | 1.63 | 31.1 |
| 178 | 26.01 | 56% | 89.2 | 880 | 3.62 | 0.03 | 51.7 |

| Record No. | Temperature (°C) | RH (%) | TOW (%) | Precipitation (mm) | pH | Cl (mg/L) | Corrosion (µm) |
|---|---|---|---|---|---|---|---|
| 179 | 27.85 | 54% | 64.7 | 1030 | 5.01 | 74.45 | 141 |
| 180 | 13 | 42% | 62.8 | 359 | 5.048 | 1.4 | 12.6 |
| 181 | -2.36 | 67% | 88.1 | 656 | 3.64 | 9.25 | 53 |
| 182 | 21 | 20% | 56 | 1372 | 5.06 | 0.8 | 13.7 |
| 183 | 13.94 | 78% | 83 | 653 | 4.48 | 3.92 | 39.7 |
| 184 | 23.8 | 48% | 65 | 1095 | 3.52 | 0.01 | 74.2 |
| 185 | 9.4 | 69% | 81.4 | 493 | 4.42 | 44.14 | 99.8 |
| 186 | 28.17 | 41% | 34.6 | 1185 | 6.86 | 0.02 | 29 |
| 187 | 27.1 | 53% | 65.3 | 2427 | 4.905 | 1.5 | 23 |
| 188 | 29.66 | 48% | 66.3 | 778 | 6.86 | 9.64 | 37 |
| 189 | 13.34 | 16% | 61.1 | 438 | 5.03 | 4.75 | 29.7 |
| 190 | 16.97 | 32% | 69.2 | 786 | 4.2 | 4.5 | 24.9 |
| 191 | 23.2 | 60% | 80 | 1152 | 4.342 | 3.2 | 61.3 |
| 192 | 28.94 | 34% | 36.2 | 1420 | 5.04 | 9.8 | 19 |
| 193 | 23.8 | 48% | 89.3 | 1122 | 4.489 | 2.3 | 52.5 |
| 194 | -3.07 | 74% | 66.4 | 1314 | 4.77 | 9.85 | 9 |
| 195 | 6.67 | 46% | 75.2 | 436 | 4.92 | 12.28 | 28 |
| 196 | 16.97 | 50% | 76.3 | 1163 | 5.49 | 2.18 | 10 |
| 197 | 27.4 | 58% | 70.7 | 2123 | 5.443 | 2.9 | 23.2 |
| 198 | 13.34 | 42% | 69.2 | 734 | 5.43 | 0.01 | 23.2 |
| 199 | 13.94 | 70% | 81.4 | 1340 | 6.23 | 8.45 | 49.9 |
| 200 | 14.2 | 37% | 68.3 | 367 | 4.366 | 1.5 | 44.1 |
| 201 | 24.24 | 49% | 76.3 | 1016 | 4.07 | 4.23 | 42.5 |
| 202 | 26.06 | 49% | 76.3 | 1225 | 4.54 | 3.69 | 39.7 |
| 203 | 15.76 | 40% | 69.2 | 866 | 5.67 | 0.01 | 11.9 |
| 204 | 13.34 | 37% | 69.2 | 636 | 4.41 | 0.62 | 30.7 |
| 205 | 17.27 | 47% | 76.3 | 984 | 5.28 | 51.41 | 35.3 |
| 206 | 24.85 | 55% | 76.3 | 1437 | 5.5 | 4.5 | 59.2 |
| 207 | -2.01 | 57% | 63.5 | 1048 | 3.65 | 71.35 | 33 |

| Record No. | Temperature (°C) | RH (%) | TOW (%) | Precipitation (mm) | pH | Cl (mg/L) | Corrosion (µm) |
|---|---|---|---|---|---|---|---|
| 208 | 20.4 | 44% | 72 | 1440 | 5.239 | 0.8 | 12.9 |
| 209 | 14.47 | 57% | 33.9 | 1037 | 6.81 | 8.83 | 15 |
| 210 | 11.21 | 58% | 76.3 | 791 | 5.15 | 0.01 | 25.2 |
| 211 | -3.1 | 28% | 84 | 114 | 4.692 | 5.4 | 35.9 |
| 212 | 6.06 | 30% | 69.2 | 337 | 4.68 | 0.92 | 5.2 |
| 213 | 12.43 | 39% | 69.2 | 563 | 3.78 | 12.02 | 69.7 |
| 214 | -2.04 | 39% | 34 | 753 | 6.87 | 0.01 | 3.4 |
| 215 | 26.97 | 58% | 76.3 | 1347 | 5.1 | 8.53 | 79.2 |
| 216 | 5.15 | 37% | 69.2 | 337 | 3.73 | 0.46 | 30.2 |
| 217 | 19.8 | 65% | 74.9 | 1409 | 4.5 | 0.8 | 14.6 |
| 218 | 6.06 | 43% | 73.1 | 357 | 4.5 | 8.22 | 36.5 |
| 219 | 17.4 | 40% | 72.4 | 685 | 4.933 | 1.9 | 29.9 |
| 220 | 14.85 | 32% | 69.2 | 745 | 5.71 | 0.01 | 11.9 |
| 221 | 24.02 | 60% | 77.3 | 918 | 4.09 | 2.18 | 20.5 |
| 222 | -2.7 | 52% | 90.2 | 729 | 6.83 | 0.02 | 21 |
| 223 | 24.8 | 64% | 53.7 | 1299 | 6.721 | 0.01 | 23.7 |
| 224 | 23 | 78% | 81 | 631 | 5.287 | 12.3 | 66.1 |
| 225 | 14 | 76% | 82 | 463 | 4.419 | 2.3 | 35.5 |
| 226 | 14.28 | 58% | 65.4 | 858 | 6.82 | 9.61 | 26 |
| 227 | 16.97 | 40% | 69.2 | 873 | 4.82 | 2.18 | 30.2 |
| 228 | 26.06 | 50% | 76.3 | 1453 | 5.81 | 0.01 | 19.9 |
| 229 | 20 | 65% | 77.3 | 890 | 4.32 | 0.01 | 19.9 |
| 230 | 13 | 42% | 62.8 | 359 | 4.689 | 1.4 | 10.8 |
| 231 | 15.15 | 33% | 69.2 | 762 | 5.22 | 0.01 | 10.4 |
| 232 | 4.51 | 35% | 69.2 | 261 | 4.89 | 0.62 | 14.3 |
| 233 | 3.64 | 60% | 77.3 | 321 | 4.58 | 0.17 | 17.7 |
| 234 | 22.9 | 48% | 91.1 | 1471 | 4.614 | 2 | 47.2 |
| 235 | 15.8 | 50% | 82.3 | 989 | 7.12 | 67.53 | 123.2 |
| 236 | 22.9 | 84% | 88.3 | 3677 | 5.229 | 4 | 69.3 |

| Record No. | Temperature (°C) | RH (%) | TOW (%) | Precipitation (mm) | pH | Cl (mg/L) | Corrosion (µm) |
|---|---|---|---|---|---|---|---|
| 237 | 12.43 | 58% | 76.3 | 458 | 3.73 | 29.59 | 95.1 |
| 238 | 10.6 | 27% | 64.5 | 495 | 4.495 | 0.8 | 22.5 |
| 239 | 13.34 | 16% | 61.1 | 663 | 4.01 | 47.62 | 54.8 |
| 240 | 12.12 | 56% | 76.3 | 828 | 5.12 | 0.01 | 37.1 |
| 241 | 26.06 | 55% | 76.3 | 1480 | 5.66 | 0.01 | 30.2 |
| 242 | 5.76 | 15% | 61.1 | 338 | 4.59 | 12.37 | 23.2 |
| 243 | 7.28 | 37% | 69.2 | 383 | 5.11 | 7.59 | 33.7 |
| 244 | 19.09 | 71% | 81.4 | 1272 | 5.31 | 3.92 | 19.9 |
| 245 | 16.06 | 37% | 69.2 | 718 | 3.98 | 4.97 | 53.2 |
| 246 | 26.06 | 55% | 76.3 | 1408 | 5.34 | 7.59 | 30.2 |
| 247 | 26.3 | 51% | 46.3 | 947 | 4.88 | 8.3 | 24.5 |
| 248 | 15.6 | 27% | 57.5 | 266 | 5.113 | 0.8 | 6.4 |
| 249 | 27.1 | 59% | 74 | 1387 | 4.878 | 2.5 | 28.3 |
| 250 | 4.55 | 45% | 75.2 | 302 | 4.36 | 3.69 | 26 |
| 251 | 28.39 | 68% | 33.6 | 855 | 3.53 | 0.03 | 41 |
| 252 | -1.94 | 82% | 34.7 | 1049 | 4.87 | 65.44 | 22 |
| 253 | 14.4 | 42% | 88.8 | 1294 | 6.83 | 0.03 | 38 |
| 254 | 6.9 | 10% | 72 | 624 | 4.821 | 0.8 | 3.6 |
| 255 | 17.88 | 15% | 61.1 | 552 | 5.17 | 0.01 | 16 |
| 256 | 14.24 | 65% | 77.3 | 861 | 4.89 | 13.05 | 43.2 |
| 257 | 13.83 | 53% | 89.2 | 1511 | 6.95 | 66.66 | 119 |
| 258 | 14.34 | 45% | 85.2 | 767 | 4.75 | 0.01 | 34.4 |
| 259 | 28.81 | 29% | 33.8 | 793 | 3.62 | 67.54 | 71 |
| 260 | 16.97 | 50% | 76.3 | 1089 | 5.14 | 2.54 | 14.9 |
| 261 | 24.2 | 58% | 77 | 716 | 5.145 | 43.1 | 128.4 |
| 262 | 13.97 | 81% | 35.9 | 648 | 4.91 | 8.01 | 13 |
| 263 | 15.8 | 31% | 68.1 | 1704 | 4.415 | 2.6 | 29.6 |
| 264 | 23.03 | 60% | 77.3 | 1081 | 4.45 | 2.18 | 49.9 |
| 265 | 27.7 | 51% | 75 | 983 | 4.586 | 3.4 | 23 |

| Record No. | Temperature (°C) | RH (%) | TOW (%) | Precipitation (mm) | pH | Cl (mg/L) | Corrosion (µm) |
|---|---|---|---|---|---|---|---|
| 266 | 13.93 | 43% | 89 | 1759 | 7.01 | 8.82 | 49 |
| 267 | 13.68 | 38% | 36.4 | 635 | 6.84 | 0.02 | 9 |
| 268 | -1.17 | 46% | 35.6 | 1363 | 3.5 | 8.37 | 35 |
| 269 | 6.67 | 46% | 75.2 | 492 | 5.35 | 5.58 | 23.8 |
| 270 | 26.06 | 60% | 77.3 | 1458 | 5.52 | 4.26 | 39.7 |
| 271 | 13.34 | 45% | 75.2 | 693 | 4.4 | 5.58 | 27.6 |
| 272 | 16.94 | 19% | 61.1 | 622 | 4.49 | 0.01 | 35.7 |
| 273 | 27.82 | 49% | 88.5 | 401 | 7.01 | 67.84 | 188 |
| 274 | 11.1 | 24% | 62.7 | 334 | 4.4 | 0.8 | 19.7 |
| 275 | 13.9 | 71% | 78.8 | 805 | 5.101 | 8 | 54.8 |
| 276 | 2.12 | 40% | 69.2 | 208 | 4.53 | 1.63 | 19.9 |
| 277 | 15.7 | 16% | 65.5 | 655 | 4.579 | 1.7 | 18.1 |
| 278 | 14.38 | 47% | 34.5 | 1112 | 3.63 | 73.85 | 47 |
| 279 | 10.8 | 45% | 74 | 451 | 5.213 | 2.3 | 18.2 |
| 280 | 14.24 | 25% | 67.7 | 648 | 4.64 | 1.4 | 39.7 |
| 281 | 7.8 | 10% | 72 | 681 | 4.822 | 0.8 | 4.8 |
| 282 | 25.2 | 47% | 79.5 | 1591 | 4.377 | 3.4 | 36 |
| 283 | 17.88 | 49% | 76.3 | 1076 | 5.22 | 26.75 | 32.6 |
| 284 | 11.96 | 29% | 69.2 | 577 | 4.43 | 1.4 | 34.2 |
| 285 | 15.2 | 79% | 34.3 | 1275 | 4.62 | 0.01 | 8.3 |
| 286 | 16.02 | 1% | 68.3 | 110 | 5.9 | 0.01 | 14.8 |
| 287 | 29.61 | 61% | 35.3 | 1068 | 3.63 | 8.94 | 43 |
| 288 | 3.64 | 35% | 36.8 | 618 | 5.39 | 0.01 | 5 |
| 289 | 14.55 | 32% | 46.2 | 726 | 5.3 | 0.01 | 8.7 |
| 290 | 23.03 | 20% | 36.1 | 785 | 4.86 | 0.01 | 13 |
| 291 | 27.3 | 58% | 71.6 | 2171 | 5.046 | 4.5 | 20.1 |
| 292 | 5.6 | 28% | 63.2 | 747 | 4.53 | 0.79 | 5.1 |
| 293 | -3 | 49% | 34.8 | 1105 | 4.82 | 0.03 | 4 |
| 294 | 28.57 | 62% | 65.5 | 1284 | 6.79 | 69.4 | 122 |

| Record No. | Temperature (°C) | RH (%) | TOW (%) | Precipitation (mm) | pH | Cl (mg/L) | Corrosion (µm) |
|---|---|---|---|---|---|---|---|
| 295 | 13.9 | 60% | 36.5 | 1023 | 5.05 | 70.01 | 17 |
| 296 | 25.4 | 47% | 79.4 | 1303 | 4.356 | 2.7 | 26.4 |
| 297 | 17.2 | 32% | 61.9 | 374 | 5.344 | 0.8 | 21 |
| 298 | 26.9 | 56% | 69.1 | 2210 | 5.19 | 2.5 | 20.9 |
| 299 | 6.67 | 37% | 69.2 | 361 | 4.89 | 12.19 | 21.3 |
| 300 | 7.58 | 37% | 69.2 | 396 | 5.22 | 3.42 | 21.3 |
| 301 | 14.2 | 80% | 73.4 | 1800 | 5.265 | 0.8 | 19.6 |
| 302 | 26.1 | 55% | 71.4 | 936 | 5.214 | 0.8 | 19.5 |
| 303 | 16.8 | 17% | 65.1 | 443 | 4.402 | 1.3 | 17.9 |
| 304 | 27.88 | 60% | 77.3 | 1265 | 4.79 | 6.63 | 30.2 |
| 305 | -1.68 | 47% | 64.9 | 1281 | 4.91 | 0.02 | 8.8 |
| 306 | 27.2 | 57% | 68.7 | 2082 | 4.712 | 3 | 14.2 |
| 307 | 14.85 | 31% | 69.2 | 711 | 4.43 | 3.92 | 39.7 |
| 308 | 15.2 | 29% | 64.5 | 747 | 5.038 | 0.8 | 8.6 |
| 309 | -1.5 | 48% | 63.2 | 1211 | 6.79 | 0.03 | 15 |

# APPENDIX B. SUPPORT VECTORS $\mathbf{x}_i$ AND CONSTANTS $\nu_i$

The final corrosion rate model was defined by support vectors $\mathbf{x}_i$, optimization constants $\nu_i$, and constant $b$ as:

$$A(\mathbf{x}) = \sum_{i=1}^{N_{SV}} \nu_i \exp\left(-\gamma \left\|\mathbf{x}_i - \mathbf{x}\right\|^2\right) + b$$

The predictive function to estimate the corrosion rate was determined as:

$$A(\mathbf{x}) = \sum_{i=1}^{175} \nu_i \exp\left(-0.091 \left\|\mathbf{x}_i - \mathbf{x}\right\|^2\right) + 85.95$$

with $\gamma = 0.091$ found as the optimal RBF kernel parameter and the constant calculated as $b$ =85.95. Table B-1 lists the complete set of 175 support vectors $\mathbf{x}_i$, and their associated constants $\nu_i$.

Table B-1: Support vectors $\mathbf{x}_i$ and associated constants $\nu_i$

| Support Vector No. | $\nu_i$ | Support Vectors $\mathbf{x}_i$ | | | |
|---|---|---|---|---|---|
| | | Temperature | RH | pH | Cl |
| 1 | 45.020 | 0.060 | 0.066 | -0.953 | -1.000 |
| 2 | -45.020 | -0.443 | 0.242 | -0.372 | -0.991 |
| 3 | -45.020 | -0.022 | 0.021 | -0.288 | -0.986 |
| 4 | 45.020 | -0.443 | 0.242 | -0.560 | -0.983 |

| Support Vector No. | $v_i$ | Support Vectors $\mathbf{x}_i$ | | | |
|---|---|---|---|---|---|
| | | Temperature | RH | pH | Cl |
| 5 | 45.020 | 0.550 | 0.522 | -0.040 | -0.862 |
| 6 | 45.020 | -0.443 | 0.377 | -0.464 | -0.915 |
| 7 | 45.020 | 0.217 | -0.038 | -0.469 | -1.000 |
| 8 | 1.168 | -0.001 | 0.017 | -0.861 | -1.000 |
| 9 | 45.020 | 0.598 | 0.616 | -0.544 | -0.967 |
| 10 | -45.020 | -0.951 | 0.789 | -0.353 | -0.967 |
| 11 | 45.020 | 0.812 | 0.131 | -0.948 | -0.264 |
| 12 | 45.020 | -0.517 | 0.488 | -0.305 | -0.966 |
| 13 | 45.020 | 0.033 | 0.574 | -0.157 | -0.917 |
| 14 | 45.020 | 0.878 | 0.910 | 0.816 | -0.296 |
| 15 | 45.020 | 0.051 | 0.211 | -0.532 | -0.985 |
| 16 | 4.698 | 0.634 | 0.938 | -0.469 | -0.976 |
| 17 | -45.020 | 0.772 | 0.488 | 0.204 | -1.000 |
| 18 | 45.020 | -0.883 | -0.920 | -0.973 | -0.913 |
| 19 | 45.020 | 0.164 | 0.242 | -0.729 | -0.949 |
| 20 | -45.020 | 0.871 | 0.443 | -0.420 | -0.965 |
| 21 | 45.020 | 0.587 | 0.522 | -0.489 | -0.977 |
| 22 | 45.020 | 0.698 | 0.488 | 0.046 | -0.953 |
| 23 | 45.020 | -0.001 | -0.038 | -0.203 | -0.991 |
| 24 | 45.020 | 0.272 | 0.488 | -0.545 | -0.033 |
| 25 | 45.020 | -0.241 | 0.664 | -0.504 | -0.542 |
| 26 | 45.020 | -0.976 | 0.910 | 0.745 | -0.910 |

| Support Vector No. | $v_i$ | Support Vectors $\mathbf{x}_i$ | | | |
|---|---|---|---|---|---|
| | | Temperature | RH | pH | Cl |
| 27 | -27.496 | -0.914 | 0.093 | -0.254 | -1.000 |
| 28 | 45.020 | -0.057 | 0.488 | -0.005 | -1.000 |
| 29 | 45.020 | 0.798 | 0.512 | 0.060 | -0.955 |
| 30 | -28.297 | 0.091 | 0.242 | 0.153 | -1.000 |
| 31 | 45.020 | 0.586 | 0.651 | -0.062 | -0.872 |
| 32 | 45.020 | -0.085 | 0.242 | -0.499 | -0.986 |
| 33 | -45.020 | 0.827 | 0.450 | -0.300 | -0.959 |
| 34 | -45.020 | 0.640 | 0.651 | -0.206 | -0.981 |
| 35 | -45.020 | 0.661 | 0.664 | 0.572 | -0.983 |
| 36 | -45.020 | 0.841 | 0.225 | -0.355 | -0.969 |
| 37 | -45.020 | 0.391 | 0.439 | -0.464 | -0.992 |
| 38 | -45.020 | 0.045 | 0.588 | -0.156 | -0.945 |
| 39 | 45.020 | 0.275 | 0.550 | -0.775 | -0.994 |
| 40 | 45.020 | 0.785 | 0.055 | -0.933 | -1.000 |
| 41 | -45.020 | 0.348 | 0.720 | -0.545 | -0.959 |
| 42 | -45.020 | -0.392 | 0.339 | -0.300 | -0.992 |
| 43 | -45.020 | 0.772 | 0.488 | -0.035 | -0.921 |
| 44 | 45.020 | 0.774 | 0.488 | -0.275 | -0.447 |
| 45 | -45.020 | -0.020 | 0.720 | -0.147 | -1.000 |
| 46 | -45.020 | 0.428 | 0.339 | -0.087 | -0.992 |
| 47 | 45.020 | 0.899 | -0.972 | 0.735 | -0.905 |
| 48 | -45.020 | 0.062 | -0.958 | -0.907 | -0.234 |

| Support Vector No. | $v_i$ | Support Vectors $\mathbf{x}_i$ | | | |
|---|---|---|---|---|---|
| | | Temperature | RH | pH | Cl |
| 49 | 45.020 | 0.053 | 0.190 | -0.392 | -0.986 |
| 50 | 25.343 | 0.770 | 0.048 | 0.822 | -1.000 |
| 51 | -45.020 | 0.136 | -0.163 | -0.151 | -0.992 |
| 52 | -45.020 | -0.443 | 0.242 | -0.193 | 1.000 |
| 53 | -45.020 | 0.841 | 0.280 | -0.383 | -0.976 |
| 54 | 45.020 | 0.035 | 0.664 | 0.419 | -0.912 |
| 55 | 45.020 | 0.532 | 0.522 | 0.771 | 0.013 |
| 56 | -45.020 | 0.330 | 0.737 | -1.000 | -0.960 |
| 57 | 45.020 | -0.988 | 0.772 | -0.285 | -0.944 |
| 58 | 45.020 | 0.416 | 0.740 | -0.475 | -0.968 |
| 59 | 45.020 | 0.809 | 0.720 | -0.780 | 0.603 |
| 60 | -45.020 | -0.934 | 0.045 | -0.897 | -0.260 |
| 61 | -45.020 | 0.219 | 0.488 | -0.137 | -0.974 |
| 62 | -45.020 | 0.275 | 0.488 | -0.096 | -0.722 |
| 63 | 45.020 | 0.809 | 0.862 | -0.668 | 0.888 |
| 64 | 45.020 | -0.001 | -0.038 | -0.193 | -0.951 |
| 65 | -45.020 | 0.148 | -0.156 | -0.304 | -0.992 |
| 66 | 45.020 | -0.443 | 0.377 | -0.586 | -0.915 |
| 67 | 45.020 | 0.698 | 0.522 | -0.158 | -0.326 |
| 68 | -45.020 | 0.146 | 0.242 | 0.133 | -1.000 |
| 69 | -45.020 | 0.823 | 0.239 | -0.112 | -0.974 |
| 70 | -45.020 | 0.221 | 0.394 | -0.095 | -0.975 |

| Support Vector No. | $v_i$ | Support Vectors $\mathbf{x}_i$ | | | |
|---|---|---|---|---|---|
| | | Temperature | RH | pH | Cl |
| 71 | 45.020 | -0.891 | -0.927 | 0.791 | -0.910 |
| 72 | 45.020 | 0.827 | 0.488 | -0.158 | -0.912 |
| 73 | -45.020 | 0.109 | 0.242 | -0.096 | -1.000 |
| 74 | 45.020 | 0.900 | -0.955 | 0.740 | -1.000 |
| 75 | 45.020 | -0.075 | 0.488 | -0.147 | -1.000 |
| 76 | -45.020 | 0.238 | 0.190 | -0.071 | -1.000 |
| 77 | -45.020 | 0.091 | 0.242 | -0.045 | -1.000 |
| 78 | -45.020 | 0.772 | 0.488 | -0.152 | -1.000 |
| 79 | 45.020 | -0.001 | -0.038 | -0.928 | -0.942 |
| 80 | -45.020 | 0.648 | 0.522 | -0.673 | -0.977 |
| 81 | 45.020 | 0.880 | 0.087 | -0.203 | -0.227 |
| 82 | -45.020 | -0.028 | 0.131 | 0.154 | -0.997 |
| 83 | 45.020 | 0.219 | 0.242 | -0.739 | -0.775 |
| 84 | -45.020 | 0.367 | 0.450 | -0.514 | -0.992 |
| 85 | 45.020 | -0.369 | 0.242 | -0.147 | -0.811 |
| 86 | 45.020 | 0.924 | 0.114 | 0.704 | -0.280 |
| 87 | 45.020 | 0.587 | 0.720 | -0.249 | -0.953 |
| 88 | -45.020 | 0.379 | 0.478 | -0.445 | -0.992 |
| 89 | 45.020 | 0.053 | 0.522 | -0.265 | -0.865 |
| 90 | -45.020 | -0.338 | 0.339 | -0.299 | -0.992 |
| 91 | 45.020 | 0.865 | 0.623 | -0.093 | -0.915 |
| 92 | -45.020 | 0.219 | 0.522 | 0.046 | -0.977 |

| Support Vector No. | $v_i$ | Support Vectors $\mathbf{x}_i$ | | | |
|---|---|---|---|---|---|
| | | Temperature | RH | pH | Cl |
| 93 | -45.020 | 0.847 | 0.325 | -0.185 | -0.953 |
| 94 | 45.020 | -0.388 | 0.450 | -0.045 | -0.963 |
| 95 | -21.078 | -0.966 | 0.896 | -0.193 | -0.230 |
| 96 | 35.861 | 0.843 | -0.948 | 0.816 | -0.314 |
| 97 | 45.020 | 0.803 | 0.754 | -0.096 | -0.125 |
| 98 | 45.020 | 0.154 | -0.003 | -0.693 | -0.573 |
| 99 | 45.020 | -0.001 | -0.038 | -0.509 | -0.942 |
| 100 | -45.020 | 0.337 | 0.734 | -0.014 | -0.966 |
| 101 | 45.020 | 0.787 | 0.927 | 0.825 | -0.161 |
| 102 | -45.020 | 0.403 | 0.522 | -0.555 | -1.000 |
| 103 | 45.020 | 0.069 | 0.626 | -0.116 | -0.859 |
| 104 | 45.020 | 0.580 | 0.903 | -0.092 | -0.959 |
| 105 | 45.020 | -0.369 | 0.242 | -0.152 | -0.921 |
| 106 | -45.020 | 0.725 | 0.595 | -0.399 | -0.972 |
| 107 | -45.020 | 0.045 | 0.664 | -0.072 | -0.992 |
| 108 | -45.020 | 0.403 | -0.446 | -0.375 | -0.992 |
| 109 | -45.020 | 0.033 | -0.889 | -0.183 | -0.274 |
| 110 | 45.020 | 0.219 | 0.664 | 0.041 | -0.976 |
| 111 | -45.020 | 0.209 | 0.100 | -0.514 | -0.987 |
| 112 | 45.020 | 0.029 | 0.934 | 0.786 | -0.308 |
| 113 | -45.020 | -0.935 | -0.976 | -0.963 | -1.000 |
| 114 | 45.020 | 0.818 | 0.955 | 0.750 | -0.895 |

| Support Vector No. | $v_i$ | Support Vectors $\mathbf{x}_i$ | | | |
|---|---|---|---|---|---|
| | | Temperature | RH | pH | Cl |
| 115 | -45.020 | -0.934 | -0.927 | 0.811 | 0.238 |
| 116 | 45.020 | 0.227 | 0.484 | -0.385 | -0.978 |
| 117 | -45.020 | 0.774 | 0.318 | -0.099 | -0.992 |
| 118 | -45.020 | 0.731 | 0.595 | -0.537 | -0.972 |
| 119 | -45.020 | -0.942 | 0.163 | 0.720 | -0.260 |
| 120 | 45.020 | 0.569 | 0.488 | -0.392 | -0.994 |
| 121 | -45.020 | -0.022 | 0.021 | -0.367 | -0.986 |
| 122 | 45.020 | 0.643 | 0.664 | 0.220 | -0.969 |
| 123 | -45.020 | 0.219 | 0.488 | 0.041 | -0.977 |
| 124 | -45.020 | -0.976 | 0.969 | 0.725 | -1.000 |
| 125 | -45.020 | -0.471 | 0.035 | -0.448 | -0.992 |
| 126 | 45.020 | -0.185 | -0.830 | -0.076 | -1.000 |
| 127 | 45.020 | 0.659 | 0.512 | -0.135 | -0.553 |
| 128 | -45.020 | 0.057 | 0.235 | -0.226 | -0.973 |
| 129 | -45.020 | 0.293 | -0.038 | 1.000 | -1.000 |
| 130 | 45.020 | -0.425 | 0.242 | -0.219 | -0.947 |
| 131 | -45.020 | 0.349 | 0.824 | -0.875 | -0.917 |
| 132 | 45.020 | -0.020 | 0.488 | -0.152 | -1.000 |
| 133 | -45.020 | 0.219 | 0.488 | -0.530 | -0.604 |
| 134 | -45.020 | -0.591 | 0.522 | -0.423 | -0.998 |
| 135 | -45.020 | 0.348 | 0.664 | -0.050 | -0.959 |
| 136 | -45.020 | 0.282 | -0.401 | -0.497 | -0.992 |

| Support Vector No. | $v_i$ | Support Vectors $\mathbf{x}_i$ | | | |
|---|---|---|---|---|---|
| | | Temperature | RH | pH | Cl |
| 137 | -29.186 | -0.315 | 0.488 | -0.275 | -0.979 |
| 138 | -45.020 | 0.798 | 0.242 | -0.532 | -0.983 |
| 139 | 45.020 | -0.057 | 0.242 | -0.831 | -0.875 |
| 140 | -45.020 | 0.191 | 0.616 | -0.973 | -0.995 |
| 141 | 45.020 | -0.951 | 0.962 | -0.110 | -0.944 |
| 142 | 45.020 | -0.388 | 0.242 | 0.046 | -0.966 |
| 143 | 45.020 | 0.148 | 0.696 | 0.873 | -0.299 |
| 144 | -45.020 | -0.020 | 0.242 | -0.152 | -0.977 |
| 145 | 5.118 | 0.987 | -0.931 | -0.907 | -0.907 |
| 146 | -45.020 | 0.238 | 0.488 | -0.066 | -0.467 |
| 147 | -45.020 | 0.227 | 0.322 | -0.134 | -0.974 |
| 148 | -45.020 | 0.033 | -0.969 | 0.725 | -0.241 |
| 149 | 45.020 | 0.017 | 0.488 | 0.301 | -1.000 |
| 150 | -25.357 | -0.986 | -0.934 | -0.953 | -0.265 |
| 151 | -45.020 | 0.459 | 0.450 | -0.147 | -1.000 |
| 152 | 45.020 | -0.388 | 0.242 | -0.423 | -0.970 |
| 153 | 45.020 | -0.425 | 0.242 | -0.453 | -0.986 |
| 154 | 45.020 | 0.661 | 0.488 | -0.764 | -0.962 |
| 155 | -45.020 | 0.112 | 0.080 | -0.189 | -0.992 |
| 156 | -45.020 | -0.979 | 0.934 | -0.183 | -1.000 |
| 157 | 45.020 | 0.046 | 0.045 | -0.953 | -0.909 |
| 158 | -45.020 | 0.275 | 0.488 | -0.305 | -0.506 |

| Support Vector No. | $v_i$ | Support Vectors $\mathbf{x}_i$ | | | |
|---|---|---|---|---|---|
| | | Temperature | RH | pH | Cl |
| 159 | -45.020 | 0.804 | 0.516 | -0.178 | -0.941 |
| 160 | -45.020 | 0.017 | 0.242 | -0.142 | -1.000 |
| 161 | -30.814 | 0.947 | -0.900 | -0.188 | -0.898 |
| 162 | 45.020 | 0.091 | 0.242 | -0.499 | -0.959 |
| 163 | -45.020 | -0.642 | 0.339 | -0.303 | -0.991 |
| 164 | -45.020 | -0.143 | 0.512 | -0.137 | -0.973 |
| 165 | -45.020 | -0.998 | 0.145 | -0.326 | -0.898 |
| 166 | -45.020 | 0.882 | 0.522 | -0.316 | -0.931 |
| 167 | 45.020 | 0.032 | 0.121 | -0.219 | -0.320 |
| 168 | 45.020 | 0.634 | 0.097 | -0.963 | -1.000 |
| 169 | 45.020 | -0.057 | 0.488 | -0.856 | -0.693 |
| 170 | 45.020 | 0.913 | -0.990 | -0.958 | -1.000 |
| 171 | -45.020 | 0.403 | -0.038 | 0.342 | -1.000 |
| 172 | 45.020 | -0.425 | 0.242 | -0.759 | -0.991 |
| 173 | -45.020 | 0.829 | 0.512 | -0.396 | -0.955 |
| 174 | 45.020 | -0.001 | -0.038 | -0.729 | -0.942 |
| 175 | -45.020 | 0.853 | 0.294 | 0.017 | -0.970 |